

# INTEGRATED DESIGN AND CONTROL OF REACTIVE DISTILLATION PROCESSES

MASTER OF SCIENCE IN ENGINEERING  
(CHEMICAL)

ASHFAQ IFTAKHER



Department of Chemical Engineering  
Bangladesh University of Engineering and Technology

January, 2021

# **Integrated Design and Control of Reactive Distillation Processes**

by

Ashfaq Iftakher

(1018022031)

Under the supervision of

Professor Dr. Md. Ali Ahammad Shoukat Choudhury

Submitted in partial fulfillment of the requirements for the degree of

MASTER OF SCIENCE IN ENGINEERING

(CHEMICAL)



Department of Chemical Engineering

BANGLADESH UNIVERSITY OF ENGINEERING AND TECHNOLOGY

January, 2021

### CERTIFICATE OF THESIS WORK

The thesis titled “**Integrated Design and Control of Reactive Distillation Processes**” submitted by **Ashfaq Iftakher**, Student ID. **1018022031F** Session **November, 2018** has been accepted as satisfactory in partial fulfillment of the requirement for the degree of **Master of Science in Engineering (Chemical)** on **January 02, 2021**.

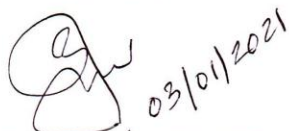
#### BOARD OF EXAMINERS



---

Dr. Md. Ali Ahammad Shoukat Choudhury  
Professor  
Department of Chemical Engineering, BUET, Dhaka-1000

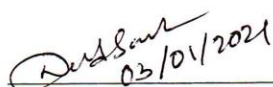
Chairman



---

Dr. Md. Mominur Rahman  
Professor & Head  
Department of Chemical Engineering, BUET, Dhaka-1000

Member (Ex-officio)



---

Dr. Nahid Sanzida  
Associate Professor  
Department of Chemical Engineering, BUET, Dhaka-1000

Member



---

Dr. Biplob Kumar Biswas  
Professor  
Department of Chemical Engineering  
Jashore University of Science and Technology  
Jashore-7408, Bangladesh

Member (External)

## DECLARATION

The thesis on “Integrated Design and Control of Reactive Distillation Processes” completed by Ashfaq Iftakher has been submitted in partial fulfillment of the degree of Master of Science in Chemical Engineering. This thesis is my original work and wherever contributions of others are involved, every effort is made to indicate this clearly, with due reference to the literature, and acknowledgement of collaboration is made explicitly.

**Ashfaq Iftakher**

**Student ID: 1018022031 F**

Department of Chemical Engineering

Bangladesh University of Engineering and Technology

In my capacity as supervisor of the candidate’s thesis, I certify that the above statements are true to the best of my knowledge.

**Thesis supervisor**

**Dr. Md. Ali Ahammad Shoukat Choudhury**

**Professor**

Department of Chemical Engineering

Bangladesh University of Engineering and Technology

Dhaka -1000

## ABSTRACT

Superior controllability of reactive distillation (RD) systems designed at the maximum driving force (design-control solution) is demonstrated in this work. Binary or multi-element single or double feed RD systems are considered. Reactive phase equilibrium data, needed for driving force analysis and design of the RD system, is generated through an in-house property prediction tool. Next, rigorous steady state simulation is carried out in ASPEN plus in order to verify that the predefined design targets and dynamics are met. Finally, a multi-objective performance function is employed to quantify the performance of the RD systems in terms of energy consumption, sustainability metrics (total CO<sub>2</sub> footprint), and the control performance. Controllability of the designed system is evaluated using relative gain array (RGA) and Niederlinski Index ( $N_I$ ), to indicate the degree of loop interactions, and system stability respectively. Further verification is done through the dynamic simulations of the RD systems using proportional integral (PI) controllers and model predictive controllers (MPC). The design-control of the RD systems corresponding to other alternative designs that do not take advantage of the maximum driving force is also investigated. The analysis shows that the RD designs at the maximum driving force, compared to the alternative designs exhibit the followings: 1) superior design, as indicated by less energy consumption and lower carbon footprint, 2) enhanced controllability, as indicated by Integral Absolute Error (IAE) and total variation of input (TV). Finally, the integrated design-control framework to perform all the design and control tasks is converted to a computer-aided toolbox for quick implementation, design and control of the desired RD systems.

## ACKNOWLEDGEMENTS

All praise and gratitude be to the Almighty Allah for enabling me to complete the thesis work successfully.

There are several people whom I would like to acknowledge. At first, I would like to express my most sincere gratitude to my supervisor – Professor Dr. Md. Ali Ahammad Shoukat Choudhury for his inspiration, instruction, support and guidance. He has been instrumental in shaping my philosophy towards academic research. I am deeply indebted to him for his sincere effort to teach me the art of doing research. His patience, enthusiasm, immense knowledge and encouragement have always been inspirational to me.

I would also like to gratefully acknowledge the support and directions of Professor Rafiqul Gani. He has so generously provided the financial support through his family trust fund to buy the high performance computer, necessary to complete this work. His work ethic and dedication to research has been truly eye-opening for me.

I would also like to acknowledge the support and encouragement of Ahaduzzaman Nahid, Assistant Professor, Dept. of Chemical Engineering, BUET. Being able to conduct research with him has been a life changing experience for me.

I express my deepest thanks to Dr. Seyed Soheil Mansouri and Dr. Anjan Tula for the collaboration and help regarding many aspects of the thesis work.

Finally, and most importantly, I acknowledge and thank my parents for their immense sacrifice in bringing me up, and allowing me to pursue my dream.

# TABLE OF CONTENTS

ABSTRACT.....	v
ACKNOWLEDGEMENT.....	vi
TABLE OF CONTENTS.....	vii
LIST OF FIGURES .....	x
LIST OF TABLES .....	xiii
NOMENCLATURE.....	xiv
ABBREVIATIONS.....	xv
1 INTRODUCTION.....	2
1.1 Background .....	2
1.2 Framework for the integrated design and control of RD systems.....	3
1.3 Scope of the work.....	3
1.4 Objective of the study .....	4
1.5 Thesis organization .....	4
2 REACTIVE DISTILLATION COLUMNS – A LITERATURE REVIEW .....	7
2.1 Notable reactive distillation systems.....	7
2.2 Design methods for reactive distillation systems.....	8
2.3 Control of reactive distillation systems.....	8
2.4 Methodologies for integrated design control of reactive distillation systems.....	9
2.4.1 Dynamic optimization approach .....	11
2.4.2 Embedded control optimization .....	13
2.4.3 Decomposition approach.....	14
2.5 Concepts and Theories for integrated design control of reactive distillation systems...	14
2.5.1 Chemical and physical equilibrium and element-based method.....	15
2.5.2 Driving force concept for reactive and nonreactive separations .....	21
2.5.3 Driving force based integrated design and control.....	23
2.6 Review of Model Predictive Controller .....	25

2.7	Review of State-space models.....	27
3	DESIGN-CONTROL FRAMEWORK AND ALGORITHMS .....	30
3.1	Overview of Integrated process design and control framework.....	30
3.2	Description of Integrated design-control framework .....	33
3.2.1	Step 1: Data collection and Problem formulation .....	33
3.2.2	Step 2: Integrated design-control .....	35
3.2.3	Step 3: Verification through simulation and analysis .....	44
4	APPLICATION EXAMPLES .....	48
4.1	Case Studies .....	48
4.2	Case study 1: MTBE production without inert .....	49
4.2.1	Step 1: Data collection and problem formulation .....	49
4.2.2	Step 2: Integrated Design-Control .....	50
4.2.3	Step 3: Verification through simulation and analysis .....	52
4.2.4	Step 4: Comparison with RD design not at maximum driving force .....	55
4.3	Case study 2: MTBE production with inert .....	57
4.3.1	Step 1: Data collection and problem formulation .....	57
4.3.2	Step 2: Integrated Design-Control .....	58
4.3.3	Step 3: Verification through simulation and analysis .....	59
4.3.4	Step 4: Comparison with RD design not at the maximum driving force .....	61
4.4	Case study 3: Methyl Acetate production .....	62
4.4.1	Step 1: Data collection and problem formulation .....	62
4.4.2	Step 2: Integrated Design-Control .....	63
4.4.3	Step 3: Verification through simulation and analysis .....	65
4.4.4	Step 4: Comparison with RD design not at the maximum driving force .....	68
4.5	Case study 4: Toluene disproportion.....	69
4.5.1	Step 1: Data collection and problem formulation .....	69
4.5.2	Step 2: Integrated Design-Control .....	70
4.5.3	Step 3: Verification through simulation and analysis .....	72
4.5.4	Step 4: Comparison with RD designs not at the maximum driving force.....	73
4.6	Case study 5: ETBE production .....	74



4.6.1	Step 1: Data collection and problem formulation .....	74
4.6.2	Step 2: Integrated Design-Control .....	75
4.6.3	Step 3: Verification through simulation and analysis .....	76
4.6.4	Step 4: Comparison with RD design not at the maximum driving force .....	78
4.7	Case study 6: TAME production.....	79
4.7.1	Step 1: Data collection and problem formulation .....	79
4.7.2	Step 2: Integrated Design-Control .....	80
4.7.3	Step 3: Verification through simulation and analysis .....	81
4.7.4	Step 4: Comparison with RD design not at the maximum driving force .....	83
4.8	Summarized results and discussions .....	84
5	OVERVIEW OF THE REACTIVE DISTILLATION TOOLBOX.....	97
5.1	The Reactive Distillation Toolbox .....	97
5.2	Setting up steady state simulation .....	97
5.3	Generating state space matrices and MPC scripts.....	103
5.4	Running the simulation and observing the dynamic responses.....	106
6	CONCLUSION AND FUTURE WORKS.....	111
6.1	Conclusions .....	111
6.2	Directions for future works .....	112
References .....		113
Appendix A .....		II
Appendix B .....		VI
Appendix C .....		VIII
Appendix D .....		IX

## LIST OF FIGURES

Figure 2.1 Production of methyl-acetate at Eastman-Kodak. Left: without intensification; Right: with intensification – reactive distillation column (Schoenmakers & Bessling, 2003).	7
Figure 2.2 Driving force based design of distillation columns – on the left is the driving force diagram and on the right is the corresponding design of the reactive distillation column (adapted from Babi et al., 2014)	22
Figure 2.3 A Driving force diagram with the important distillation design parameters (Bek-Pedersen & Gani, 2004).	25
Figure 2.4 Basic concepts for model predictive control (Seborg, 2010).	27
Figure 3.1 Integrated RD process design-control framework.	31
Figure 3.2 Process-controller block diagram highlighting PI and MPC controller.	44
Figure 4.1 Reactive McCabe-Thiele method for designing MTBE binary element reactive distillation system.	52
Figure 4.2 Open-loop response of the optimal design control solution to step change in feed flow rate, Case study 1: A) top; B) bottom.	54
Figure 4.3 Close-loop response of the optimal design control solution for step change in feed flow rate, Case study 1: A) PI controller; B) MPC controller	54
Figure 4.4 Comparison between controlled outputs under MPC and PI controllers for the design-control solution, Case study 1: A) composition B) percent deviation.	55
Figure 4.5 Close-loop response of the alternative design for step change in feed flow rate, Case study 1: A) PI controller; B) MPC controller	56
Figure 4.6 Comparison between controlled outputs under MPC and PI controllers for the alternative design, Case study 1: A) composition B) percent deviation	57
Figure 4.7 Reactive McCabe-Thiele diagram and calculations for MTBE multi-element system.	59
Figure 4.8 Open-loop response of the optimal design control solution to step change in feed flow rate, Case study 2: A) top; B) bottom.	60
Figure 4.9 Close-loop response of the optimal design control solution for step change in feed flow rate, Case study 2: A) PI controller; B) MPC controller	60
Figure 4.10 Comparison between controlled outputs under MPC and PI controllers for the design-control solution, Case study 2: A) composition B) percent deviation	61
Figure 4.11 Close-loop response of the alternative design for step change in feed flow rate, , Case study 2: A) PI controller; B) MPC controller	62
Figure 4.12 Comparison between controlled outputs under MPC and PI controllers for the alternative design, Case study 2: A) composition B) percent deviation	62
Figure 4.13 Reactive distillation column design for methyl-acetate multi-element system at 1 atm.	64
Figure 4.14 Open-loop response of the optimal design control solution to step change in feed flow rate, Case study 3: A) +10% methanol; B) +10% acetic acid.	66

Figure 4.15 Close-loop response of the optimal design control solution for a step change in the feed flow rate, Case study 3: A) PI controller, +10% methanol; B) PI controller, +10% acetic acid; C) MPC controller, +10% methanol; D) MPC controller, +10% acetic acid. _____	67
Figure 4.16 Comparison between the controlled outputs under the MPC and PI controllers for the design-control solution, Case study 3: A) +10% methanol; composition B) +10% methanol; percent deviation; C) +10% acetic acid; composition D) +10% acetic acid; percent deviation. _____	67
Figure 4.17 Close-loop response of the alternative design for a step change in the feed flow rate, Case study 3: A) PI controller, +10% methanol; B) PI controller, +10% acetic acid; C) MPC controller, +10% methanol; D) MPC controller, +10% acetic acid. _____	68
Figure 4.18 Comparison between the controlled outputs under the MPC and PI controllers for the alternative design, Case study 3: A) +10% methanol; composition B) +10% methanol; percent deviation; C) +10% acetic acid; composition D) +10% acetic acid; percent deviation. _____	69
Figure 4.19 Reactive distillation column design for toluene disproportionation binary element system at 1 atm. ____	71
Figure 4.20 Open-loop response of the optimal design control solution to step change in feed flow rate, Case study 4: A) top; B) bottom. _____	72
Figure 4.21 Close-loop response of the optimal design control solution for step change in feed flow rate, Case study 4: A) PI controller; B) MPC controller _____	72
Figure 4.22 Comparison between controlled outputs under MPC and PI controllers for the design-control solution, Case study 4: A) composition B) percent deviation _____	73
Figure 4.23 Close-loop response of the alternative design for step change in feed flow rate, Case study 4: A) PI controller; B) MPC controller. _____	74
Figure 4.24 Comparison between controlled outputs under MPC and PI controllers for the alternative design, Case study 4: A) composition B) percent deviation. _____	74
Figure 4.25 Reactive distillation column design for ETBE binary -element system at 15 atm. _____	76
Figure 4.26 Open-loop response of the optimal design control solution to step change in feed flow rate, Case study 5: A) top; B) bottom. _____	77
Figure 4.27 Close-loop response of the optimal design control solution for step change in feed flow rate, Case study 5: A) PI controller; B) MPC controller _____	77
Figure 4.28 Comparison between controlled outputs under MPC and PI controllers for the design-control solution, Case study 5: A) composition B) percent deviation _____	78
Figure 4.29 Close-loop response of the alternative design for step change in feed flow rate, Case study 5: A) PI controller; B) MPC controller. _____	78
Figure 4.30 Comparison between controlled outputs under MPC and PI controllers for the alternative design, Case study 5: A) composition B) percent deviation. _____	79
Figure 4.31 Reactive distillation column design for TAME at 4 bar. _____	81
Figure 4.32 Open-loop response of the optimal design control solution to step change in feed flow rate, Case study 6: A) top; B) bottom. _____	82

Figure 4.33 Close-loop response of the optimal design control solution for step change in feed flow rate, Case study 6: A) PI controller; B) MPC controller	82
Figure 4.34 Comparison between controlled outputs under MPC and PI controllers for the design-control solution, Case study 6: A) composition B) percent deviation	83
Figure 4.35 Close-loop response of the alternative design for step change in feed flow rate, Case study 6: A) PI controller; B) MPC controller	83
Figure 4.36 Comparison between controlled outputs under MPC and PI controllers for the alternative design, Case study 6: A) composition B) percent deviation	84
Figure 4.37 Calculated VLE phase diagram for the 6 reactive systems; A) MTBE without inert (1 atm); B) MTBE with inert (11 atm); C) Methyl-acetate (1 atm); D) Toluene disproportionation (1 atm); E) ETBE (15 atm); F) TAME (4 bar).	87
Figure 4.38 Calculated reactive driving force diagram for the 6 reactive systems; A) MTBE without inert (1 atm); B) MTBE with inert (11 atm); C) Methyl-acetate (1 atm); D) Toluene disproportionation (1 atm); E) ETBE (15 atm); F) TAME (4 bar).	88
Figure 4.39 Calculated reactive differential driving force diagram for the 6 reactive systems; A) MTBE without inert (1 atm); B) MTBE with inert (11 atm); C) Methyl-acetate (1 atm); D) Toluene disproportionation (1 atm); E) ETBE (15 atm); F) TAME (4 bar).	90
Figure 5.1 Compound selection	98
Figure 5.2 Feed specification	99
Figure 5.3 Reaction Definition	99
Figure 5.4 Reaction Kinetics	100
Figure 5.5 RD Column Design parameters	101
Figure 5.6 Aspen Input file generation	101
Figure 5.7 Input file translation to ASPEN PLUS	102
Figure 5.8 Converged steady state simulation	102
Figure 5.9 Flow driven ASPEN PLUS Dynamics file	103
Figure 5.10 CDI script generation	104
Figure 5.11 Generated CDI script	104
Figure 5.12 CDI script invoke	105
Figure 5.13 State space matrices generation	105
Figure 5.14 MATLAB MPC m file generation	106
Figure 5.15 Generated m file for MPC simulation	106
Figure 5.16 Opening MPC m file in MATLAB	107
Figure 5.17 MPC simulation data	107
Figure 5.18 Dynamic MPC closed loop simulation	108
Figure 5.19 Open loop and Close loop PI response	109

## LIST OF TABLES

Table 3.1 Common variables for design and control. ....	32
Table 4.1 Design targets and product specifications for MTBE system without inert.....	50
Table 4.2 Design targets and product specifications for MTBE system with inert.....	57
Table 4.3 Design targets and product specifications for methyl acetate production. ....	63
Table 4.4 Design targets and product specifications for Toluene disproportionation.....	70
Table 4.5 Design targets and product specifications for ETBE production. ....	75
Table 4.6 Design targets and product specifications for TAME system.....	80
Table 4.7 Key information for problem formulation (step 1). ....	84
Table 4.8 The element matrix and element reaction for the binary element reactive systems.....	85
Table 4.9 The element matrix and element reaction for the multi-element reactive systems. ....	86
Table 4.10 Summary of design parameters for design-control solutions and alternative designs. ....	89
Table 4.11 RGA, Niederlinski index ( $N_I$ ) and system stability for the design at the maximum driving force. ....	91
Table 4.12 Disturbance scenarios .....	91
Table 4.13 Performance objective function values of PI and MPC controller for Case study 1,2,4,5 & 6 at the design-control solution.....	91
Table 4.14 RGA, Niederlinski index ( $N_I$ ) and system stability for the alternative designs .....	92
Table 4.15 Performance objective parameter values of the PI and MPC controllers for Case study 3 at the design-control solution. ....	93
Table 4.16 Summary of the comparison of performance objective function terms for design-control solution and alternative designs for PI and MPC control structure for case study 1, 2 & 4. ....	93
Table 4.17 Summary of the comparison of performance objective function terms for design-control solution and alternative designs for PI and MPC control structure for case study 5 & 6. ....	94
Table 4.18 Summary of the comparison of the performance objective function terms for the design-control solution and the alternative designs for the PI and MPC control structure for case study 3.....	94

## NOMENCLATURE

$x$	Vector of decision variables
$z$	Vector of dynamic state variables
$F$	Vector of objective functions
$h$	Vector of equality constraints
$g$	Vector of inequality constraints
$G$	Gibbs free energy
$\mu_i^\beta$	Chemical potential of component $i$ in phase $\beta$
$M$	Number of elements
$NC$	Number of components
$A^{M \times NC}$	Formula matrix
$NR$	Number of reactions
$W_j^\beta$	Element $j$ in phase $\beta$
$D_x$	Location of maximum driving force
$D_y$	Quantity of maximum driving force
$N_F$	Number of feed stage
$D$	Vector of model equations
$\theta$	Vector of constitutive equations
$u$	Design and manipulated variables
$d$	Disturbance variables
$y$	Controlled variables
$N_x$	Number of states

$A^{N_x \times N_x}$	System matrix
$\lambda$	Vector of eigenvalues of the system matrix
$x^D, x^B$	Product compositions (design targets)
$RR$	Reflux ratio
$Q_R$	Reboiler duty
$N_I$	Niederlinski Index

## ABBREVIATIONS

RD	Reactive distillation
PI	Proportional Integral
MPC	Model Predictive Controller
IAE	Integral Absolute Error
SISO	Single Input Single Output
MIMO	Multiple Input Multiple Output
MINLP	Mixed Integer Nonlinear Programming
MIDO	Mixed Integer Dynamic Optimization
DAE	Differential Algebraic Equation
DF	Driving Force
PH	Prediction Horizon
CH	Control Horizon
ODE	Ordinary Differential Equation
RGA	Relative Gain Array
MTBE	Methyl-tert-Butyl-Ether
ETBE	Ethyl-tert-Butyl-Ether
TAME	Tert-Amyl-Methyl-Ether
CDI	Control Design Interface



**CHAPTER 1**  
**INTRODUCTION**

# 1 INTRODUCTION

This chapter summarizes the advantages and challenges associated with the operation of reactive distillation – one of the major process intensification units. Later, the scope of the work, along with specific objectives and organization of the thesis are described.

## 1.1 Background

Reactive distillation (RD) takes advantage of the synergy created when combining heterogeneous/homogenous catalytic reactions or non-catalytic reactions with separation into a single intensified process unit (Tian et al., 2018). Some of the key advantages of RD are as follows:

- a) Improved productivity and selectivity by simultaneous removal of products from reactants as well as suppression of side reactions (H. Y. Lee et al., 2010).
- b) Reduced capital cost, and the need for solvents (Babi et al., 2014).
- c) Avoidance/degradation of azeotropes (Agreda & Partin, 1984).
- d) Reduced energy usage by using the heat of exothermic reaction *in situ* for the vaporization of the liquid, resulting in lower CO<sub>2</sub> emission and less waste among others (Kiss, 2019).

These advantages not only attract industrial perspectives and applications (G. J. Harmsen, 2007) but also make RD a suitable intensified process to combat ever-increasing worldwide energy demand, which is expected to increase about 3.5 times (7 times increase in electricity demand) over the next ten years. (Gani et al., 2020).

Although RD is highly preferable due to the obvious requirement of fewer unit operations, which translates to more economic profit, industries are yet to fully embrace this technology. The primary reason being, as an intensified process unit, RD is more difficult to design and control than corresponding non-intensified process. The complex issues regarding designing RD arise mainly due to the simultaneous consideration of separation and reaction, which results in a reduction of the degree of freedom and narrowed operating window. Consequently, the

controllability of RD strongly depends on their design (Georgiadis et al., 2002). Therefore, if there is any issue in process design, the achievement of good control performance is highly unlikely. For example, inaccurate kinetic modeling propagates exponentially through the process, greatly upsetting the nominal operation. In the case of dynamic operation, unlike non-reactive systems, holdup becomes a key design variable for RD that affects control performance. Therefore, it is of paramount importance to incorporate operability and controllability in the early design stage for a feasible steady state and dynamic operation under process disturbances.

## **1.2 Framework for the integrated design and control of RD systems**

To address the simultaneous design and control issues, the development and application of a versatile framework for systematic integration of the driving force concept based design with various control methods, such as PI(D) and MPC, are presented in this work.

The framework follows three main calculation steps. In the first step, the design targets along with the objectives are set. In the second step, the key design parameters for the steady state and dynamic simulation of the RD system are determined using the driving force concept. In the final step, the steady-state and dynamic verification of the designed systems are carried out using the state-space model of the process and open loop and closed-loop simulation. Detailed description of the framework is give in section 3.1.

## **1.3 Scope of the work**

There has been significant amount of work done on the integration of design and control for RD systems, as discussed in Chapter 2. However, most of the control structures relied on regulatory controller (PI). Work on integrated design-control using MPC has scarcely been reported. Francisco et al., 2011 reported a methodology for the simultaneous design of processes and linear MPCs, providing the plant dimensions, the control system parameters and a steady state working point. Bahakim & Ricardez-Sandoval, 2014 proposed a methodology based on stochastic simultaneous design and MPC control of chemical processes under uncertainty.

However, these processes rely on mathematical optimization formulation for process synthesis, which are computationally expensive to perform. Also, there is no integrated design-control work done where graphical design method (e.g. driving force concept) is integrated with advanced controller such as MPC. In this work, this gap is intended to reduce by developing a framework where the optimal/near optimal design parameters are easy to obtain, and dynamic operation is guaranteed to be feasible. Another issue is, there is no known single user interface/toolbox that allows user to set up an RD system for steady state and dynamic simulation. This issue is also addressed in this work by developing an integrated design-control toolbox.

#### **1.4 Objective of the study**

The major objectives of this study are reported as below:

- **Objective 1**: Development of a systematic framework for integrated design and control of RD systems through the driving force approach (Bek-Pedersen & Gani, 2004) for feasible steady-state and dynamic operation.
- **Objective 2**: Analysis of control performance for RD systems operating under a regulatory controller (PI), or a supervisory controller (MPC).
- **Objective 3**: Implementation of the framework into a software toolbox that will systematically guide the user to set up the RD system, perform steady-state and dynamic simulation, and analyze the response. Some of the most convenient features of the toolbox will be the automatic generation of flowsheet and scripts for state space matrices generation and close loop MPC simulation, resulting in a significant amount of time savings.

#### **1.5 Thesis organization**

Chapter 1 is the introduction to the thesis. Summary of the background, primary objectives of this study and the thesis organization are also included in this chapter.

Chapter 2 provides an overview of the recent developments in the RD technology. Special focus has been given in describing the relevant methodologies, theory and concepts for integrated design and control.

Chapter 3 introduces the framework for the design control along with the detailed description of each step. Required algorithms to perform each step are also included in this chapter.

Chapter 4 discusses the application of the framework described in Chapter 3 through six case studies. For each case study, the problem setup along with the design and control performance evaluation are described in detail. The results are quantified to draw the conclusion.

Chapter 5 provides an overview of the developed software. The sequence of tasks to use the toolbox is described through a case study.

Chapter 6 states the conclusion drawn from current work, and suggests future research directions.

**CHAPTER 2**  
**REACTIVE DISTILLATION COLUMNS –**  
**A LITERATURE REVIEW**

## 2 REACTIVE DISTILLATION COLUMNS – A LITERATURE REVIEW

This chapters aims to provide an extensive review on reactive distillation (RD). At first, some of the notable works on RD in terms of reaction-separation systems, process synthesis, design and control over the last 20 years are briefly reported. Later, the state of the art methodologies and concepts for integrated design-control of RD are given special focus and discussed in detail.

### 2.1 Notable reactive distillation systems

Although the theoretical foundations for the RD operation were laid out in the 1920s, the first notable industrial application was by Eastman Kodak company in 1983 when they substituted a complex network of distillation column and reactor by a single RD unit as shown in *Figure 2.1*.

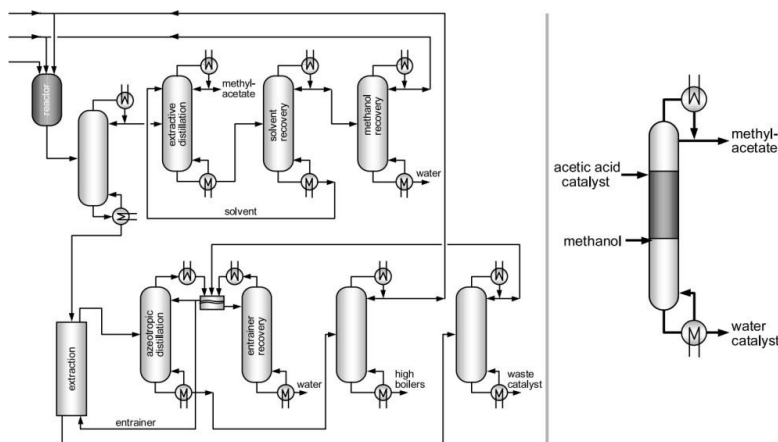


Figure 2.1 Production of methyl-acetate at Eastman-Kodak. Left: without intensification; Right: with intensification – reactive distillation column (Schoenmakers & Bessling, 2003).

Over the years, many more work on RD systems are reported in the literature. Some of the notable works in terms of chemicals handled are: production of methyl acetate (Agreda & Partin,

1984); production of methyl acetate as well as fuel additives or oxygenates (MTBE, ETBE, TAME) (G. J. Harmsen, 2007); hydrolysis of methyl acetate (Sander et al., 2007); biodiesel production (Kiss & Bildea, 2012); production of ethylene glycol (An et al., 2014); production of silanes (Medina-Herrera et al., 2017); production of acrylic and methacrylic monomers, polyesters, alkyl ethers (dimethyl ether, di-n-pentyl ether), fatty esters, and other short chain alkyl esters (Kiss, 2019). There have been more than 150 successful industrial applications of RD technology (J. Harmsen, 2010) for selective hydrogenation of mixed hydrocarbons, selective desulfurization of mid catalytic naphtha, isomerization of n-olefins to iso-olefins, etc.

## **2.2 Design methods for reactive distillation systems**

Substantial amount of research is done on the design methods for RD systems over the years. These include conceptual design (Doherty, MF; Malone, 2001); optimal design using deterministic and stochastic techniques (Segovia-Hernández et al., 2015); computer aided tool for searching for process designs (Anjan Kumar Tula et al., 2017); graphical methods (Sánchez Daza et al., 2003); model-based tool that utilizes process-group contribution method (Anjan Kumar Tula et al., 2015); boundary value methods (Dragomir & Jobson, 2005); pinch based methods (Avami et al., 2012); shortest stripping line method (Lucia et al., 2008).

To summarize, all the synthesis methods for RD can be categorized as heuristic, graphical, and optimization-based approaches. Shah et al., 2012 discussed systematic framework to characterize the feasibility of RD columns based on a set of heuristics. Almeida-Rivera et al., 2004 discussed graphical techniques for RD designs. Optimization-based approaches, however, provide a more systematic procedure for the synthesis of RD columns. These methods are based on either NLP or MINLP formulations with an objective to minimize total annual cost in the most cases (Tian et al., 2018).

## **2.3 Control of reactive distillation systems**

In the area of control of RD operations, several control studies involving RD operations have been reported. For example, the control of ethyl acetate production has been reported by Chien et



al., 2008, who employed a PI(D) controller to control tray temperature. Heath et al., 2000 employed a PI controller for ethylene glycol production through a RD process. Wang et al., 2014 controlled tray temperature using a PI control for diethyl carbonate synthesis. Al-Arfaj & Luyben, 2002 studied the use of a PI controller to control tray temperature and product purity for methyl acetate production.

Applications of advanced control algorithms such as model predictive controller (MPC) are also reported for RD operation in the literature. J. H. Lee, 2011 has reviewed the development and application of MPC in the last three decades. Some of the notable works on MPC for RD systems include: controlling product purity in a TAME synthesis process (Sharma & Singh, 2012); applying nonlinear MPC with a neural network model for controlling product purity of a methyl acetate RD system (Engell & Fernholz, 2003). In the case of ethyl acetate production, (Kawathekar & Riggs, 2007) applied nonlinear MPC for controlling product purity; (Venkateswarlu & Reddy, 2008) applied nonlinear MPC based on stochastic optimization for controlling product purity, reboiler & condenser holdups, and column pressure; (Balasubramhanya & Doyle, 2000) applied nonlinear MPC to control tray temperature.

#### **2.4 Methodologies for integrated design control of reactive distillation systems**

In section 2.2, the works on synthesis of RD systems were considered based on satisfying a steady-state design target, without taking into account the dynamic operability. In section 2.3, control of RD systems were considered without taking into account the optimal process design of RD systems. As it was discussed briefly in section 1.1, design issues and control issues must be considered simultaneously in order to ensure feasible and reliable RD operation. It is well-known that process design and process control, when considered independently, generally lead to conflicting objectives for the chemical processes e.g., process over design vs not robust design, infeasible vs economically suboptimal operating points (Rafiei & Ricardez-Sandoval, 2020), etc. Therefore, design and control issues are best to be addressed simultaneously (as in integrated process design and control) to obtain economically attractive, yet operationally feasible, and flexible processes. One of the convenient features of the simultaneous approach is the possibility to identify and eliminate potentially promising design alternatives that may have controllability

problems due to a loss of degree of freedom which shrinks the controllability region (Alvarado-Morales et al., 2010).

Since, all the work in this thesis are based on integration of design and control of RD systems, rest of this chapter is dedicated to describe some of the key methodologies and concepts for the integrated design-control approach. These methodologies can be categorized as follows:

- a) Dynamic optimization approach.
- b) Embedded control optimization.
- c) Decomposition approach.

In the forthcoming subsections, these methodologies along with some of the recent contributions that are reported in the literature are described. Note that, in all the methodologies that are reviewed, the process flowsheet is known, as well as the design targets, feed specifications and process conditions are predefined. Therefore, the objective is to find the design variables, the operating conditions (including set-points for controlled variables) and controller structure that optimize the plant controllability. It is assumed that the process model and constraints are accurate enough to capture the appropriate dynamic behavior and process specifications. The general formulation of the problem is given as follows (Sendin et al., 2004):

$$\min_x F(\dot{z}, z, p, x) = \begin{bmatrix} F_1(\dot{z}, z, p, x) \\ F_2(\dot{z}, z, p, x) \end{bmatrix} \quad \#2.1$$

Subject to:

$$f(\dot{z}, z, p, x) = 0 \quad \#2.2$$

$$z(t_0) = z_0 \quad \#2.3$$

$$h(z, p, x) = 0 \quad \#2.4$$

$$g(z, p, z) \leq 0 \quad \#2.5$$

$$x^L \leq x \leq x^U \quad \#2.6$$

Here  $x$  is the vector of decision variables,  $z$  is the vector of dynamic state variables,  $F$  is the vector of objective functions ( $F_1$  is a combination of capital cost and operating costs, and  $F_2$  is the controllability measures),  $f$  is the set of differential and algebraic equality constraints describing the system dynamics (mass, energy and momentum balances, i.e., the nonlinear

process model), and  $h$  and  $g$  are possible equality and inequality constraints which impose additional requirements for process performance.

### 2.4.1 Dynamic optimization approach

In dynamic optimization approach, the design-control problem is formulated as a mixed integer non-linear programming (MINLP) optimization problem. The continuous variables represent both design variables (flow rates, heat duties etc.) and process variables (temperatures, pressures, compositions). The binary (decision) variables express logical decisions such as whether to choose between different possible flowsheet structures and/or controller structures. In the integrated process design control context, the variables are considered in the process model in a way such that they represent both steady state and dynamic behavior of the problem. Hence, the optimization problem is referred as mixed-integer dynamic optimization (MIDO).

Disturbance rejection is an important feature for the closed-loop control performance of chemical processes. In order to get minimum time closed-loop disturbance rejection, the following optimization problem can be formulated to use in a MIDO approach (Flores-Tlacuahuac & Biegler, 2007):

$$\min \int_0^{t_f} \|z(t) - \hat{z}(t)\|^2 dt \quad \#2.7$$

subject to: semi-explicit differential algebraic equation (DAE) model of a dynamic process

$$\frac{dz(t)}{dt} = F(z(t), x(t), u(t), t, p) \quad \#2.8$$

$$0 = G(z(t), x(t), u(t), t, p) \quad \#2.9$$

Initial conditions:

$$z(0) = z^0 \quad \#2.10$$

Bounds:

$$z^L \leq z(t) \leq z^U \quad \#2.11$$

$$x^L \leq x(t) \leq x^U \quad \#2.12$$

$$u^L \leq u(t) \leq u^U \quad \#2.13$$

$$p^L \leq p \leq p^U \quad \#2.14$$

Disjunctions:

$$\bigvee_{i \in D} \{a_j \leq g_j(w) \leq b_j\} \quad \#2.15$$

where  $F$  is the vector containing the DAE model of a dynamic process,  $G$  is the vector of algebraic equations,  $t \in [0 t_f]$  is the time,  $z$  is the differential state vector,  $z^0$  the initial value of  $z$ ,  $\hat{z}$  is the set-point vector,  $x$  is the algebraic state vector,  $u$  is the control profile vector and  $p$  is a time independent parameter vector.

By definition,  $w = [z^T \ x^T \ u^T \ p^T]^T$  and  $D$  is the set of disjunctions with the inequality constraints having the property  $g_j(0) = 0$  is the  $j^{th}$  disjunction. These disjunctions can be obtained and derived in a systematic manner taking into account the logical expressions. Such DAE optimization problems are solved by applying non-linear programming (NLP) solvers to the DAE model (Biegler, 2007).

MIDO approach has been increasingly used as a result of the advancements in computational power and dynamic programming algorithms (Dimian et al., 2014). Various algorithms and solutions strategies have been developed to solve MIDO problems. Androulakis, 2000 employed complete discretization on the dynamic system where the MINLP problem is solved using the branch and bound method. Avraam et al., 1999 also employed complete discretization on the dynamic system, except, they used outer approximation (OA) method to solve the MINLP problem. A comprehensive review of state-of-the-art and progress in the optimization-based simultaneous design and control for chemical processes has been performed by Yuan et al., 2012. Note, however, the major drawback of MIDO methodologies is the complexity that is

associated with computation. Therefore, their application on large or industrial problems is difficult due to very long computation time (Ricardez-Sandoval et al., 2009).

#### **2.4.2 Embedded control optimization**

This approach is based on a novel mathematical formulation to render the combinatorial complexity of the integrated process design and control problem. Therefore, the problem is formulated as a bi-level optimization problem, which is then solved using a two-stage sequential approach (Malcolm et al., 2007). This formulation separates design decisions from control decisions to keep the problem size manageable by significantly reducing the complexity. The first stage (usually called master level) seeks optimal design decisions while the second stage tests the dynamic performance based on design decisions obtained previously by fixing a particular control strategy (for example PI or MPC) alongside its tuning parameters.

Fixing a particular control strategy in the second stage, therefore, eliminates integer decisions for selecting controller structures, and the problem complexity is reduced compared to MINLP formulation. The currently proposed solution strategies are able to reduce and solve the combinatorial complexity of the problem with less computational effort compared to the MIDO strategies. Although the design solution obtained from the embedded control optimization approach may result in suboptimal design solutions, it is attractive from a computational point of view and offers better practicality for solving industrial problems.

Malcolm et al., 2007 proposed a procedure for integrated process design and control, which is based on process dynamics and advanced control by a novel embedded control optimization approach. Their work suggests a two-stage problem decomposition leading to a massive reduction of problem size and complexity. Note that in this work, the integration of design and control is made possible using a novel problem formulation that implicitly relates closed-loop dynamics with design decisions. Moon et al., 2011 introduced a new mathematical formulation to reduce combinatorial complexity of integrating design and control by avoiding a combinatorial explosion of control configuration, using a full state space model that does not require a pairing of control variables and loops.

### **2.4.3 Decomposition approach**

The decomposition approach offers an effective solution strategy. The main idea in the decomposition-based approach is to decompose the integrated process design and control problem into an ordered set of sub-problems. Each sub- problem, except the last one, requires only the solution of a subset from the original constraints set. The final sub-problem contains the objective function and the remaining constraints. In this way, the solution of the decomposed set of sub- problems is equivalent to that of the original optimization problem. after every sequential sub-problem, the search space for feasible solutions is reduced and a sub-set of design-manipulated and/or decision variables are fixed. The advantage is a more flexible solution approach together with relatively easy to solve sub-problems.

Here, only a few decomposition algorithms in the area of integration of process design and control that have been proposed are reviewed. Mohideen et al., 1996 proposed a unified decomposition-based process design framework for obtaining integrated process and control based on a dynamic mathematical model that describes uncertain parameters and time-varying disturbances and a set of process design and control alternatives. (Kookos & Perkins, 2001) developed an algorithm based on the systematic generation of lower and upper bounds on the best achievable dynamic economics of the combined plant to effectively reduce the size of the search space. (S. S. Mansouri, Huusom, et al., 2016) have shown that by simultaneously considering design and control issues through the driving force concept, optimal design-control of reactive distillation units can be achieved. The main takeaway from this work is that a process designed based on the largest driving force consumes the minimum amount of energy and also is the easiest from the operation viewpoint. Recently, (Lopez-Arenas et al., 2019) proved theoretically that a RD column designed for operation at the maximum available driving force, corresponds to the minimum energy requirement.

### **2.5 Concepts and Theories for integrated design control of reactive distillation systems**

In this chapter, the concepts and theories that are being used in this work will be elaborated. These concepts and theories are used in various stages of the integrated process design and control methodology. First, the chemical and physical equilibrium concept is explained with

relevant mathematical information. Additionally, the element-based method which is based on the chemical and physical equilibrium concept is elaborated. Second, the driving force concept for designing reactive and non-reactive separation processes is discussed. Driving force approach is a method of distillation process design. Its objective is to achieve the design at the maximum available driving force for separation of a given mixture (reactive or non-reactive). Finally, the driving force based integrated process design and control is presented. From a process design point of view, optimal/near optimal design in terms of energy consumption is obtained at the highest driving force. From a controller design point of view, the best controller structure and set-point values for controlled and manipulated variables are obtained at this point. Later in Algorithm 4 (Chapter 3), it is demonstrated analytically that at the maximum driving force, the sensitivity of the controlled variables to disturbances is the lowest and at the same time, the sensitivity of controlled variables to manipulated variables (actuators) is the highest, thereby facilitating superior control performance.

### **2.5.1 Chemical and physical equilibrium and element-based method**

This concept is derived from chemical model theory, where the equations of chemical equilibrium together with any appropriate physical model yielding the chemical potentials are embedded into an element-based model (called the chemical model) (Michelsen, 1994). The solution of the chemical model equations together with the condition of equilibrium (equality of the component chemical potentials in all co-existing phases) provides the element phase compositions for the reactive system. One attractive feature of this concept is its capability to handle the problem of reactive-phase equilibrium in the same manner as the case when no reactions are taking place in the system. That is, this approach reduces the chemical and physical equilibrium problem to an identical physical equilibrium problem for a mixture of elements representing the system.

#### **2.5.1.1 Thermodynamic fundamentals**

For a system with  $NP$  phase and  $NC$  chemical species, the fundamental thermodynamic relation is given by the Gibbs free energy as follows:

$$G = G(T, P, n_i^\beta) \quad \#2.16$$

Where  $n_i^\beta$  ( $i = 1, 2, \dots, NC; \beta = 1, 2, \dots, NP$ ) represents the number of moles of species  $i$  in phase  $\beta$ . The Gibbs free energy is an extensive property, proportional to the amount of material in the system. From Euler's theorem on homogenous functions, it follows that

$$G = \sum_{\beta=1}^{NP} \sum_{i=1}^{NC} \mu_i^\beta n_i^\beta \quad \#2.17$$

where the chemical potential  $\mu_i^\beta$  is defined by

$$\frac{\partial G}{\partial n_i^\beta} = \mu_i^\beta(T, P, n_j^\beta) \quad \#2.18$$

Since, it is a homogenous function of degree zero in  $n_j^\beta$ ; that is  $\mu_i^\beta$  is an intensive property (extensive property is a homogenous function of degree one due to proportionality). The total differential of  $G$  from Equation 2.16 is given by:

$$dG = \left(\frac{\partial G}{\partial T}\right)_{P,n} dT + \left(\frac{\partial G}{\partial P}\right)_{T,n} dP + \sum_{\beta=1}^{NP} \sum_{i=1}^{NC} \left(\frac{\partial G}{\partial n_i^\beta}\right)_{T,P} dn_i^\beta \quad \#2.19$$

For fixed  $T, P$ , Equation 2.19 reduces to:

$$dG = \sum_{\beta=1}^{NP} \sum_{i=1}^{NC} \left(\frac{\partial G}{\partial n_i^\beta}\right)_{T,P} dn_i^\beta = \sum_{\beta=1}^{NP} \sum_{i=1}^{NC} \mu_i^\beta dn_i^\beta \quad \#2.20$$

The total differential of  $G$  from Equation 2.18 is given by:

$$dG = \sum_{\beta=1}^{NP} \sum_{i=1}^{NC} \mu_i^\beta dn_i^\beta + \sum_{\beta=1}^{NP} \sum_{i=1}^{NC} n_i^\beta d\mu_i^\beta \quad \#2.21$$

Combining Equation 2.20 and 2.21 gives the well known Gibbs-Duhem equation:

$$0 = \sum_{\beta=1}^{NP} \sum_{i=1}^{NC} n_i^\beta d\mu_i^\beta \quad \#2.22$$



If Gibbs function is used to describe a thermodynamic system, the thermodynamic equilibrium for a close system is defined as the state for which the total Gibbs free energy is minimum with respect to all possible changes at the given  $T$  and  $P$ . This can be formulated mathematically as follows:

$$\min G = \sum_{\beta=1}^{NP} \sum_{i=1}^{NC} \mu_i^{\beta} n_i^{\beta} \quad \#2.23$$

Subject to:

$$\sum_{\beta=1}^{NP} \sum_{i=1}^{NC} A_{ji} n_i^{\beta} - b_j = 0 \quad j = 1, 2, \dots, M \quad \#2.24$$

In the above formulation,  $G$  is the total Gibbs free energy of a system that has  $NC$  species and  $NP$  phases. Equation 2.24 represents the  $M$  independent element mass balances, where the coefficients  $A_{ji}$  denote the number of elements  $j$  in molecule  $i$  in the reaction mixture. The formula matrix  $A^{M \times NC}$  is a full rank matrix i.e.,  $\text{rank}(A) = M$  and  $b_j$  is the total number of moles of element  $j$  in the system. Note that any of the  $M$  independent elements can be atoms, molecules or radicals/groups. Also note that, the total number of elements ( $M$ ) is less than the number of components ( $NC$ ) in the reactive system. Because, if the reaction is allowed to occur without stoichiometric constraints,  $M = NC - NR$ , where  $NR$  is the number of independent reactions. The solution of the constrained optimization problem represented by Equation 2.23 and 2.24 is obtained through the Lagrange multiplier formulation. Further details along with the phase rule for reacting systems can be found in Pérez Cisneros et al., 1997.

### 2.5.1.2 Equilibrium conditions

In order to explain the chemical and physical equilibrium concept, only chemical and physical equilibrium for  $\beta = 1$  (a single phase) is considered. For simplicity, the superscript  $\beta$  in Equation 2.17 is omitted. Applying the stationary point conditions into Equation 2.23 and 2.24, the following Gibbs free energy equation at equilibrium is obtained (Pérez Cisneros et al., 1997).

$$G_{eq} = \sum_{i=1}^{NC} n_i \mu_i = \sum_{i=1}^{NC} n_i \left( \sum_{j=1}^M A_{ji} \lambda_j \right) = \sum_{j=1}^M b_j \lambda_j \quad \#2.25$$

The relationship between the vector  $\boldsymbol{\lambda}$  (Lagrange multiplier) and the vector  $\mathbf{b}$  (element composition) is identical to the relationship between vector  $\mathbf{n}$  (molar composition) and the vector  $\boldsymbol{\mu}$  (chemical potential). Thus, a completely consistent thermodynamic representation of a phase at chemical equilibrium is obtained in terms of  $\mathbf{b}$  as the (element) composition vector and  $\boldsymbol{\lambda}$  as the corresponding element potential vector.

One convenient feature of the chemical model approach is that the equations are identical to the set of equations used to solve a nonreactive phase equilibrium problem. This implies that the same computational methods and tools can be used for reactive systems in the same way as for nonreactive systems. Furthermore, the element mole fraction can be defined similarly as component mole fractions for nonreactive systems. The total element amount in any phase  $\beta$  is given as follows:

$$b_T^\beta = \sum_{j=1}^M b_j^\beta \quad \#2.26$$

Then the element ‘mole’ fractions are given by:

$$W_j^\beta = \frac{b_j^\beta}{b_T^\beta} = \frac{b_j^\beta}{\sum_{k=1}^M b_k^\beta} \quad \#2.27$$

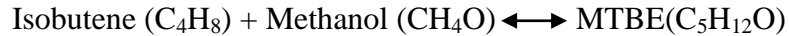
### 2.5.1.3 Element selection

It is clear that the choice of elements plays a significant role in the current formulation. As discussed previously, elements in a reaction mixture can be molecules, atoms or groups. Here two example are given to further illustrate how to choose elements for two reactive systems

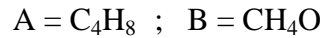
namely: (1) binary element reactive systems that can be represented by two elements, and (2) multi-element reactive systems that can be represented by more than two elements.

**Example 2.1: Binary element system**

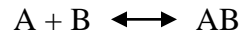
Consider the reversible reaction between Isobutene ( $C_4H_8$ ) and Methanol ( $CH_4O$ ) to produce MTBE( $C_5H_{12}O$ ). In terms of compounds, the reaction can be represented as follows:



Since there are 3 compounds and 1 reaction, the above reactive system can be represented in terms of 2 elements. Element definition is as follows:



Element based reaction is as follows:

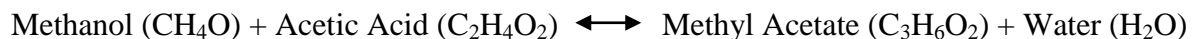


Consequently, the element matrix ( $A_{ji}$ ) is written as follows where the columns are elements and the rows are compounds.

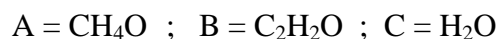
	$C_4H_8$	$CH_4O$	$C_5H_{12}O$
A	1	0	1
B	0	1	1

**Example 2.2: Multi-element systems**

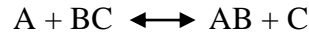
The reaction between Methanol ( $CH_4O$ ) and Acetic Acid ( $C_2H_4O_2$ ) to produce Methyl Acetate ( $C_3H_6O_2$ ) and Water ( $H_2O$ ) can be expressed in terms of compounds as follows:



Here, there are 4 compounds, and 1 reaction. Therefore, the reactive system can be expressed with 3 elements. Element definition is as follows:



Element based reaction is as follows:



Similarly, as Example 2.1, the formula matrix is constructed as follows:

	CH <sub>4</sub> O	C <sub>2</sub> H <sub>4</sub> O <sub>2</sub>	C <sub>3</sub> H <sub>6</sub> O <sub>2</sub>	H <sub>2</sub> O
A	1	0	1	0
B	0	1	1	0
C	0	1	0	1

It is to be emphasized again that the choice of elements is arbitrary as long as the elements satisfy the condition that,  $\text{rank}(A) = M$  where  $A$  is the formula matrix and  $M$  is the number of elements.

Jantharasuk et al., 2011 have shown that any multi-element system can be represented in terms of equivalent binary elements. The two key elements are noted as the light key element (LK) and the heavy key element (HK). One can assign any pair of elements (or compounds) as LK and HK, with the lower boiling compound in the pair being the LK and the heavier boiling compound in the pair being the HK. For all other non-key compounds, those that have lower boiling points than the light key, go with the LK, while those that have higher boiling points than the HK, go with the HK compound. This representation is similar in concept to the conventional method of distillation design for a non- reactive multicomponent system. Note that LK and HK are selected according to the rules of key element selection given by Jantharasuk et al., 2011. It is well-known that the sum of mole fractions is always equal to 1. Therefore, it is also the case when the mole fractions are given in terms of elements. Thus, the sum of mole fractions in a multi-element system is as follows:

$$W_{LK}^{\beta} + W_{HK}^{\beta} + W_{LNK}^{\beta} + W_{HNK}^{\beta} = 1 \quad \#2.28$$

From the above summation, one can represent the multi-element system in a new composition domain termed as ‘equivalent binary element composition’ as follows (Jantharasuk et al., 2011):

$$W_{eq}^{\beta} = W_{LK}^{\beta} + W_{HK}^{\beta} = 1 - \sum(W_{LNK}^{\beta} + W_{HNK}^{\beta}) \quad \#2.29$$

Where, the LK equivalent element composition is given as follows:

$$W_{LK,eq}^{\beta} = \frac{W_{LK}^{\beta}}{W_{LK}^{\beta} + W_{HK}^{\beta}} \quad \#2.30$$

And the element composition is given as follows (Pérez Cisneros et al., 1997):

$$W_j^{\beta} = \frac{\sum_{i=1}^{NC} A_{ji} x_i^{\beta}}{\sum_{i=1}^{NC} \sum_{j=1}^M A_{ji} x_i^{\beta}} \quad \#2.31$$

## 2.5.2 Driving force concept for reactive and nonreactive separations

The driving force approach is a method to design distillation operations (reactive or non-reactive) which was first proposed by Gani and Bek-Pedersen (Bek-Pedersen et al., 2000). Like the McCabe-Thiele method (McCabe & Thiele, 1925) it is based on the graphical representation of vapor-liquid data. However, in this approach, driving force ( $DF$ ), which is a function of vapor and liquid composition, is plotted against, liquid (or vapor) composition. It is defined as the difference between two co-existing phases (vapor and liquid) and can only represent binary interaction between compounds (for non-reactive systems) or elements (for reactive systems) in two coexisting phases. Furthermore, Sánchez Daza et al., 2003 extended the application of the driving force approach to design of reactive distillation columns. A generic driving force diagram is given in *Figure 2.2*.

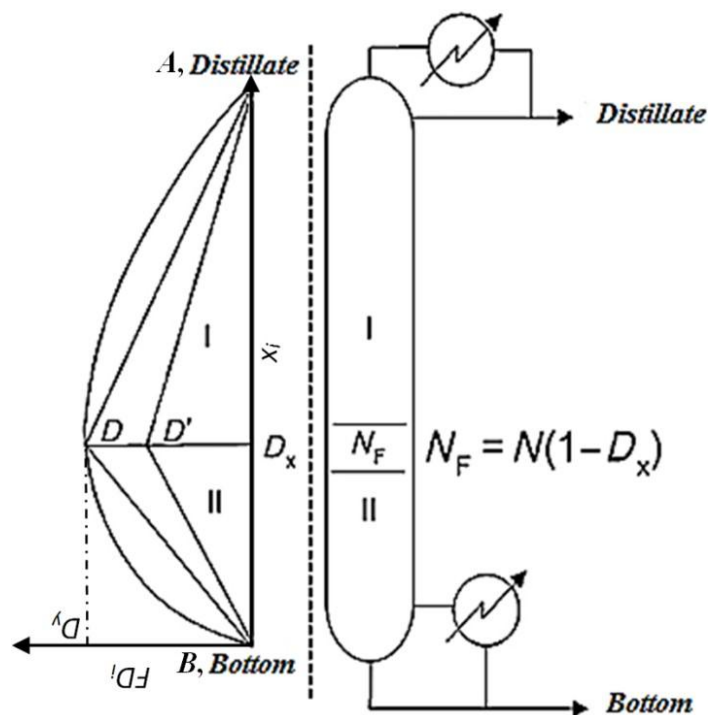


Figure 2.2 Driving force based design of distillation columns – on the left is the driving force diagram and on the right is the corresponding design of the reactive distillation column (adapted from Babi et al., 2014)

To date, driving force approach has been applied in numerous process synthesis (Babi et al., 2014; Anjan Kumar Tula et al., 2015), design (Bek-Pedersen & Gani, 2004; Bek-Pedersen et al., 2000; Sánchez Daza et al., 2003) and process control (Alvarado-Morales et al., 2010; S. S. Mansouri, Huusom, et al., 2016) applications. This approach is very well established as a powerful and simple method for design of separation operations, with or without reactions, that results in optimal/near optimal separation designs both in terms of energy consumption, control and operation when the process is designed at the maximum driving force.

The driving force is defined as the difference in composition of a specific element (equivalent element or compound) between two co-existing phases. Note however, although the driving-force diagram is plotted for a binary pair of elements or compounds, since all separation tasks are performed for specific binary pairs of compounds (or elements or equivalent elements), this

concept can be applied also to multi-compound mixtures as well. Also, the separation of a mixture of  $NC$  compounds would need  $NC - 1$  separation tasks and therefore,  $NC - 1$  binary pairs of driving forces are involved for each separation task. Note that the element-based reactive driving-force diagram fully considers the extent of reaction on an element basis. In this work, the driving force method is applied in the design of reactive distillation columns for chemical equilibrium or kinetically controlled reactions.

In the driving force approach, RD column design variables are determined in terms of two parameters. These are the location and the size of the maximum driving force,  $D_x$  and  $D_y$  respectively, as shown in *Figure 2.3*. The feed stage location ( $N_F$ ) and the minimum reflux ratio,  $RR_{\min}$  are determined from these two parameters for a given feed and product specification. A driving force diagram together with the distillation design parameters is given in *Figure 2.3*. The driving force,  $DF$ , has concrete thermodynamic basis. Its definition from a thermodynamic perspective along with its relation to chemical and physical equilibrium can be found in S. Mansouri, 2016.

### 2.5.3 Driving force based integrated design and control

The integrated process design and control is explained conceptually through the use of a process model represented by balance equations (mass, energy and momentum), constitutive equations (phenomena models usually as a function of intensive variables) and conditional equations (equilibrium, controller and defined relations). In a generic form, the model equations are given by:

$$D = f(x, y, u, d, \theta, t) \#2.32$$

Where  $D = \frac{dx}{dt}$  for dynamic model and  $D = 0$  for steady-state model.

Constitutive equations:

$$\theta = g_1(u, x, y) \#2.33$$

Conditional equations:

$$0 = g_2(u, x, y, d, \delta) \#2.34$$

In Equation 2.32-2.34,  $y^{(Ny \times 1)}$  contains output controlled variables;  $d^{Nd \times 1}$  contains feed stream disturbance variables;  $u^{Nu \times 1}$  contains design-manipulated variables;  $\theta$  is a vector of constitutive variables;  $x^{Nx \times 1}$  contains process-state variables and  $\delta^{N\delta \times 1}$  contains controller parameter.

From a driving force based process design point of view, for specified inputs of design variables ( $u$ ) and disturbances in feed stream variables ( $d$ ), values for process variables ( $x$ ) and output variables ( $y$ ) that satisfy a set of design specifications (process design objectives) are determined at the maximum driving force.

From a driving force based controller design point of view, for any changes in  $d$  and/or set point values in  $y$ , values of  $u$  that restores the process to its optimal designed condition are determined corresponding to the maximum driving force. In other words, to maintain  $x$  and  $y$  at their target values for a disturbance in  $d$ ,  $u$  needs to be manipulated. Alternatively, for fixed  $d$  and a change in set points for  $y$ ,  $u$  needs to be manipulated.

Therefore, the process design and control work with the same set of variables and the goal is to select and determine the values of these variables. The analysis of the model equations in Equation 2.32 reveals that the variables are classified in terms of  $x, y, u, d, \theta$  for integrated design and control problems. Equation 2.33 relates  $\theta$  to  $x, y$ . In other words, the solution for  $x$  and  $y$  is directly influenced by  $\theta$ . As discussed above  $\theta$  contains the constitutive variables such as driving force. Hence it is established that the driving force influences the process design, as well as the control performance. Note that, Algorithm 5 in Chapter 3 provides an analytic derivation of the relation between  $\theta$  to  $x, y$  while calculating controller sensitivity. Further discussion and a sample derivation of the terms of controller sensitivity can be found in S. Mansouri, 2016.



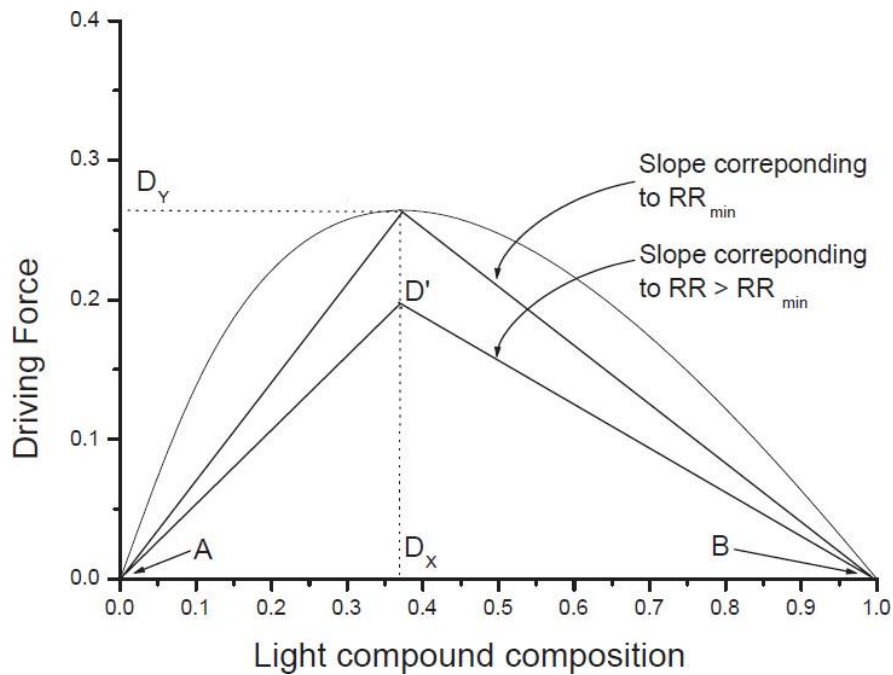


Figure 2.3 A Driving force diagram with the important distillation design parameters (Bek-Pedersen & Gani, 2004).

## 2.6 Review of Model Predictive Controller

Model predictive controller (MPC) is suitable for controlling multiple-input multiple-output (MIMO) process while satisfying inequality constraints on the input and output variables (constrained MIMO problems). If a reasonably accurate dynamic model of the process is available, model and current measurements can be used to predict future values of the outputs. Then the appropriate changes in the input variables can be calculated based on both predictions and measurements.

In the MPC implementation, a process model is used to predict the current values of the output variables. The residuals, the difference between the actual and predicted outputs, serve as the feedback signal to a prediction block. The predictions are used in two types of MPC calculations that are performed at each sampling instant: set-point calculations and control calculations. Inequality constraints on the input and output variables, such as upper and lower limits, can be included in either type of calculations. The set points for the control calculations, also called ‘targets’, are calculated from an optimization based on a steady state model of the process, traditionally, a linear model.

The MPC calculations are based on current measurements and predictions of the future values of the outputs. The objective of the MPC control calculations is to determine a sequence of control moves (manipulated input changes) so that the predicted response moves to the set point in an optimal manner. The actual output  $y$ , predicted output  $\hat{y}$ , and manipulated input  $u$  for a single input single output control is shown in *Figure 2.4*. At the current sampling instant, denoted by  $k$ , the MPC strategy calculates a set of  $M$  input values  $\{u(k+i-1), i = 1, 2, \dots, M\}$ . The set consists of the current input  $u(k)$  and  $M - 1$  future inputs (control moves). The input is held constant after the  $M$  control moves. The inputs are calculated so that a set of  $P$  predicted outputs  $\{\hat{y}(k+i), i = 1, 2, \dots, P\}$  reaches the set point in an optimal manner. The number of predictions  $P$  is referred to as prediction horizon while the number of control moves  $M$  is called the control horizon. Although a sequence of  $M$  control moves is calculated at each sampling instant, only the first move is implemented at each sampling instant. Then a new sequence is calculated based on the objective function, which generally is the minimization of residuals over  $P$  predicted outputs. Further discussion can be found in Seborg, 2010.

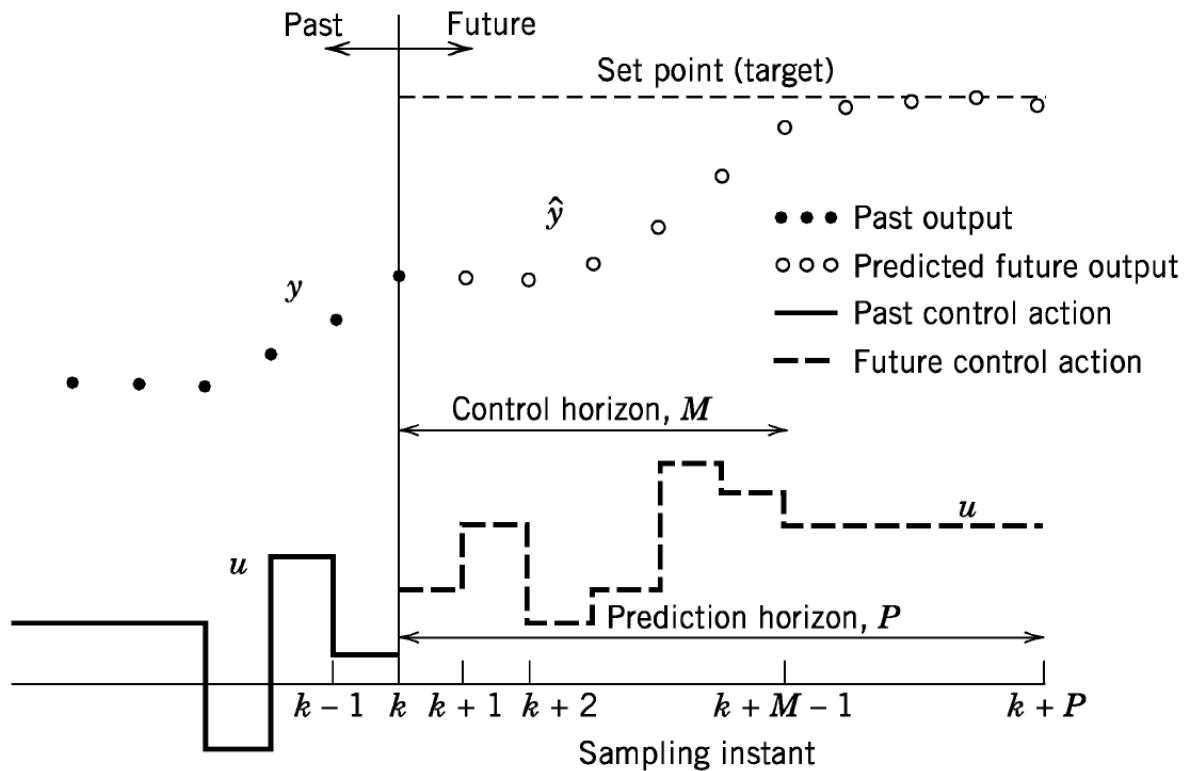


Figure 2.4 Basic concepts for model predictive control (Seborg, 2010).

## 2.7 Review of State-space models

If a dynamic model is expressed by one or more ordinary differential equations (ODEs), it can be expressed as state-space models, that provide a compact and useful representation of the underlying dynamic systems. In this work, linear state space models are obtained by linearizing the dynamic model around a steady-state consistent operating point. Therefore, this section will focus only on linear state-space models.

A continuous time state-space model can be expressed as follows:

$$\dot{x} = Ax + Bu \quad \#2.35$$

$$y = Cx + Du \quad \#2.36$$

In the above model formulation,  $x$  is the state vector,  $u$  is the input vector of manipulated variables, and  $y$  is the output vector of measured variables. The elements of  $x$  are referred to as state variables. The elements of  $y$  are typically a subset of  $x$ , namely, the state variables that are measured. In general,  $x, u, y$  are functions of time. The time derivative of  $x$  is denoted by  $\hat{x} = \frac{dx}{dt}$ , is also a vector. Matrices  $A, B, C, D$  are constant matrices. For a plant with  $Nx$  states,  $Ny$  outputs, and  $Nu$  inputs, the state space matrices have the following dimensions:  $A^{Nx \times Nx}, B^{Nx \times Nu}, C^{Ny \times Nx}, D^{Ny \times Nu}$ . If there is no disturbance introduced through the manipulated variables,  $D$  matrix is zero. A more detailed discussion along with some examples can be found in Seborg, 2010.

**CHAPTER THREE**

**DESIGN-CONTROL FRAMEWORK AND**

**ALGORITHMS**

### 3 DESIGN-CONTROL FRAMEWORK AND ALGORITHMS

This chapter describes the framework that is used in this thesis work. The framework systematically integrates the driving force-based method for design with the established control methods of PI(D) and MPC.

#### 3.1 Overview of Integrated process design and control framework

The framework for integrated design and control of RD processes based on the driving force concept is illustrated in *Figure 3.1*. This framework consists of three main steps as follows:

1. Data collection and problem formulation, consisting of sub steps:
  - 1a. Objective function definition.
  - 1b. Reactive system representation in terms of binary key elements.
  - 1c. Key elements selection in the case of multi-element systems.
2. Integrated design-control, consisting of sub steps:
  - 2a. RD process design issues.
  - 2b. Optimal design-control issues.
3. Verification, consisting of sub steps:
  - 3a. Controller structure verification.
  - 3b. Dynamic open loop and closed loop simulation and analysis.
  - 3c. Final selection.

The integration of process design and control objectives is achieved in step 2 through operation at the maximum driving force, if feasible. The verification in step 3 is carried out through simulations in open-loop and closed-loop to evaluate the performance of the designed reactive distillation process with and without the controllers. The integration of design and control is achieved through a set of variables that have dual roles, that is, each of these variables has a role in design and a role in control as given in *Table 3.1*. This framework has been implemented in a

new version of ProCADC (Anjan K. Tula et al., 2020), an integrated software tool for process design and control, which also provides a link to the needed property estimation tool as well as links to external tools (ASPEN PLUS, MATLAB). An overview of this toolbox is presented in Chapter 5.

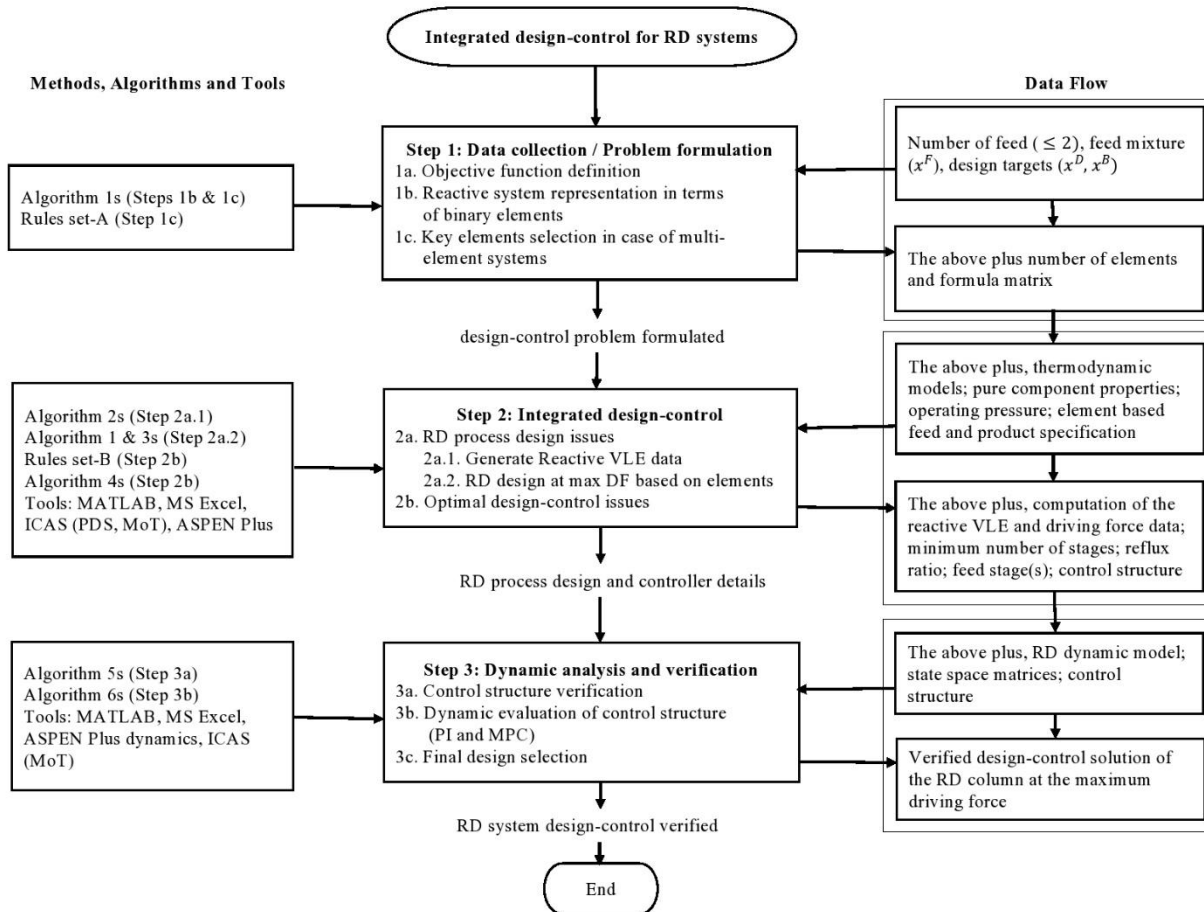


Figure 3.1 Integrated RD process design-control framework.

Table 3.1 Common variables for design and control.

Variables	Role in design	Role in control
Product composition ( $x^D, x^B$ )	Design specification (constraint)-provides the setpoint for the controlled variable	Controlled variable- the controller maintains the RD column at the set point
Reflux ratio ( $RR$ )	Design variable (calculated as a function of the available driving force diagram) – provides the reference value for the actuator	Manipulated variable- adjusted to control top product composition
Reboiler duty ( $Q_R$ )	Design variable (used to calculate the carbon footprint of the process; function of the available driving force) – provides reference for actuator	Manipulated variable- adjusted to control bottom product purity
Light key / equivalent light key element composition ( $D_x$ )	There exists a unique light key / equivalent light key element composition for which the driving force is maximum. At this point, the key design variables (reflux ratio/rate and/or reboil ratio) are calculated. This is also a design variable since it can be used to calculate the feed stage using the formula $N_F = N(1 - D_x)$	At this point, the sensitivity of controlled variables with respect to disturbance, and the sensitivity of manipulated variables to controlled variables are calculated analytically to show the optimal controllability (Algorithm 5)



## 3.2 Description of Integrated design-control framework

In this section, the steps of the framework presented in section 3.1 and in *Figure 3.1*, along with the algorithms to perform each task will be described.

### 3.2.1 Step 1: Data collection and Problem formulation

This step starts after a decision to use a reactive distillation column has been made. Data/information on raw materials, products, catalysts, reaction conversions, and feed conditions (temperature, pressure, and composition) are collected, and design targets and product specifications are given. An objective function, which could be maximized (or minimized) from both the design and control perspectives, is defined. RD system representation based on elements are also done in this step.

#### 3.2.1.1 Step 1a. Design targets and Objective function definition

The objective function can be defined as a set of process design and control performance metrics which are to be maximized (or minimized). or in the form of a weighted multi objective function as follows (S. S. Mansouri, Sales-Cruz, et al., 2016a):

$$f_{obj} = \min \left( w_1 P_1 + w_2 P_2 + w_3 \left( \frac{1}{P_3} \right) \right) \#3.1$$

Here,  $P_1$  represents costs associated to the reboiler and condenser duties.  $P_2$  is the sensitivity of the controlled variables ( $y$ ) to disturbances ( $d$ ) in the feed ( $dy/dd$ ),  $P_3$  is the sensitivity of manipulated variables  $u$  with respect to controlled variables  $y$  ( $dy/du$ ). Note that in Equation 3.1  $w_1, w_2, w_3$  are weight factors.

### 3.2.1.2 Step 1b. Reactive system representation

In this step, the number and identity of elements needed to represent the reactive system is determined through the algorithm of Pérez Cisneros et al., 1997. A revised version of this algorithm is given in Algorithm 1.

If a binary element system is encountered, go to step 2. Otherwise, a multi-element system (more than two elements) is identified, in that case go to Step 1c to identify the key pair of elements.

### 3.2.1.3 Step 1c. Identify the key elements

The equivalent binary elements, that is the light key and heavy key elements, are selected according to the rules of key element selection for a multi-element system (Jantharasuk et al., 2011), which are given as a sub algorithm in Algorithm 1.

#### **Algorithm 1: Identification of number of elements**

*Objective: To identify the number of elements present in the system*

*Step (i): Calculate the number of elements (NE) using the following formula:*

$$NE = NC - NR \#3.2$$

where  $NC$  is the number of compounds, and  $NR$ , is the number of reactions.

*Step (ii): If the number of elements (NE) is equal to two go to Step (iii), otherwise, for more than two elements, go to Rules set-A to select reactive key binary pairs – then go to Step (iii).*

#### **Rules set-A:**

**Rule I:** The mixture on component basis is arbitrarily considered as attaining the expected reaction conversion. The corresponding compositions are later applied with the ‘Rule of key element selection’ in the next steps.

**Rule II:** The element that is contained by the remaining lightest component should not be specified as heavy key and/or heavy non-key element.

**Rule III:** The element that is contained by the remaining heaviest component should not be specified as light key and/or light non-key element.

**Rule IV:** The key element should be present along the whole column (should be contained in both distillate and bottom products).

*Step (iii):* Write the formula matrix ( $A_e$ ) from the formula coefficients  $a_{ji}$  with the constituent elements ( $j = 1, 2, \dots, NE$ ) as rows and the species ( $i = 1, 2, \dots, NC$ ) as columns.

**End of Algorithm 1**

### **3.2.2 Step 2: Integrated design-control**

The objective of this step is to determine the process design and control structure. In Step 2a design parameters are obtained by applying the driving force approach (Bek-Pedersen & Gani, 2004). In Step 2b, the associated controller design (pairing of controlled and manipulated variables) for the RD system are determined. Steady state simulation of the designed RD systems is carried out to verify that the design targets defined in Step 1 are matched. The steady state values of controlled variables are selected as set points for the dynamic (open-loop and closed-loop) analysis.

#### **3.2.2.1 Step 2a.1: Generate reactive vapor-liquid equilibrium data**

The reactive vapor-liquid equilibrium (VLE) data is either obtained from experiments or computation of reactive bubble points and/or dew points. In this work, the reactive bubble point data are calculated using the algorithm proposed by Sánchez Daza et al., 2003, available through ProCADC Algorithm 2 presents the algorithm to generate binary and equivalent binary element reactive phase diagram. Note that in this algorithm, the choice of discretization may affect the accuracy of the results. A discretization interval 0.05 is used in this work to perform the calculation. Since the calculation of the reactive VLE data is not computationally expensive,

one can decrease the discretization interval (in absence of miscibility gaps) to obtain a smoother curve.

**Algorithm 2: Construction of reactive phase VLE diagram for binary/multi element systems**

*Objective: To calculate the vapor-liquid equilibrium data at given temperature or pressure and element feed composition*

*Step (i):* Give element composition in the feed ( $W_j^l, j = 1, 2, \dots, NE$ ) and pressure ( $P$ ).

*Step (ii):* Assume a temperature ( $T$ ) between bubble point and dew point.

*Step (iii):* Solve for component moles  $n_i^l$  in the liquid phase (chemical equilibrium).

$$W_j^l \sum_{k=1}^{NE} \sum_{i=1}^{NC} A_{ki} n_i^l - \sum_{i=1}^{NC} A_{ji} n_i^l = 0, \quad \forall j \in \{1, 2, \dots, NE\} \quad \#3.3$$

$$\sum_{i=1}^{NC} Z_{ik} \mu_i^l = 0, \quad \forall k \in \{1, 2, \dots, NR\} \quad \#3.4$$

where  $Z_{ik}$  is the stoichiometric coefficient of the compounds in the reaction mixture.

*Step (iv):* Compute vapor mole fractions  $y_i$  at equilibrium implicitly.

$$y_i \phi_i^v = x_i \phi_i^l \quad \forall i \in \{1, 2, \dots, NC\} \quad \#3.5$$

Note that activity coefficient models can be also used for fugacity balances.

*Step (v):* Calculate a correction for temperature using the check equation ( $\sum_{i=1}^{NC} y_i - 1 = 0$ ). If not converged, return to *Step (iii)*, else, go to *Step (vi)*

*Step (vi):* Compute element mole fractions for the vapor phase (Pérez Cisneros et al., 1997).

$$W_j^v = \frac{\sum_{i=1}^{NC} A_{ji} y_i}{\sum_{k=1}^{NE} \sum_{i=1}^{NC} A_{ki} y_i} \quad \#3.6$$

The element composition in the liquid phase is calculated using the below equation.

$$W_j^l = \frac{\sum_{i=1}^{NC} A_{ji} x_i}{\sum_{k=1}^{NE} \sum_{i=1}^{NC} A_{ki} y_i} \#3.7$$

It should be noted that with the element mole fractions it is not possible to obtain negative values for composition variables.

*Step (vii):* If more than two elements are encountered, calculate the equivalent binary composition for the entire composition domain using the key elements (LK and HK) identified in Algorithm 1. The light key equivalent element composition is given as follows:

$$W_{LK,eq}^l = \frac{W_{LK}^l}{W_{LK}^l + W_{HK}^l} \#3.8$$

$$W_{LK,eq}^v = \frac{W_{LK}^v}{W_{LK}^v + W_{HK}^v} \#3.9$$

*Step (viii):* Repeat *Steps (i)-(vi)* for new values of  $W_j^l$  to obtain the reactive phase diagram for the entire composition domain (0-1). For systems without miscibility gaps, a constant discretization step of 0.05 in the  $x$ -axis composition is used and recommended. Note that this phase diagram needs to be generated only once and it is not computationally expensive.

**End of Algorithm 2**

### 3.2.2.2 Step 2a.2: Reactive distillation design

The objective of this step is to find the reactive distillation column design (i.e. number of stages, reflux ratio and feed location) based on binary or equivalent binary element at the maximum driving force. The steps required to perform this task are given in the Algorithm 3 (S. Mansouri, 2016) for a single feed reactive distillation column; and Algorithm 4 for a double feed reactive distillation column. After application of Algorithm 3 or 4, perform steady-state simulation of the process to verify that the design objectives are satisfied.

The reactive driving-force based on the binary elements (or binary equivalent elements) is calculated using Equation 3.10 as described by Sánchez Daza et al., 2003. In case of equivalent

binary elements, light key equivalent element compositions are used to calculate the driving force.

$$DF = W_i^v - W_i^l = \frac{W_i^l \alpha_{ij}}{1 + W_i^l (\alpha_{ij} - 1)} - W_i^l \quad \#3.10$$

As part of Algorithm 3, the reactive McCabe-Thiele algorithm is given as a sub-algorithm, which is to be applied to calculate the minimum number of stages to obtain the desired product specifications (targets) defined in step 1. The calculation is based on the well-known McCabe and Thiele method (McCabe & Thiele, 1925) for non-reactive distillation design. Sánchez Daza et al., 2003 extended this method to include reactive binary distillation columns, which can also be used for equivalent binary element columns.

For a double feed RD system with feed flowrates  $H$  and  $K$ , Algorithm 4 is proposed to design the column at the maximum driving force. Note that this algorithm is adapted from the original McCabe-Thiele method (McCabe & Thiele, 1925) for design of distillation columns with two feeds.

**Algorithm 3: Reactive distillation design using driving force approach for Single feed reactive distillation column**

*Objective: To find the reactive distillation column design (number of stages, reflux ratio, feed location) at the maximum driving force using the specified design targets*

*Step (i):* Retrieve vapor-liquid element data (binary or equivalent binary) from Algorithm 2.

*Step (ii):* Calculate the corresponding driving force for the entire composition domain using Equation 3.10, then plot  $|DF|$  vs  $W_i^l$  based on the light key element.

*Step (iii):* Identify the area of operation of the driving force diagram, which is feed, distillate and bottom compositions based on the light key element (or the light key equivalent element) using the design targets set in Step 1.

*Step (iv):* Determine the reflux ratio and reboil ratio. To do this, determine the slopes of lines which are formed by the coordinates (bottoms element composition, maximum driving force),

(distillate element composition, maximum driving force). Determine the corresponding minimum reflux ratio ( $RR_{\min}$ ) and reboil ratio ( $RB_{\min}$ ). Next, Determine the real reflux ratio ( $RR$ ) and reboil ratio ( $RB$ ) from  $RR = 1.2(RR_{\min})$  and  $RB = 1.2(RB_{\min})$ .

*Step (v):* If the number of stages,  $N$ , are given go to *Step (vi)*, else, use reactive McCabe-Thiele algorithm to obtain minimum number of stages as follows:

*Sub-Algorithm for generating reactive McCabe Thiele diagram*

*Sub-Step (i):* Retrieve information from *Step 2a.1* and draw reactive equilibrium curve ( $W_A^v - W_A^l$  diagram – for the light element).

*Sub-Step (ii):* Draw the angle bi-sector line ( $45^\circ$  line), locate  $W_{A,D}^l$  (composition of element  $A$  in distillate),  $W_{A,B}^l$  (composition of product  $AB$  in the bottom) and  $W_A^F$  (composition of element  $A$  in the feed) on the  $45^\circ$  line.

*Sub-Step (iii):* Use the reflux ratio and reboil ratio obtained at the maximum driving force (Algorithm 3, *Step (iv)*) to calculate the slopes of the operating lines.

*Sub-Step (iv):* Draw the rectifying and stripping operating lines from  $W_{A,D}^l$  and  $W_{A,B}^l$  on the  $45^\circ$  line. Find the minimum number of stages by drawing the steps.

*End of Sub-Algorithm*

*Step (vi):* Identify the feed stage location,  $N_F$ , from  $N_F = N(1 - D_x)$ .

*Step (vii):* Check the design targets in terms of low key and heavy key elements in the feed, distillate and bottom as well as the location of maximum driving force on the  $x$  axis ( $D_x$ ) with the following additional conditions (Bek-Pedersen et al., 2000), (Bek-Pedersen & Gani, 2004). If one or more conditions apply, use the guidelines to further retrofit the design.

**If** condition 1a is satisfied, then relocate NF between 5% and 10% up in the column.

**Else**, if condition 1b is satisfied, then relocate NF between 5% and 10% down in the column.

**If** condition 2a is satisfied then relocate NF 10% down.

**Else**, if condition 2b is satisfied, then relocate NF 5% down.

**Else**, if condition 2c is satisfied, then relocate NF 5% up.

**Else**, if condition 2d is satisfied, then relocate NF 10% up.

Condition 1	
a)	$W_{HK,z} < 0.8$ and $D_x < 0.7$
b)	$W_{HK,z} < 0.8$ and $D_x > 0.3$
Condition 2	
a)	$\frac{1-W_{LK,D}}{1-W_{HK,B}} < 0.01$ and $D_x < 0.7$
b)	$\frac{1-W_{LK,D}}{1-W_{HK,B}} < 0.1$ and $D_x < 0.7$
c)	$\frac{1-W_{HK,B}}{1-W_{LK,D}} < 0.1$ and $D_x > 0.3$
d)	$\frac{1-W_{HK,B}}{1-W_{LK,D}} < 0.01$ and $D_x > 0.3$

*Step (viii):* Perform steady-state simulation to confirm that the design targets are satisfied. These steady-state values are the nominal values for control.

### End of Algorithm 3

### Algorithm 4: Reactive distillation design using driving force approach for two feed reactive distillation column

The objective is to find the reactive distillation column design (number of stages, reflux ratio, feed location) with two feeds at the maximum driving force using the specified design targets. This algorithm is an adopted version, proposed earlier by S. Mansouri, 2016.

*Step (i):* Retrieve vapor-liquid element data (for the binary or equivalent binary system using Algorithm 2.

*Step (ii):* Calculate the driving forces for the entire composition domain using Equation 3.10, then plot  $|DF|$  vs  $W_i^l$  based on the light key element (or the equivalent light key element).

*Step (iii):* Identify the area of operation of the driving force diagram (reactive zone information), i.e., feed compositions (feed one and two), distillate ( $W^D$ ) and bottom ( $W^B$ ) compositions based on the light key element (or the equivalent light key element) using design targets set in Step 1.

In the text above,  $W_k$  and  $W_h$  are the compositions of the feeds;  $W_g$  is the composition if the mixture with the two feeds were mixed such that it corresponds to the maximum driving force on



the  $x$ -axis of the driving force diagram ( $D_x$ ). Note also, if  $W_h > W_k$ , then the  $H$  feed is indeed placed higher in the RD column. If the area of operation is not between 0 and 1 on the  $x$ -axis, then re-scale the  $x$ -axis between 0-1.

*Step (iv):* Determine the reflux ratio and boil-up ratio similarly as Algorithm 3s *Step (iv)*.

*Step (v):* Construct the XY diagram using the vapor liquid (binary or equivalent binary) element data from Algorithm 2.

*Step (vi):* Draw the angle bi-section line ( $45^\circ$  line), and locate  $W^D, W^B, W_h, W_k$ , and  $W_g$  on the  $x$ -axis of the  $PTXY$  diagram.

*Step (vii):* The rectifying and stripping lines from *Step (iv)* are exactly the same as in the case of a single feed (see Algorithm 3), i.e., they start from the product compositions. The enrichment line for the middle of the column is found by joining the points where enrichment lines for the rectifying and stripping sections intersect the lines  $x = W_h$  and  $x = W_k$ .

*Step (viii):* Find the minimum number of reactive stages by drawing the steps.

*Step (ix):* Perform a steady-state simulation, and if further purification is required by the problem formulation, then add non-reactive stages one-at-a-time to the top and bottom of the reactive section until the desired purification of the products is achieved.

#### **End Algorithm 4**

#### **3.2.2.3 Step 2b: Optimal design-control issues**

In this step, the control structure is selected with respect to two main criteria (sensitivity of controlled variables with respect to disturbances in the feed and sensitivity of manipulated variables to controlled variables), and verified at the maximum driving force analytically using Algorithm 5. Note that the detailed mathematical derivations for binary and multi elements systems are reported in S. S. Mansouri et al., 2016b and S. S. Mansouri, Huusom, et al., 2016. For multi-element reactive systems, the only difference is that the derivations are based on equivalent binary elements instead of binary elements.

### Algorithm 5: Optimal design-control structure determination

*Objective:* The best controller structure at the maximum driving force is analytically identified by applying this algorithm.

*Criteria: Sensitivity of  $(dy/dd)$ :* If the sensitivity of controlled variables,  $y$ , with respect to disturbances in the feed,  $d$  is low it means that the process is less sensitive to disturbances and therefore, it is more robust in maintaining the controlled variables at their set-point in the presence of disturbances.

*Sensitivity of  $(du/dy)$ :* If the sensitivity of manipulated variables to controlled variables is high it will determine the best controller pairing and consequently controller action.

*Step (i):* Selection of controlled variables

In this algorithm, the primary controlled variable is  $W_i^{l,max}$  ( $D_x$ ), which is the  $x$ -axis value corresponding to the maximum driving force ( $D_y$ ). The secondary controlled variables are the product composition (design targets), which are measurable variables and they are the distillate and bottom product purities of the light key element,  $W_A^D$  and  $W_A^B$  (or  $W_{LK,eq}^D$  and  $W_{LK,eq}^B$  for a multi-element system), respectively. The reason behind this selection is that conceptual variables (that is driving force,  $DF$ ) cannot be measured directly.

*Step (ii):* Sensitivity of controlled variables to disturbances

In order to calculate the sensitivity, apply a chain rule to relate the derivatives of primary controlled variable to the derivatives of the secondary controlled variables. In order to apply the chain rule, use the following key concepts:

The desired element product at the top and the bottom is  $W_A^D$  and  $W_A^B$  (or  $W_{LK,eq}^D$  and  $W_{LK,eq}^B$  for a multi-element system), the distillate and bottom composition of light key element (element  $A$ ), respectively. At the maximum point of the driving force diagram,  $W_A^D$  and  $W_A^B$  (controlled variables) are the least sensitive to the imposed disturbances in the feed. The design variables vector is  $y = [W_A^D \ W_A^B]$ ,  $x = W_A^l$  and  $\theta = DF$  is selected on the  $y$ -axis of the driving force diagram. The disturbance vector is,  $= [F_f \ z_{wAf}]$ . (feed flowrate and feed composition of element  $A$ ). Therefore, the chain rule is expressed as follows:

$$\frac{dy}{dd} = \begin{bmatrix} \frac{dW_A^D}{dF_f} & \frac{dW_A^D}{dz_{wAf}} \\ \frac{dW_A^B}{dF_f} & \frac{dW_A^B}{dz_{wAf}} \end{bmatrix} = \begin{bmatrix} \left(\frac{dW_A^D}{dDF}\right) \left(\frac{dDF}{dW_A^l}\right) \left(\frac{dW_A^l}{dF_f}\right) & \left(\frac{dW_A^D}{dDF}\right) \left(\frac{dDF}{dW_A^l}\right) \left(\frac{dW_A^l}{dz_{wAf}}\right) \\ \left(\frac{dW_A^B}{dDF}\right) \left(\frac{dDF}{dW_A^l}\right) \left(\frac{dW_A^l}{dF_f}\right) & \left(\frac{dW_A^B}{dDF}\right) \left(\frac{dDF}{dW_A^l}\right) \left(\frac{dW_A^l}{dz_{wAf}}\right) \end{bmatrix} \quad \#3.11$$

Since the driving force diagram is always concave, therefore, the value of  $\frac{dDF}{dW_A^l} = 0$  at the maximum driving force. Therefore, the least sensitivity of controlled variables to disturbances is achieved at the maximum driving force and is obtained as follows:

$$\frac{dy}{dd} = \begin{bmatrix} \frac{dW_A^D}{dF_f} & \frac{dW_A^D}{dz_{wAf}} \\ \frac{dW_A^B}{dF_f} & \frac{dW_A^B}{dz_{wAf}} \end{bmatrix} = \begin{bmatrix} 0 & 0 \\ 0 & 0 \end{bmatrix} \quad \#3.12$$

*Step (iii): Selection of the controller structure*

The potential manipulated variables are,  $u = [L V]$ , which are represented by reflux ratio ( $RR$ ) and boilup ratio ( $RB$ ). Hence, the sensitivity of the secondary controlled variables to the manipulated variables can be expressed as follows:

$$\frac{dy}{du} = \begin{bmatrix} \frac{dW_A^D}{dRR} & \frac{dW_A^D}{dRB} \\ \frac{dW_A^B}{dRR} & \frac{dW_A^B}{dRB} \end{bmatrix} = \begin{bmatrix} DF + (1 + RR) \left(\frac{dDF}{dW_A^l}\right) \left(\frac{dW_A^l}{dRR}\right) + \frac{dW_A^l}{dRR} & (RR + 1) \left(\frac{dDF}{dW_A^l}\right) \left(\frac{dW_A^l}{dRB}\right) + \frac{dW_A^l}{dRB} \\ \frac{dW_A^l}{dRR} - \left(\frac{dDF}{dW_A^l}\right) \left(\frac{dW_A^l}{dRR}\right)_{RB} & \frac{dW_A^l}{dRB} - DF \end{bmatrix} \quad \#3.13$$

Assuming that  $\frac{dW_A^l}{dRR} = \frac{dW_A^l}{dRB} = 0$ , the following is obtained (this corresponds to a system with no or little cross interactions between  $y$  and  $u$  since changes in  $u$  cannot propagate through column). The best controller structure is easily determined by looking at the value of  $dy/du$ . It is noted from the following that since the values of  $\frac{dW_A^D}{dRR}$  and  $\frac{dW_A^B}{dRB}$  are bigger, controlling  $W_A^D$  by manipulating  $RR$  and controlling  $W_A^B$  by manipulating  $RB$  will require less control action. Therefore, for the optimal design obtained at the maximum driving force, the control structure is always as follows, and it is verified by analytical analysis that it is the optimal-design control structure.

$$\frac{dy}{du} = \begin{bmatrix} \frac{dW_A^D}{dRR} & \frac{dW_A^D}{dRB} \\ \frac{dW_A^B}{dRR} & \frac{dW_A^B}{dRB} \end{bmatrix} = \begin{bmatrix} DF & 0 \\ 0 & -DF \end{bmatrix} \#3.14$$

Or the following for a multi-element system:

$$\frac{dy}{du} = \begin{bmatrix} \frac{dW_{LK,eq}^D}{dRR} & \frac{dW_{LK,eq}^D}{dRB} \\ \frac{dW_{LK,eq}^B}{dRR} & \frac{dW_{LK,eq}^B}{dRB} \end{bmatrix} = \begin{bmatrix} DF_{LK,eq} & 0 \\ 0 & -DF_{LK,eq} \end{bmatrix} \#3.15$$

### End of Algorithm 5

#### 3.2.3 Step 3: Verification through simulation and analysis

The objective of this step is to verify the design-control solution (obtained at the maximum driving force) through steady state and dynamic simulation and analysis. *Figure 3.2* shows the process design – control block diagram employed for verification steps.

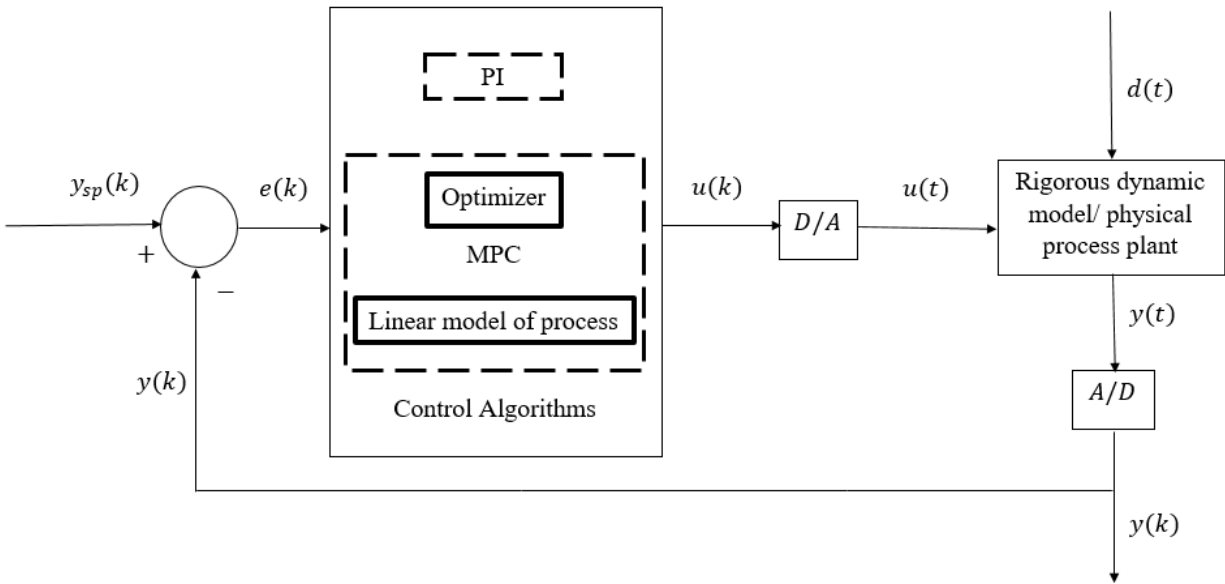


Figure 3.2 Process-controller block diagram highlighting PI and MPC controller.

### 3.2.3.1 Step 3a: Controller structure verification

The appropriateness of the controller structure obtained at the maximum binary element or equivalent binary element driving force, is verified by applying Algorithm 6. The control structure is verified by inspecting independently, the Relative Gain Array (RGA) values and the Niederlinski Index ( $N_I$ ) values.

#### Algorithm 6: Control structure verification

*Step (i):* Obtain the linear representation of the optimal design control process at the maximum driving force; either by using the transfer functions from step test between each manipulated ( $u$ ) and control variable ( $y$ ) or linearizing the model and obtaining state-space matrices ( $A, B, C, D$ ).

*Step (ii):* Construct the steady-state gain matrix ( $G$ ) from the transfer functions.

*Step (iii):* Verify that the gain matrix  $G$  has non-zero determinant.

*Step (iv):* Calculate the relative gain matrix (RGA) using the following equation(Bristol, 1966):

$$RGA(G) = G \otimes (G^{-1})^T \#3.16$$

*Step (v):* Verify that pairings such that the rearranged system, with the selected pairings along the diagonal, has an RGA matrix element close to unity, and off-diagonal elements close to zero (for a  $2 \times 2$  system); therefore, control structure at the maximum driving force has the least interactions with each other for the pairing given in Algorithm 5.

*Step (vi):* Calculate Niederlinski Index (Chiu & Arkun, 1991).(Corriou, 2004) as follows:

$$N_I = \frac{\det|G|}{\prod_i G_{ii}} \#3.17$$

If this index is negative the system is unstable irrespective of the tuning of the controllers. It is a sufficient condition, except for multivariable systems of dimensions lower than or equal to 2, where it is also necessary.

## **End of Algorithm 6**

### **3.2.3.2 Step 3b: Dynamic closed-loop analysis**

The objective of this step is to apply Algorithm 7 to evaluate the close-loop performance of the control structure identified and verified in Step 2b and Step 3a, respectively, in the presence of disturbances. The disturbance is introduced through feed (and composition).

#### **Algorithm 7: Control structure evaluation**

*Step (i):* Select a disturbance scenario in the feed.

*Step (ii):* Perform open-loop simulation in the presence of the disturbance to observe to what extent the control variables deviate from the set-point.

*Step (iii):* Select an appropriate control algorithm at supervisory (MPC) or regulatory (PI) level.

*Step (iv):* Retrieve nominal steady-state values for the control variables that are obtained after performing steady state simulation with the design parameters from Step 2a.2.

*Step (v):* Select appropriate prediction and control horizon for MPC and tuning method for PI (IMC rules(Rivera et al., 1986) or SIMC rules (Skogestad, 2003) to obtain tuned controller parameters.

*Step (vi):* Perform closed-loop simulation and verify that the disturbance is rejected and the system is recovered to its original set-points.

## **End of Algorithm 7**

### **3.2.3.3 Step 3c: Final selection**

In this step each parameter (scalar/vector) of the performance objective function is calculated to evaluate the performance of the steady-state and/or dynamic behavior of the process.

# **CHAPTER FOUR**

## **APPLICATION EXAMPLES**

## 4 APPLICATION EXAMPLES

This chapter describes the application of the integrated design-control framework which was introduced in Chapter 3. For each case study the steady state design and dynamic control performance under both PI and MPC controller are quantified through a multi parametric objective function. The summarized results and discussions demonstrate that, the RD systems, if designed at the maximum driving force, exhibit superior close loop control performance irrespective of the choice of the controllers.

### 4.1 Case Studies

The integrated design-control framework is tested through the following six case studies:

1. Case study 1: Methyl-tert-Butyl-Ether (MTBE) production without inert.
2. Case study 2: Methyl-tert-Butyl-Ether (MTBE) production in the presence of inert.
3. Case study 3: Methyl Acetate production.
4. Case study 4: Toluene disproportionation.
5. Case study 5: Ethyl-tert-Butyl Ether (ETBE) production without inert.
6. Case study 6: Tert-Amyl-Methyl-Ether (TAME) production.

Case study 1 and 2 covers the single feed binary and multi-element system. Case study 3 consists of double feed multi element system. Case study 4 is chosen to demonstrate that the framework is applicable for vapor phase reactive systems as well. Note that the other 5 case studies involve liquid phase catalytic reactions. Case study 5 validates the consistency of the framework by attaining qualitatively similar result as Case study 1. It is expected since, MTBE and ETBE have similar thermodynamic properties. Finally, Case study 6 proposes a novel process design for TAME synthesis. It replaces the conventional flowsheet as discussed by Luyben, 2013 which contains prereactor and multiple post processing units by a single intensified RD column. The results show that the newly attained flowsheet not only achieves high purity TAME, but also is dynamically controllable with minimal process upset.

As chemical reaction for each case study takes place very fast, it is reasonable to assume that the equilibrium is achieved. In order to verify the integrated design and control, a multi-objective



performance function involving a set of metrics to evaluate control performance is considered, as given below:

$$f_{obj} = \text{minimize } J_1, J_2, J_3, J_4, J_5, J_6 \quad 4.1$$

where,  $J_1$  = energy consumption associated with the process,  $J_2$  = integral absolute error (IAE),  $J_3$  = total variation of the manipulated variables,  $J_4$  = relative gain array (RGA),  $J_5$  = Niederlinski Index ( $N_I$ ), and  $J_6$  = total CO<sub>2</sub> footprint per kg feed.

Note that this is a multi-objective performance function, which takes into account both design objectives and control objectives. The values of steady state metrics,  $J_1$  and  $J_6$ , measure energy-efficiency and environment friendliness of the process.  $J_2$  and  $J_3$  are controller performance metrics which are defined below:

$$J_2 = IAE = \int_0^{\infty} |y - y_{sp}| dt \quad 4.2$$

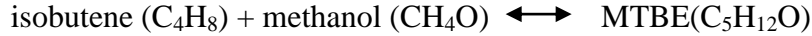
$$J_3 = TV = \sum_{i=1}^{\infty} |u_{i+1} - u_i| \quad 4.3$$

The diagonal values of  $J_4$  indicate the degree of interaction between control loops.  $J_5$  indicates the system stability. Note that for a  $2 \times 2$  system,  $N_I$  and RGA are clearly related because  $N_I = 1/(1,1)_{RGA}$ . Hence, the condition is that both have to be positive. Both metrics are included here to check the appropriateness of the control structure. The aim is not to get a weighted scalar value of this function, but to evaluate each of the metrics separately and verify that  $J_1, J_2, J_3$  and  $J_6$  are the lowest, while  $J_4$  and  $J_5$  satisfy the controllability criteria for a design at the maximum driving.

## 4.2 Case study 1: MTBE production without inert

### 4.2.1 Step 1: Data collection and problem formulation

The reaction of methanol with isobutene yields MTBE. This is a reversible and exothermic reaction. The reaction takes place in liquid phase (Al-Jarallah et al., 1988) at 25°C. It can be expressed as follows:



The pure component properties (critical properties, molecular weight, boiling and melting points) are retrieved from ICAS Database (Nielsen et al., 2001). The feed conditions for the production of MTBE are taken from Sánchez Daza et al., 2003 and they are summarized in *Table 4.1*.

Table 4.1 Design targets and product specifications for MTBE system without inert.

Component	Molar composition		
	Feed	Distillate	Bottom
Isobutene (C <sub>4</sub> H <sub>8</sub> )	0.7	0.98	-
Methanol (CH <sub>4</sub> O)	0.3	-	-
MTBE (C <sub>5</sub> H <sub>12</sub> O)	0.0	-	> 0.8
Feed flowrate: 100 kmol/h; Feed temperature and Pressure: 300K and 101.3 kPa			

A summary of the key information for all six case studies is given in Table 4.7. The choice of elements and corresponding element matrix are given in *Table 4.8*.

## 4.2.2 Step 2: Integrated Design-Control

### 4.2.2.1 Step 2a: Design issues

At first, appropriate thermodynamic models are chosen to generate the reactive VLE data, Wilson model is selected to calculate liquid phase activity coefficients and SRK equation is used to calculate the vapor phase fugacity coefficients. The resulting  $T - W_A^l - W_A^v$  phase diagrams is shown in *Figure 4.37(A)*. Using the VLE data, the corresponding reactive driving force diagram is constructed as illustrated in *Figure 4.38(A)*.

Subsequently, the RD column is designed using the driving force diagram. Note that, in the diagram, point A denotes the location for the column design at the maximum driving force,

whereas Point B denotes the location of the driving force for the alternative design 1 (design parameters are summarized in *Table 4.10*). Operating area is defined by selecting light key element distillate composition ( $W_A^D$ ) and light key element bottom composition ( $W_A^B$ ) by following Algorithms 3. To do so, consider the light key element liquid mole fraction as follows: When  $x_1 = 1$  (pure isobutene),  $x_2 = x_3 = 0$ , then  $W_A^l = 1$  and  $W_B^l = 0$ . When  $x_2 = 1$  (pure methanol),  $x_1 = x_3 = 0$ , then  $W_A^l = 0$  and  $W_B^l = 1$ . Therefore, when  $x_3 = 1$  (pure MTBE),  $x_1 = x_2 = 0$ , then  $W_A^l = 0.5$  and  $W_B^l = 0.5$ . Consequently, distillate ( $W_A^D$ ) and bottom ( $W_A^B$ ) are selected to be 0.99 and 0.5 on the  $x$ -axis of the reactive driving force diagram based on  $W_A^l$  element composition. The points  $D_x$  and  $D_y$  corresponding to the location and size of the maximum driving force are identified and consequently the slopes of the operating lines are calculated. These correspond to the minimum reflux ratio ( $RR_{min}$ ) and reboil ratio ( $RB_{min}$ ). Actual  $RR$  and  $RB$  values are obtained after multiplying the minimum  $RR_{min}$  and  $RB_{min}$  by 1.2. After that, the slopes of the operating lines are determined. For all the case studies, the number of stages ( $N$ ) is not given; therefore, the reactive McCabe-Thiele method is applied. The total number of stages includes the number of the reactive stages, nonreactive stages (if any) plus the reboiler and the condenser (the two non-reactive stages). As mentioned above, *Table 4.10* presents the reactive distillation column design parameters at the maximum driving force. The result of application of reactive McCabe-Thiele method is shown below

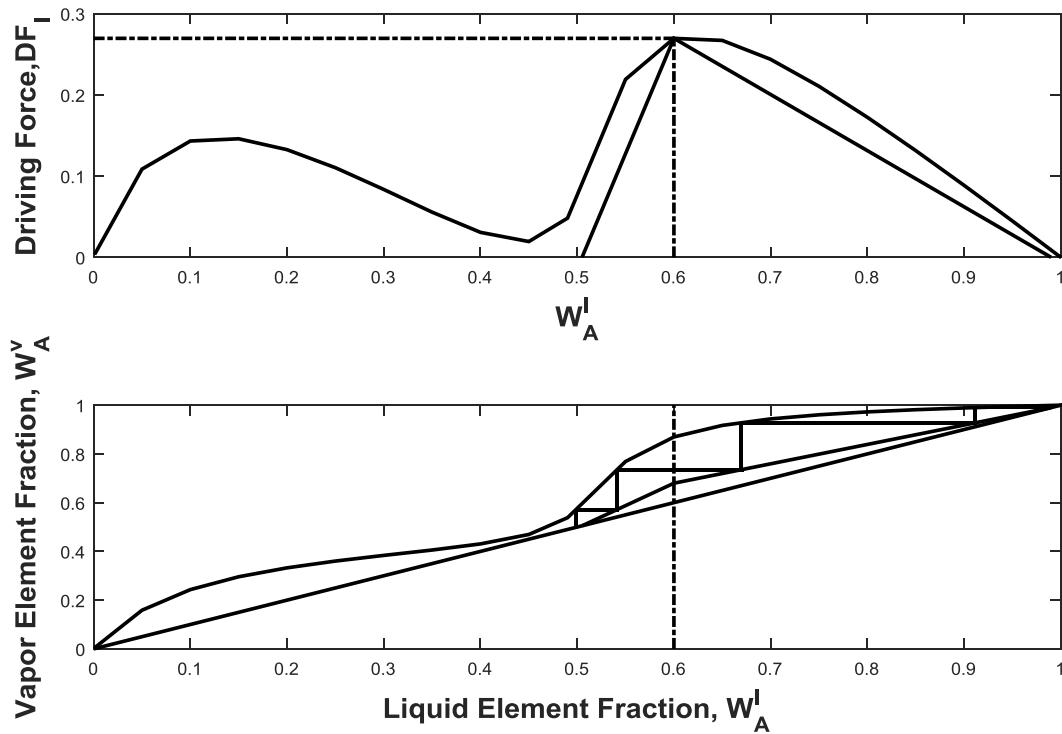


Figure 4.1 Reactive McCabe-Thiele method for designing MTBE binary element reactive distillation system.

#### 4.2.2.2 Step 2b: Optimal design-control issues

The controlled variables ( $y$ ) are the top and bottom compositions, and the manipulated variables ( $u$ ) are the reflux rate and the reboiler duty. The values of  $dDF/dW_A^l$  are calculated and plotted versus  $W_A^l$  as shown in *Figure 4.39(A)*. Note that there is a unique minimum at the maximum driving force, which indicates the least sensitivity of the controlled variables to the disturbances, and the highest sensitivity to the manipulated variables.

#### 4.2.3 Step 3: Verification through simulation and analysis

##### 4.2.3.1 Step 3a: Control structure verification

In order to verify the control structure, the linearized model of the process, i.e., the state-space model is obtained and the steady state gain matrix is constructed for the  $2 \times 2$  system. After that,

Algorithm 6 is applied to find the relative gain array (*RGA*) and Niederlinski index ( $N_I$ ), to verify the extent of loop interactions, which are listed in *Table 4.11*. It is found that the loop interactions are minimal, since diagonal values are close to unity ( $N_I \approx 1$ ). Note that *RGA* and  $N_I$  are checked to test the control schemes.

#### 4.2.3.2 Step 3b: Dynamic open loop and closed-loop analysis

In order to evaluate dynamic open-loop and closed-loop performance, Algorithm 7 is applied. The disturbance scenarios are presented in *Table 4.12* which are introduced through the feed, and expressed in terms of the percentage of feed flow rate.

At first the open-loop responses of the system to the disturbance has been determined. Next, the closed loop simulation results under PI control structure are obtained. The controller tuning parameters have been obtained using IMC rules (Rivera et al., 1986). In addition to the controller pairings mentioned above, the distillate drum level, and sump level are controlled by manipulating the distillate and bottom flow rates, respectively. The level controllers are the proportional (P) type, and they are included in the model equation to maintain the dynamic model's consistency and stability. Furthermore, a perfect pressure control is assumed. Therefore, the pressure changes in the column are neglected.

After that, closed-loop responses of the design-control solution under MPC are reported. The *A*, *B*, and *C* matrices for a standard continuous-time state-space model are obtained for the design control solution at the maximum driving force. *D* matrix is zero. For a linear system with *p* inputs, *q* outputs and *n* state variables,  $A^{n \times n}$  is the system matrix,  $B^{n \times p}$  is the input matrix,  $C^{q \times n}$  is the output matrix. Using the linear model of the process, a MPC controller is implemented to perform the closed-loop simulation on the design control solution at the maximum driving force. The plant inputs are, the condenser duty -  $Q_c$ , the reflux mass flow rate -  $R$  (kg/hr), the reboiler duty -  $Q_R$ , the distillate mass flow rate -  $D$  (kg/hr), the bottoms mass flow rate -  $B$  (kg/hr), and the feed molar flow rate (kmol/hr). The plant outputs are: the column pressure (stage 1) -  $P$  (atm), the mole fraction of the distillate of interest -  $x^D$ , the mole fraction of the bottoms of interest -  $x^B$ , the reflux drum liquid level -  $R_{lev}$  (m), and the sump liquid level -  $S_{lev}$  (m).

Finally, a comparison based on the end compositions and a comparison based on percentage deviations of the controlled outputs ( $x^D$  and  $x^B$ ) using the MPC and PI controllers for the design control solution at the maximum driving force to previously defined disturbance scenarios are reported. For the comparison based on percentage deviation, the step change is introduced at time 0. The nominal set point is at 50%.

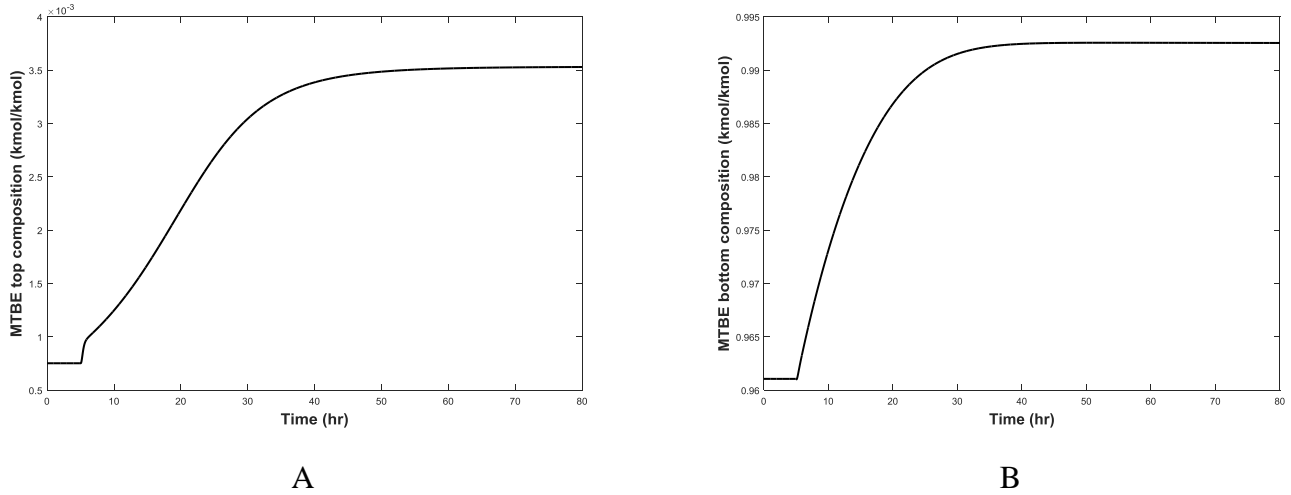


Figure 4.2 Open-loop response of the optimal design control solution to step change in feed flow rate, Case study 1: A) top; B) bottom.

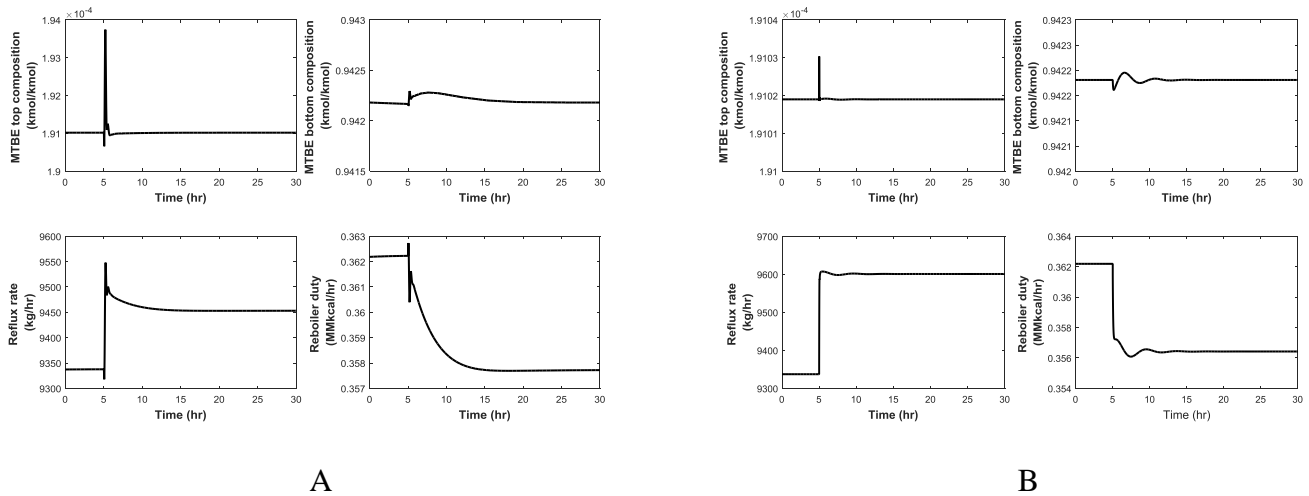


Figure 4.3 Close-loop response of the optimal design control solution for step change in feed flow rate, Case study 1: A) PI controller; B) MPC controller

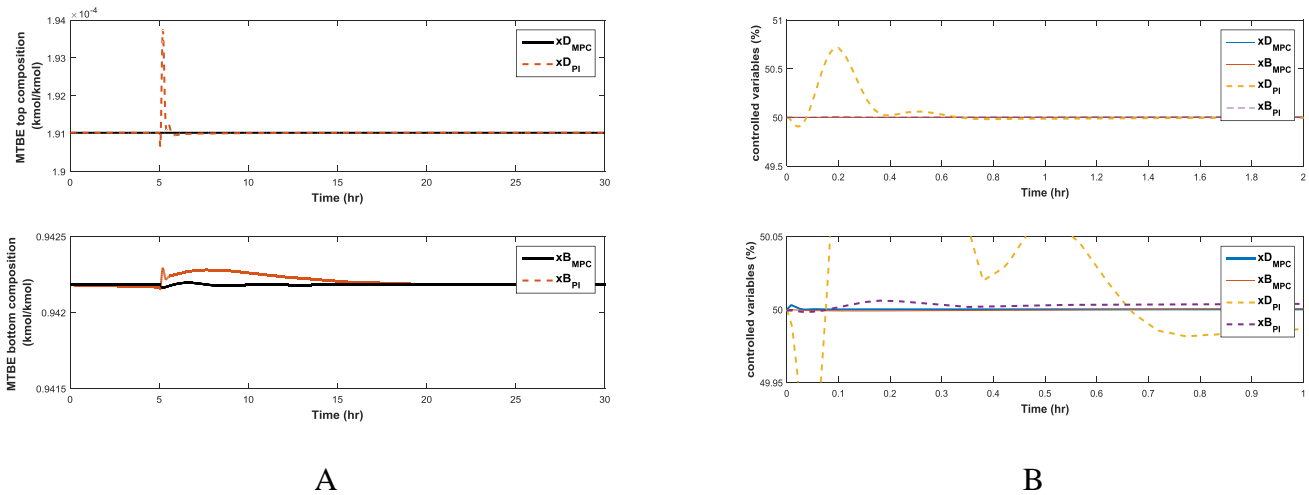


Figure 4.4 Comparison between controlled outputs under MPC and PI controllers for the design-control solution, Case study 1: A) composition B) percent deviation.

#### 4.2.3.3 Step 3c: Final selection

The values of the parameters included in the performance objective function (Equation 4.1) are calculated. The results are presented in Table 4.13.

#### 4.2.4 Step 4: Comparison with RD design not at maximum driving force

In order to establish the appropriateness of the design-control solution, an alternative reactive distillation column design not at the maximum driving force is selected for comparison. This selection confirms that by going away from the maximum driving force, the control of the reactive distillation process becomes more difficult. For the purpose of comparison, the number of stages is kept the same for all cases. Feed locations, reflux and boil-up ratios are varied and the same control structure and controlled variables as the ones in the maximum driving force design are used for the consistency of the comparison. Both the PI and MPC controllers are used for closed-loop simulation for all the alternatives. The selected design alternatives for all the cases are summarized in Table 4.10. The steady-state simulation of all the design alternatives for

all the cases is performed. All satisfied the design targets. The  $RGA$  and  $N_I$  values for the alternative designs are summarized in *Table 4.14*. For all the case studies, at first, the closed-loop performance under PI controllers for all the alternatives is evaluated. Similarly, as with the PI controllers, closed-loop performance under MPC controllers for all the alternatives is evaluated. For both cases, the disturbance scenario remained the same as for the design-control solution. After that, similarly as with the design-control solution, a comparison based on the compositions and a comparison based on the percentage deviation of the controlled outputs ( $x^D$  and  $x^B$ ) using the MPC and PI controllers for all the alternative designs are reported.

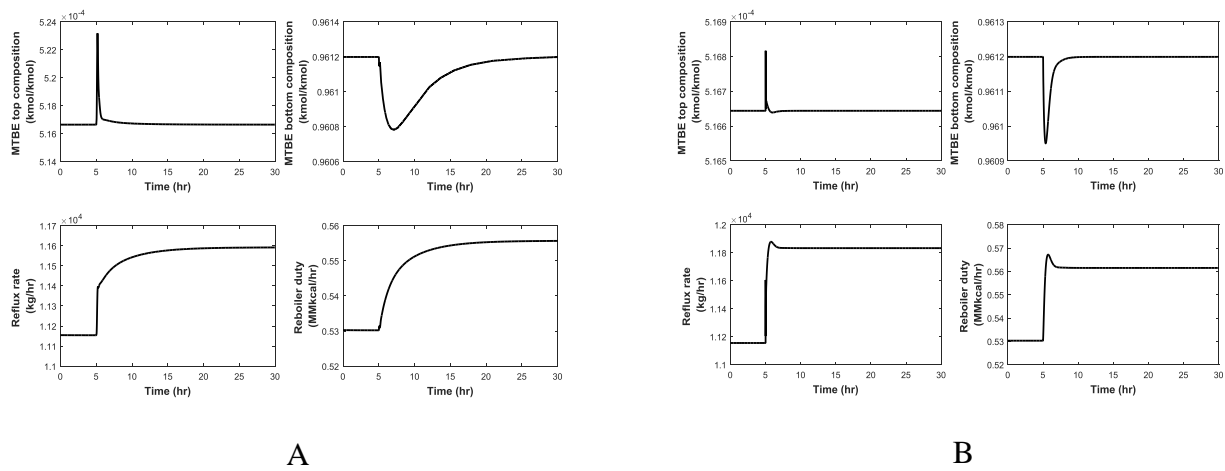


Figure 4.5 Close-loop response of the alternative design for step change in feed flow rate, Case study 1: A) PI controller; B) MPC controller

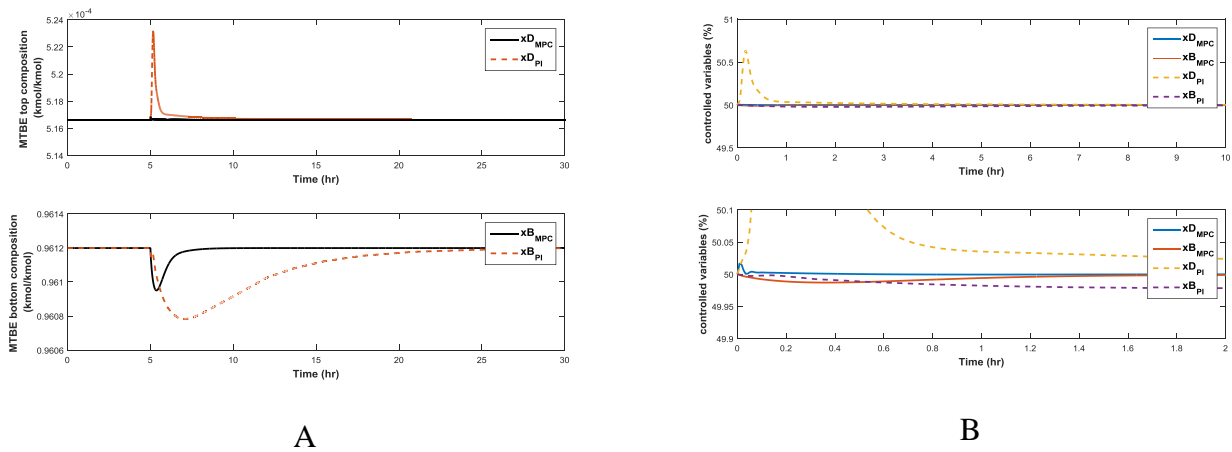




Figure 4.6 Comparison between controlled outputs under MPC and PI controllers for the alternative design, Case study 1: A) composition B) percent deviation

Finally, the objective function values for both the design-control solution and the alternative design under both the PI and MPC controllers are given in Table 4.16.

### 4.3 Case study 2: MTBE production with inert

#### 4.3.1 Step 1: Data collection and problem formulation

The reaction of methanol with isobutene with the presence of 1-butene (inert) that yields MTBE is reversible and exothermic and it takes place in presence of an acidic catalyst (Al-Jarallah et al., 1988). The reaction can be expressed as follows:



The design feed compositions and product specifications (Pérez Cisneros et al., 1997) are summarized in Table 4.2. Note however, the main target to be satisfied is the MTBE bottom composition.

Table 4.2 Design targets and product specifications for MTBE system with inert.

Component	Molar composition		
	Feed	Distillate	Bottom
Isobutene (C <sub>4</sub> H <sub>8</sub> )	0.590	0.773	0.061
Methanol (CH <sub>4</sub> O)	0.343	0.0	0.012
1-butene(C <sub>4</sub> H <sub>8</sub> )	0.067	0.196	0.024

MTBE (C <sub>5</sub> H <sub>12</sub> O)	0.0	0.031	0.907
Feed flowrate: 100 kmol/h; Feed temperature and Pressure: 320K and 11 atm.			

The choice of elements and corresponding element matrix are given in

*Table 4.9.* C is selected as the non-key element. B and A are selected to be the light key (LK) and the heavy key (HK), respectively.

### 4.3.2 Step 2: Integrated Design-Control

#### 4.3.2.1 Step 2a: Design issues

Here, the thermodynamic models to generate the reactive VLE data are as follows: Wilson model is selected to calculate liquid phase activity coefficients and SRK equation is used to calculate the vapor phase fugacity coefficients. The resulting  $T - W_{LK,eq}^l - W_{LK,eq}^v$  phase diagrams for multi-element reactive systems is given in *Figure 4.37(B)*. Using the VLE data, the reactive driving force diagram is constructed as illustrated in *Figure 4.38(B)*.

Following the same steps as mentioned in Case study 1, the RD column is designed using the driving force diagram, expect for this case study, since it is a multi-element system, equivalent light key element distillate composition ( $W_{LK,eq}^D$ ) and equivalent light key element bottom composition ( $W_{LK,eq}^B$ ) are used to define the area of operation. The result of application of reactive McCabe-Thiele method is shown below

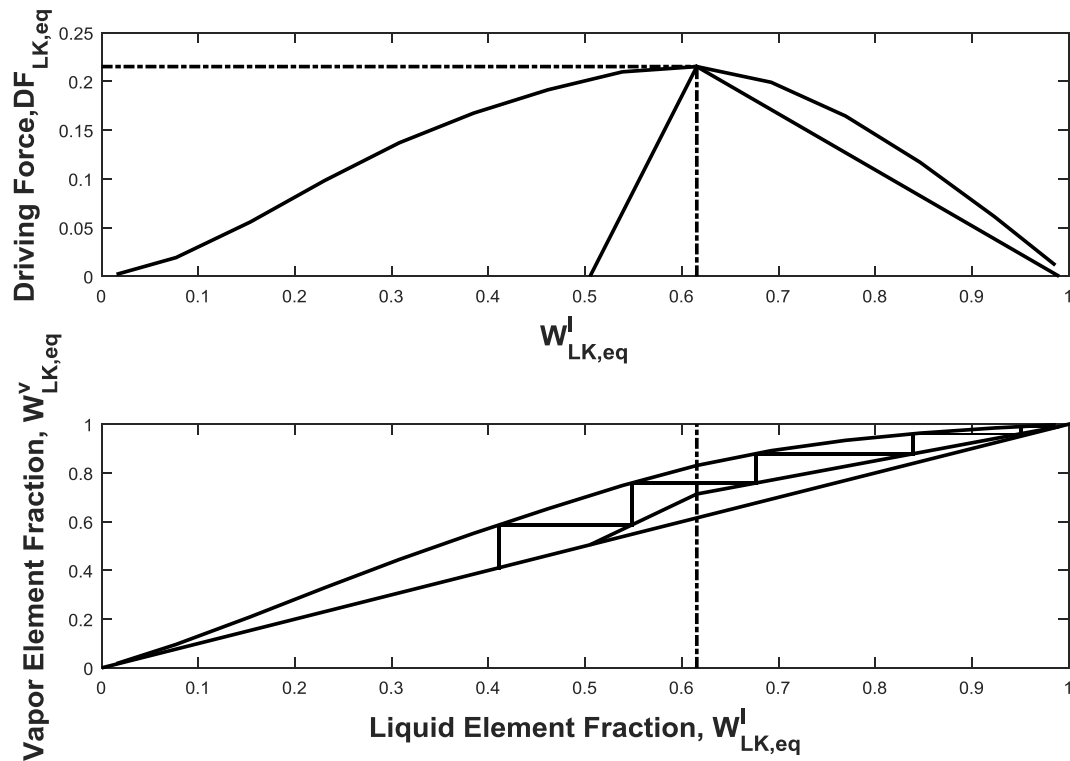


Figure 4.7 Reactive McCabe-Thiele diagram and calculations for MTBE multi-element system.

#### 4.3.2.2 Step 2b: Optimal design-control issues

As shown in *Figure 4.39 (B)*,  $dDF_{LK,eq}/dW_{LK,eq}^l$  vs  $W_{LK,eq}^l$  is minimum at the maximum driving force, which concurs with the discussion as in Case study 1.

### 4.3.3 Step 3: Verification through simulation and analysis

#### 4.3.3.1 Step 3a: Control structure verification

As shown in *Table 4.11*, the  $RGA$  and  $N_I$  values suggest that the design parameters obtained through the maximum driving force approach should result in minimal loop interaction during dynamic closed loop operation.

### 4.3.3.2 Step 3b: Dynamic Open loop and closed-loop analysis

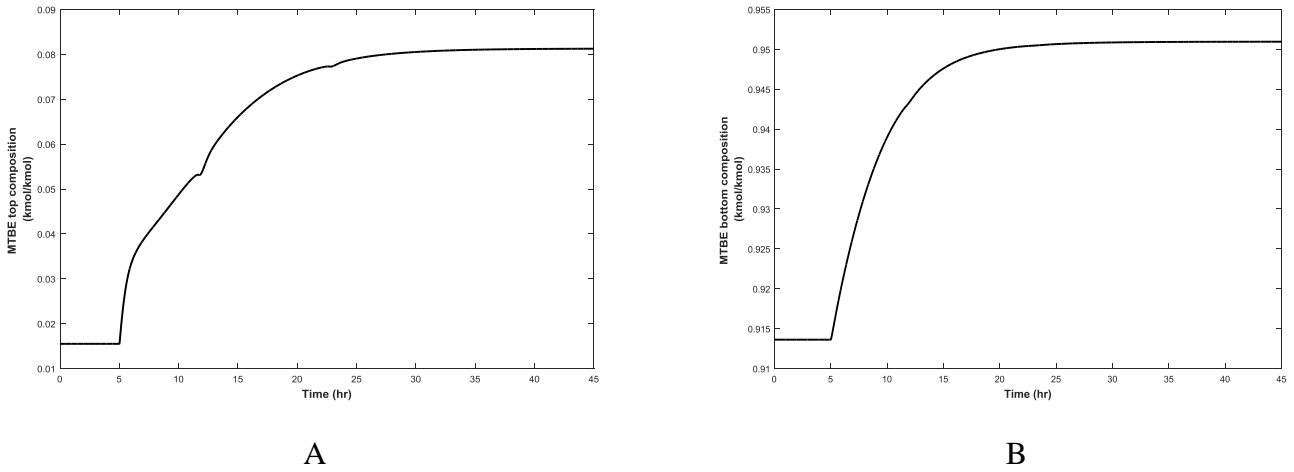


Figure 4.8 Open-loop response of the optimal design control solution to step change in feed flow rate, Case study 2: A) top; B) bottom.

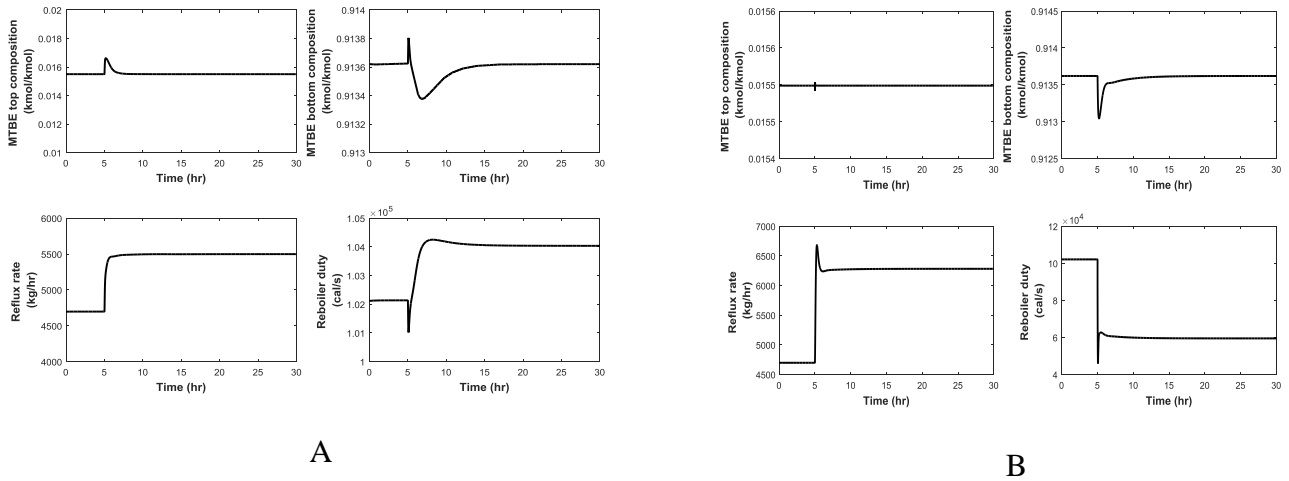
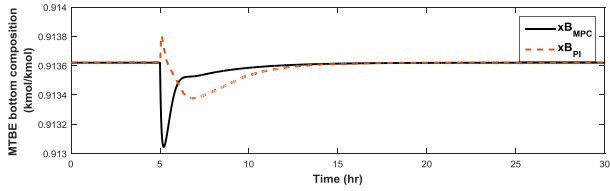
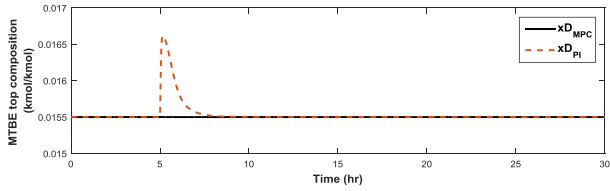
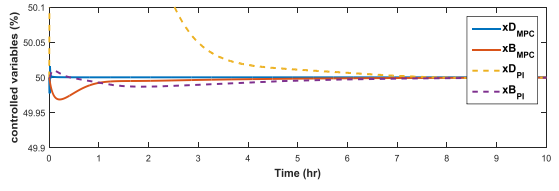
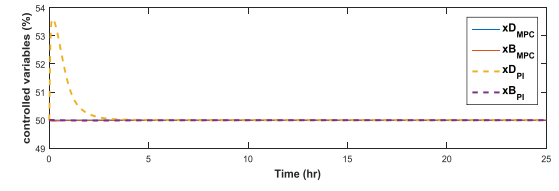


Figure 4.9 Close-loop response of the optimal design control solution for step change in feed flow rate, Case study 2: A) PI controller; B) MPC controller



A



B

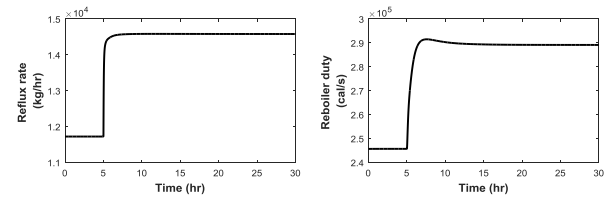
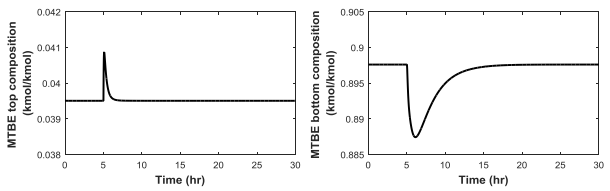
Figure 4.10 Comparison between controlled outputs under MPC and PI controllers for the design-control solution, Case study 2: A) composition B) percent deviation

### 4.3.3 Step 3c: Final selection

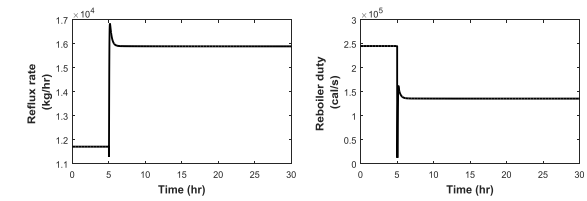
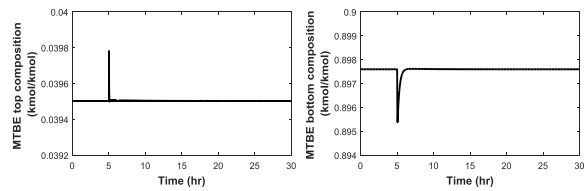
The objective function values are calculated and listed in *Table 4.13*.

### 4.3.4 Step 4: Comparison with RD design not at the maximum driving force

Following the steps as described in Case study 1, the following dynamic responses are achieved:



A



B

Figure 4.11 Close-loop response of the alternative design for step change in feed flow rate, ,  
Case study 2: A) PI controller; B) MPC controller

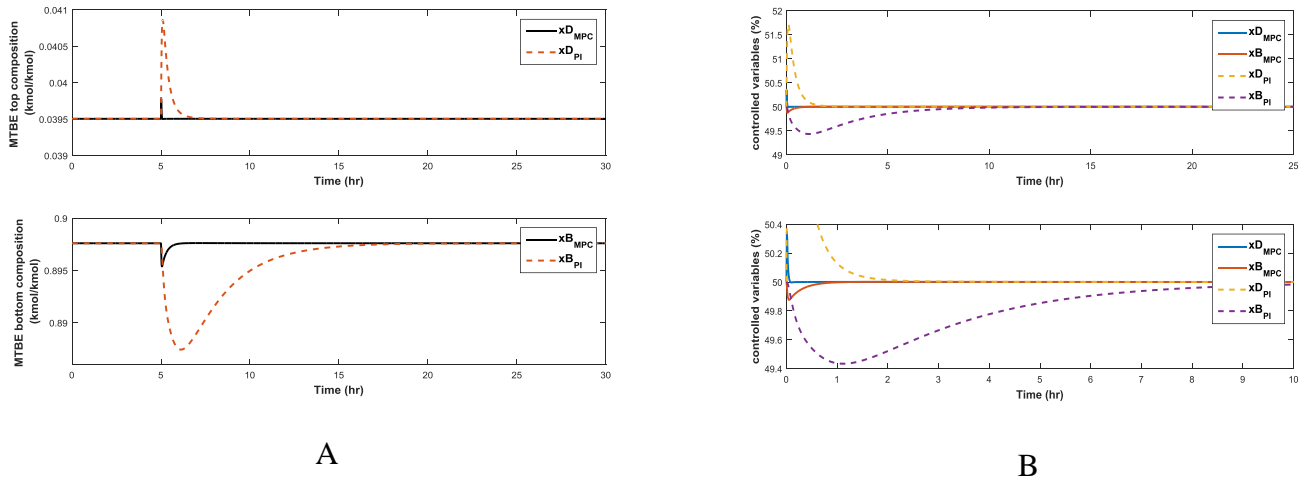


Figure 4.12 Comparison between controlled outputs under MPC and PI controllers for the alternative design, Case study 2: A) composition B) percent deviation

Finally, the performance of the design-control solution and the alternative design is quantified in Table 4.16.

#### 4.4 Case study 3: Methyl Acetate production

##### 4.4.1 Step 1: Data collection and problem formulation

For the production of methyl-acetate via a reactive distillation column, two feeds of same amount of flowrate of methanol and acetic acid and both reactive and non-reactive sections are considered. The design objective in this section is to obtain the RD column design operating at the maximum driving force to produce high purity methyl-acetate. The reaction between methanol (MeOH) and acetic acid (HOAc) yields methyl acetate (MeOAc) and water (H<sub>2</sub>O). The reaction takes place in liquid phase over a catalyst (Jantharasuk et al., 2011). It is exothermic with a heat of reaction of  $-5.42$  kJ/mol and is given as follows:



The design target for a reactive distillation column with only reactive section (Jantharasuk et al., 2011) is given in *Table 4.3*

Table 4.3 Design targets and product specifications for methyl acetate production.

Component	Molar composition			
	Feed (1)	Feed (2)	Distillate	Bottom
Methanol (CH <sub>4</sub> O)	1	0	0.0694	0.0
Acetic Acid (C <sub>2</sub> H <sub>4</sub> O <sub>2</sub> )	0	1	0.0089	0.3345
Methyl Acetate (C <sub>3</sub> H <sub>6</sub> O <sub>2</sub> )	0	0	0.7612	0.0
Water (H <sub>2</sub> O)	0	0	0.1606	0.6651
Feed (1): 230.28 kmol/h methanol; Feed temperature and Pressure: 328K and 1 atm.				
Feed (2): 230.28 kmol/h acetic acid; Feed temperature and Pressure: 328K and 1 atm.				

The choice of elements and corresponding element matrix are given in

*Table 4.9*. C is selected as the non-key element. Element A is the light key element (LK) and element B is the heavy key element (HK).

#### 4.4.2 Step 2: Integrated Design-Control

##### 4.4.2.1 Step 2a: Design Issues

Wilson model is selected to calculate liquid phase activity coefficients and SRK equation is used to calculate the vapor phase fugacity coefficients. The resulting  $T - W_{LK,eq}^l - W_{LK,eq}^v$  phase diagrams for multi-element reactive systems is given in *Figure 4.37 (C)*. Using the VLE data, the corresponding reactive driving force diagram is constructed as illustrated in *Figure 4.38 (C)*.

For this case study, since it is a two feed and multi element system, the area of operation is based on equivalent element compositions. Note that the area of operation is rescaled between 0-1 in the composition domain on the axis of the driving force diagram by following Algorithm 4. The composition of the feeds ( $W_h, W_k$ ) and the design targets in the distillate and bottom compositions ( $W^D, W^B$ ), i.e., the light key equivalent element is in pure state in one feed ( $W_k = 1$ ) and does not exist in the other feed ( $W_h = 0$ ). The feed that contains the light key element (methanol) is introduced at the last reactive stage and the other feed (which does not contain the light key element – acetic acid) is introduced at the first reactive stage (counting from the top) to ensure countercurrent flow. Non-reactive stages are added to the top and bottom of the reactive zone, one at a time, until the design targets are satisfied. The result of application of reactive McCabe-Thiele method is shown below

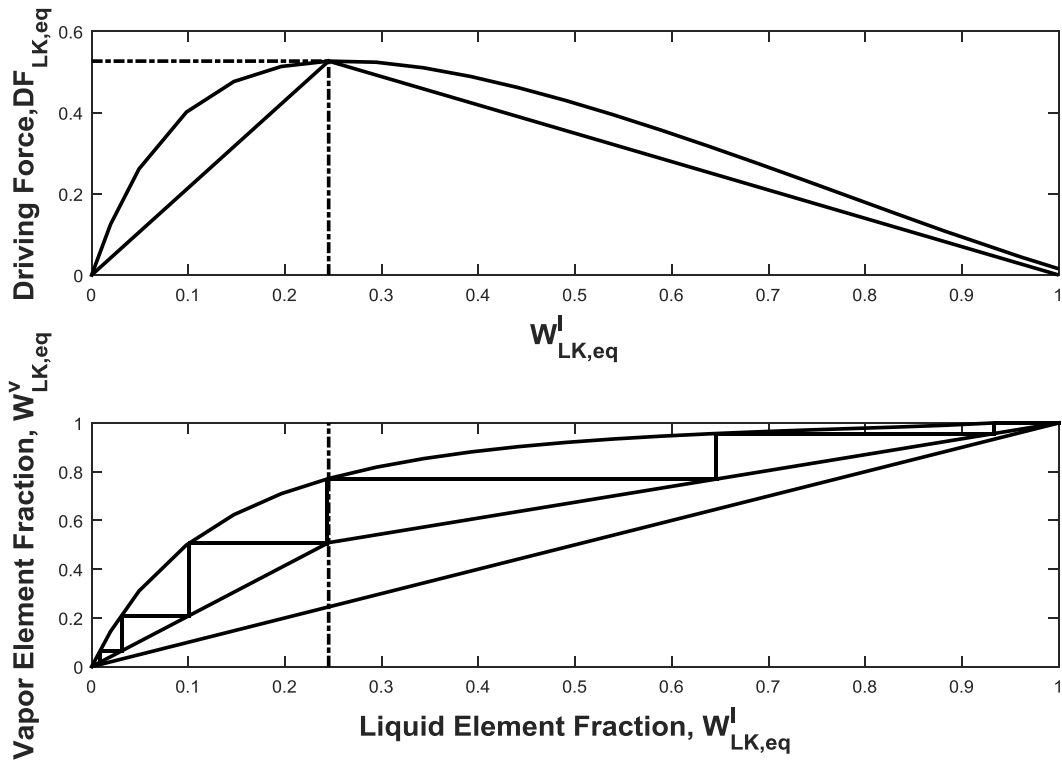


Figure 4.13 Reactive distillation column design for methyl-acetate multi-element system at 1 atm.



#### 4.4.2.2 Step 2b: Optimal design-control issues

As shown in *Figure 4.39 (C)*,  $dDF_{LK,eq}/dW_{LK,eq}^l$  vs  $W_{LK,eq}^l$  is minimum at the maximum driving force, which concurs with the discussion as in Case study 1.

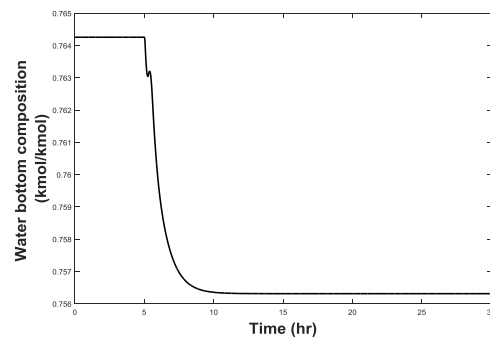
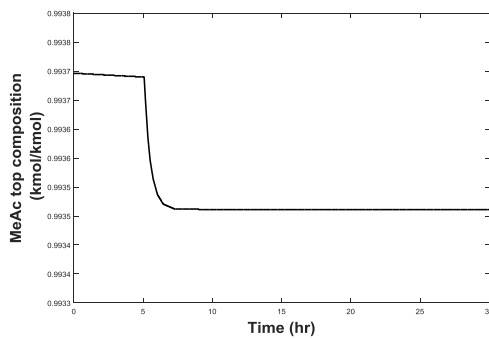
#### 4.4.3 Step 3: Verification through simulation and analysis

##### 4.4.3.1 Step 3a: Control Structure verification

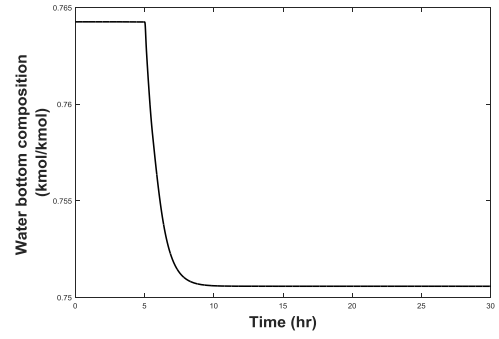
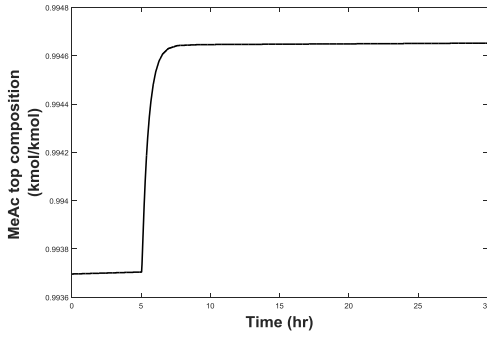
$RGA$  and  $N_I$  values as listed in *Table 4.11* suggest that this system is stable and should exhibit minimal loop interaction.

##### 4.4.3.2 Step 3b: Dynamic Open loop and closed loop analysis

Since, this is a double feed system, dynamic response for disturbances introduced through both feed streams are analyzed and shown below:

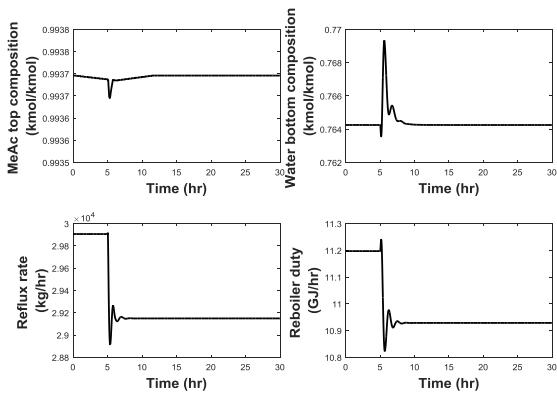


A

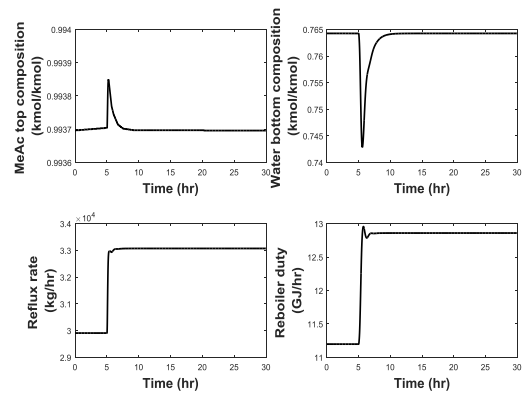


B

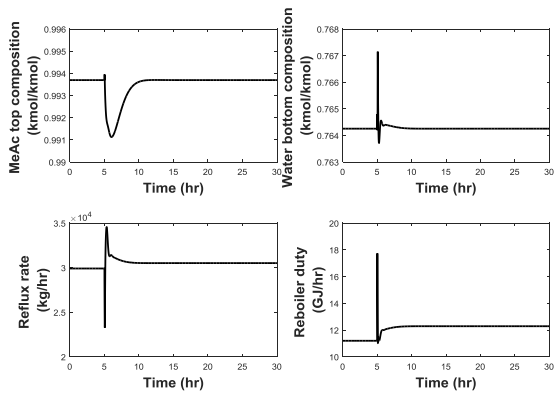
Figure 4.14 Open-loop response of the optimal design control solution to step change in feed flow rate, Case study 3: A) +10% methanol; B) +10% acetic acid.



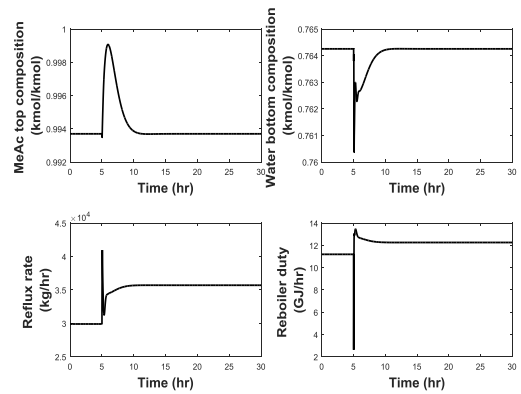
A



B



C



D

Figure 4.15 Close-loop response of the optimal design control solution for a step change in the feed flow rate, Case study 3: A) PI controller, +10% methanol; B) PI controller, +10% acetic acid; C) MPC controller, +10% methanol; D) MPC controller, +10% acetic acid.

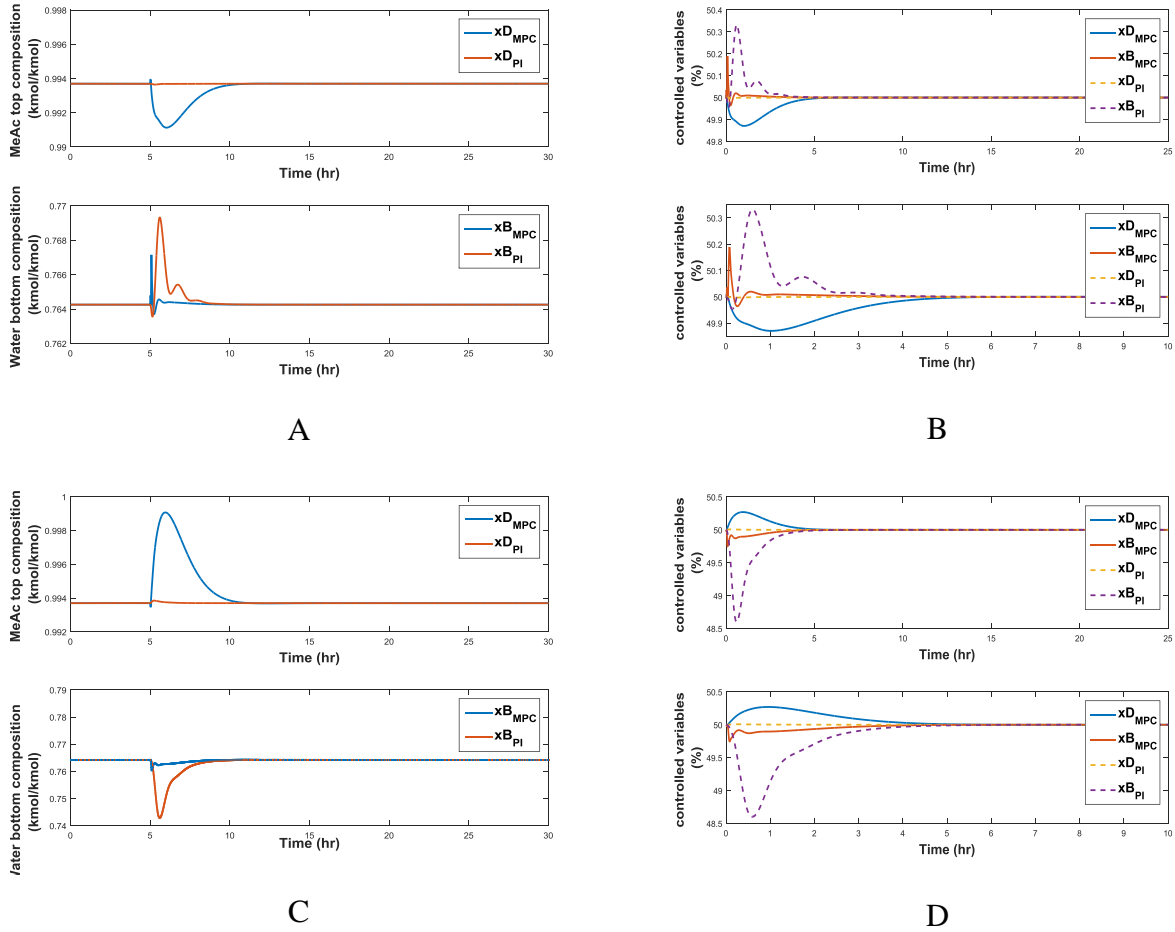


Figure 4.16 Comparison between the controlled outputs under the MPC and PI controllers for the design-control solution, Case study 3: A) +10% methanol; composition B) +10% methanol; percent deviation; C) +10% acetic acid; composition D) +10% acetic acid; percent deviation.

#### 4.4.3.3 Step 3c: Final selection

The quantified control performance for both disturbance scenarios are listed in Table 4.15,

#### 4.4.4 Step 4: Comparison with RD design not at the maximum driving force

Following the steps described in Case study 1, the dynamic responses for alternative design are obtained which are shown below:

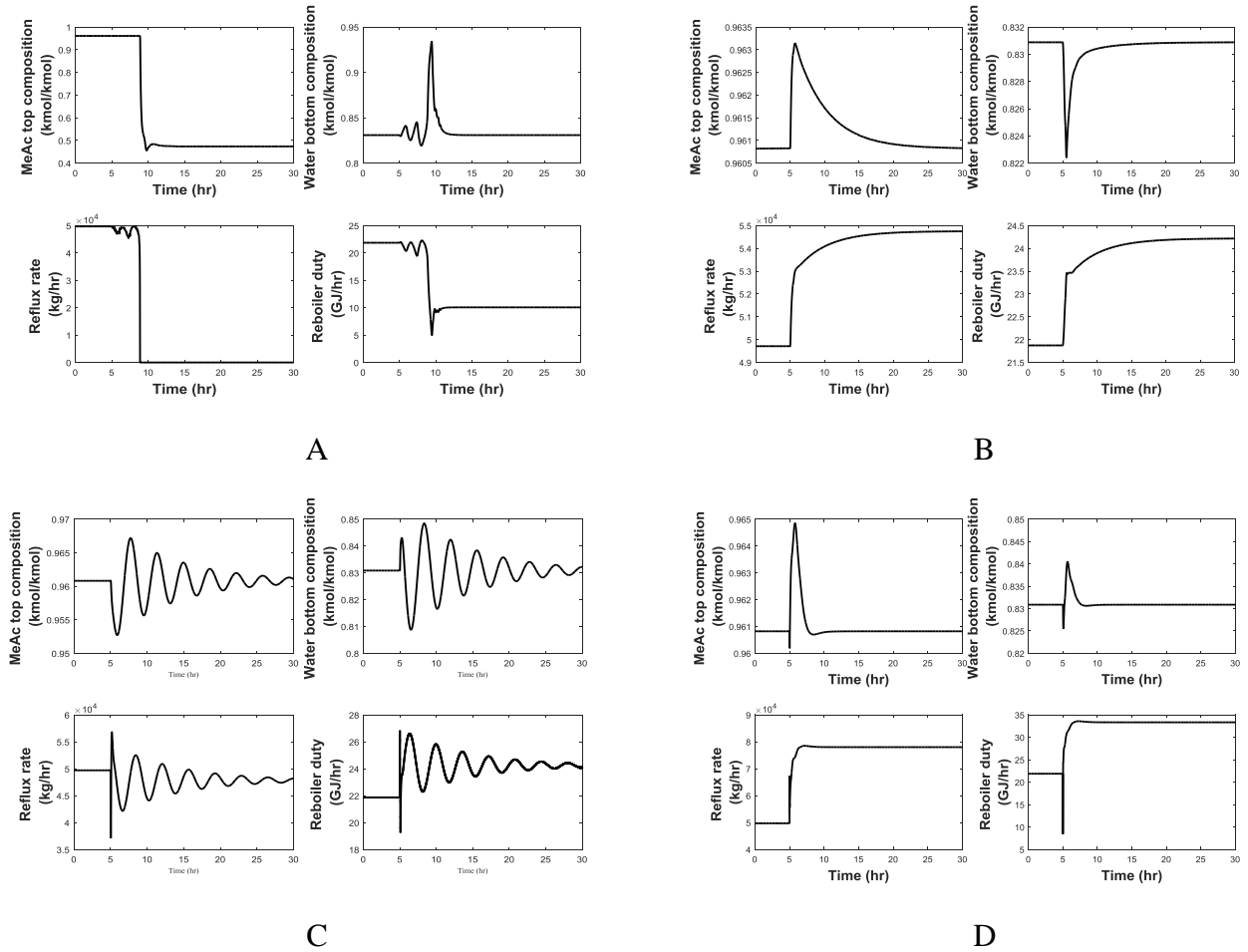


Figure 4.17 Close-loop response of the alternative design for a step change in the feed flow rate, Case study 3: A) PI controller, +10% methanol; B) PI controller, +10% acetic acid; C) MPC controller, +10% methanol; D) MPC controller, +10% acetic acid.

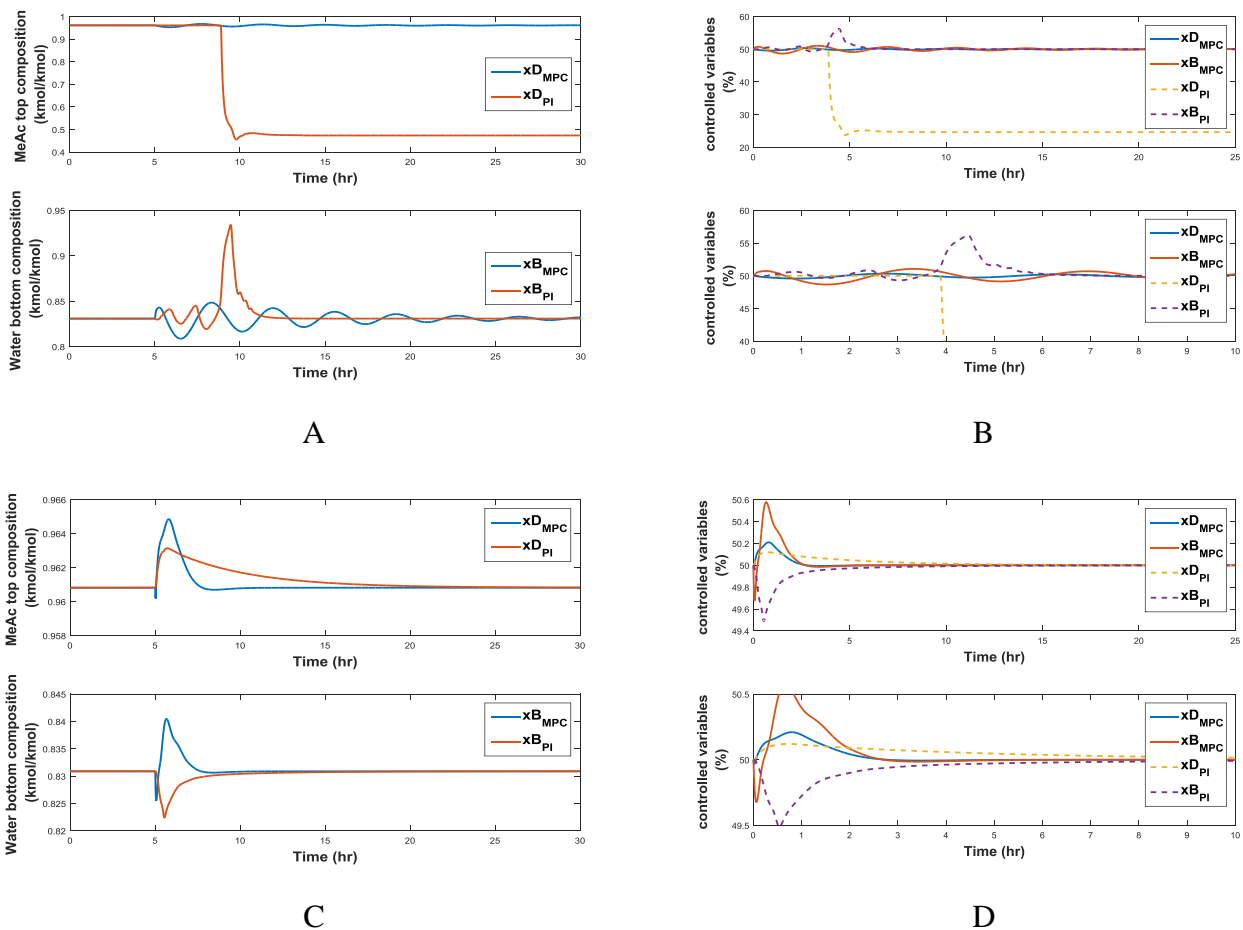


Figure 4.18 Comparison between the controlled outputs under the MPC and PI controllers for the alternative design, Case study 3: A) +10% methanol; composition B) +10% methanol; percent deviation; C) +10% acetic acid; composition D) +10% acetic acid; percent deviation.

The quantified comparison between design-control solution and the alternative design is summarized in Table 4.18.

## 4.5 Case study 4: Toluene disproportion

### 4.5.1 Step 1: Data collection and problem formulation

The disproportionation of toluene to produce benzene and *o*-xylene, is an equilibrium-limited reaction that can be improved through reactive distillation (Sánchez Daza et al., 2003). The

reaction takes place in vapor phase (Lobão et al., 2012) at 350°C. The reaction can be expressed as follows:



The feed conditions for the disproportionation of toluene (Sánchez Daza et al., 2003) are summarized in *Table 4.4*. Note however, that the primary objective is to achieve high purity Benzene in the distillate.

Table 4.4 Design targets and product specifications for Toluene disproportionation.

Component	Molar composition		
	Feed	Distillate	Bottom
Benzene (C <sub>6</sub> H <sub>6</sub> )	0.0	0.979624	0.010322
Toluene (C <sub>6</sub> H <sub>6</sub> (CH <sub>2</sub> ))	0.1	0.020344	0.312690
<i>o</i> -xylene (C <sub>6</sub> H <sub>6</sub> (CH <sub>2</sub> ) <sub>2</sub> )	0.0	0.000032	0.676988
Feed flowrate: 100 kmol/h; Feed temperature and Pressure: 623K and 101.3 kPa			

The choice of elements and corresponding element matrix are given in *Table 4.8*.

## 4.5.2 Step 2: Integrated Design-Control

### 4.5.2.1 Step 2a: Design Issues

NRTL model is selected to calculate liquid phase activity coefficients and Ideal gas equation is used to calculate the vapor phase fugacity coefficients. Note that for the case study 4, the element *B* is 'CH<sub>2</sub>' which is not a whole molecule and, therefore, cannot exist by itself. However, since it is associated with toluene and *o*-xylene, *AB*<sub>2</sub> (*o*-xylene) is used while plotting the phase diagrams. Note also that the reaction zone is only located for  $0.33 < W_A^l < 1$  (Sánchez Daza et

al., 2003). The resulting  $T - W_A^l - W_A^v$  phase diagrams is shown in *Figure 4.37 (D)*. Using the VLE data, the corresponding reactive driving force diagram is constructed as illustrated in *Figure 4.38 (D)*.

After that, the RD column is designed at the maximum driving force, except for this case, when identifying the area of operation, the design target for bottoms component composition of *o*-xylene is 0.67. Hence, corresponding element composition,  $W_A^l = 0.375$ . Consequently, distillate ( $W_A^D$ ) and bottom ( $W_A^B$ ) are selected to be 0.98 and 0.375. The result of application of reactive McCabe-Thiele method is shown below

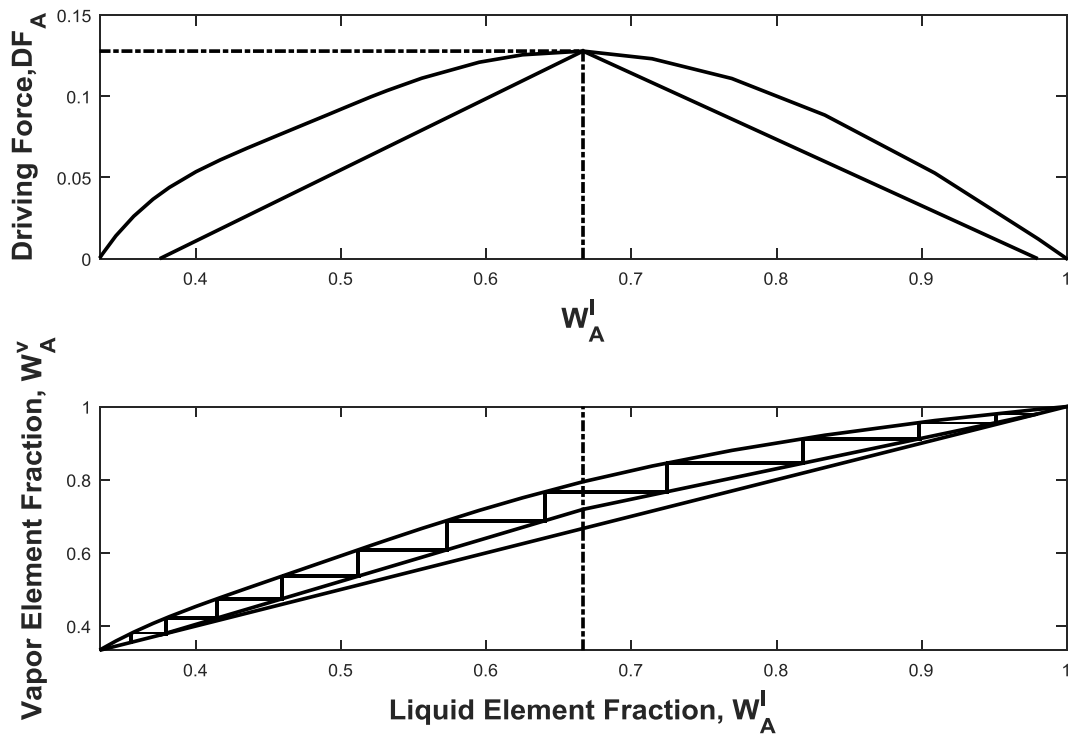


Figure 4.19 Reactive distillation column design for toluene disproportionation binary element system at 1 atm.

#### 4.5.2.2 Step 2b: Optimal design-control issues

The differential driving force diagram for this case study as shown in *Figure 4.39(D)* exhibits a unique minimum at the maximum driving force which supports the discussion in Case study 1.

### 4.5.3 Step 3: Verification through simulation and analysis

#### 4.5.3.1 Step 3a: Control structure verification

Parameters listed in *Table 4.11*, suggest closed-loop performance with minimal loop interaction.

#### 4.5.3.2 Step 3b: Dynamic Open loop and closed-loop analysis

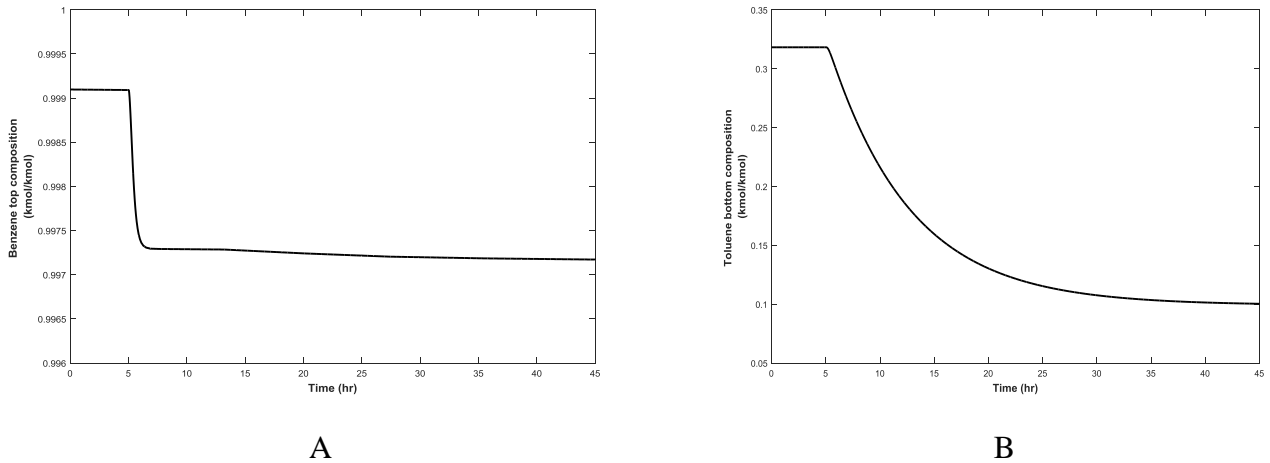


Figure 4.20 Open-loop response of the optimal design control solution to step change in feed flow rate, Case study 4: A) top; B) bottom.

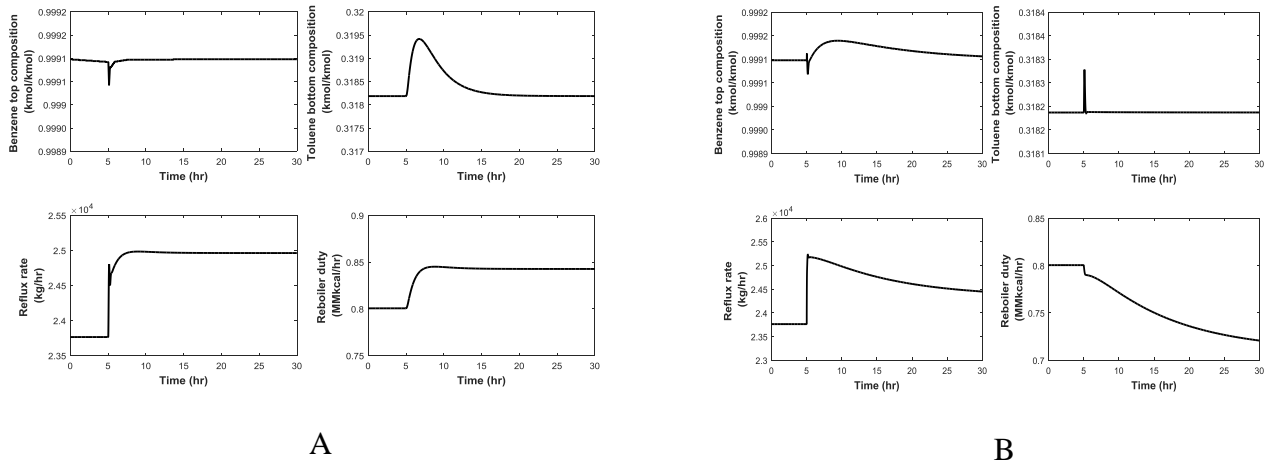
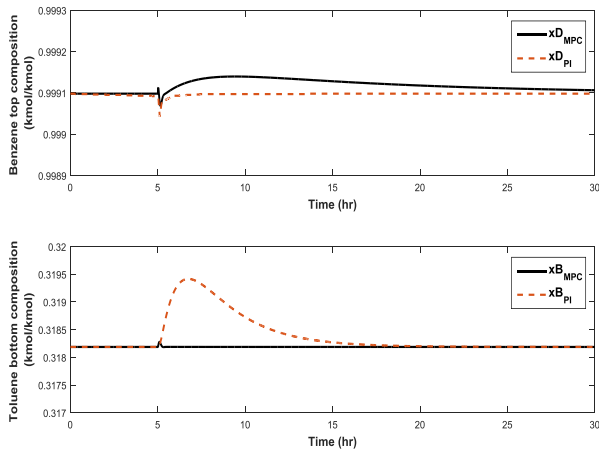
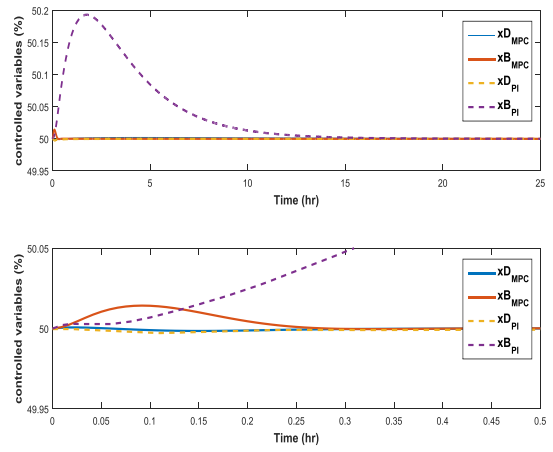


Figure 4.21 Close-loop response of the optimal design control solution for step change in feed flow rate, Case study 4: A) PI controller; B) MPC controller





A



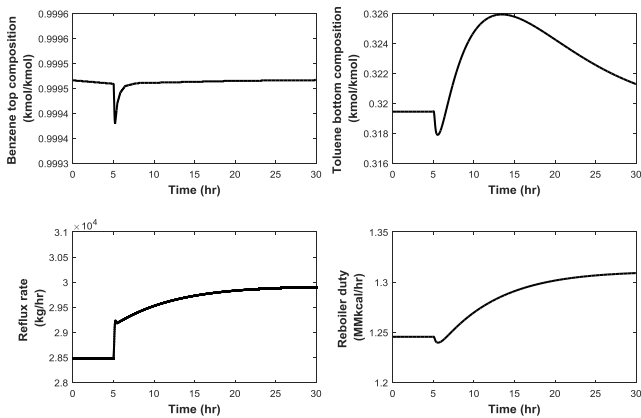
B

Figure 4.22 Comparison between controlled outputs under MPC and PI controllers for the design-control solution, Case study 4: A) composition B) percent deviation

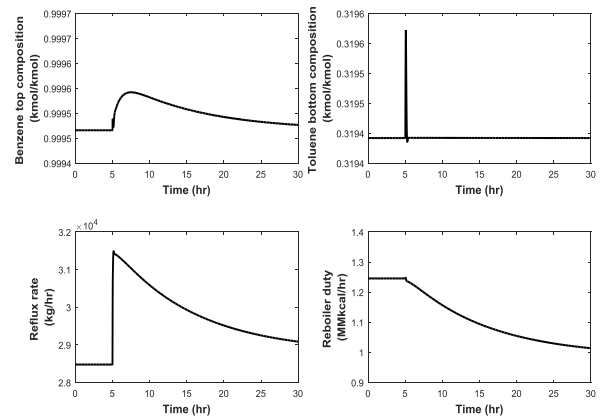
### 4.5.3.3 Step 3c: Final selection

The design-control performance at the maximum driving force is quantified in Table 4.13.

### 4.5.4 Step 4: Comparison with RD designs not at the maximum driving force



A



B

Figure 4.23 Close-loop response of the alternative design for step change in feed flow rate, Case study 4: A) PI controller; B) MPC controller.

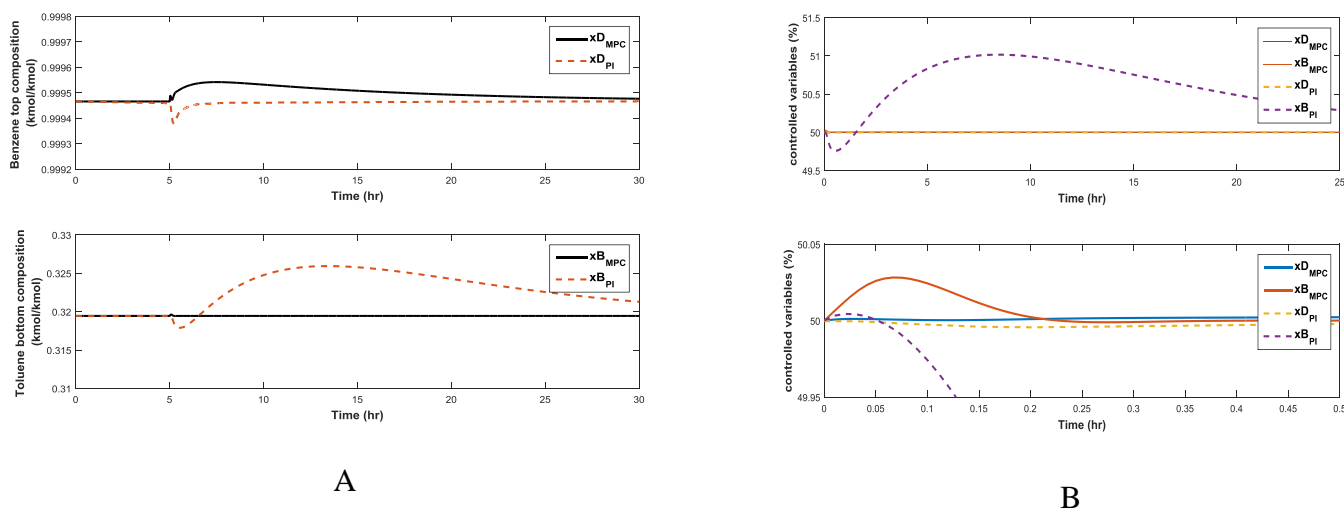


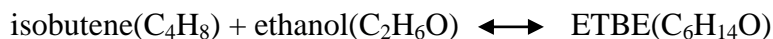
Figure 4.24 Comparison between controlled outputs under MPC and PI controllers for the alternative design, Case study 4: A) composition B) percent deviation.

Comparison of the performance under both designs is summarized in Table 4.16.

## 4.6 Case study 5: ETBE production

### 4.6.1 Step 1: Data collection and problem formulation

The reaction of ethanol with isobutene yields ETBE. This is a reversible and exothermic reaction. The reaction takes place in liquid phase (François & Thyron, 1991) at 25°C. It can be expressed as follows:



ETBE RD synthesis utilizes the same principles as the MTBE process. Conventional ETBE RD synthesis follows a similar route to MTBE synthesis. However, reaction and phase differences

create slightly different operating conditions and change the expected conversion and purity. The more restrictive equilibrium lowers the conversion achieved in the reaction stage by 1-2% (Sneesby et al., 1997).

Therefore, the feed compositions for the production of ETBE are kept the same as for MTBE (Sánchez Daza et al., 2003). However, the feed temperatures and pressures are selected to be 323K and 15atm as suggested by Umar et al., 2009 and Françoisse & Thyron, 1991. Since the conversion achieved in the reactive stage is 1-2% less than the MTBE process, the expected product purity is slightly less than that for MTBE. The selected design targets and product specifications are summarized in *Table 4.5*.

Table 4.5 Design targets and product specifications for ETBE production.

Component	Molar composition		
	Feed	Distillate	Bottom
Isobutene (C <sub>4</sub> H <sub>8</sub> )	0.7	> 0.9	-
Ethanol (C <sub>2</sub> H <sub>6</sub> O)	0.3	-	-
ETBE (C <sub>6</sub> H <sub>14</sub> O)	0.0	-	> 0.8
Feed flowrate: 100 kmol/h; Feed temperature and Pressure: 323K and 15 atm.			

The choice of elements and corresponding element matrix are given in *Table 4.8*.

## 4.6.2 Step 2: Integrated Design-Control

### 4.6.2.1 Step 2a: Design issues

Wilson model is selected to calculate liquid phase activity coefficients and SRK equation is used to calculate the vapor phase fugacity coefficients. The resulting  $T - W_A^l - W_A^p$  phase diagram is

shown in *Figure 4.37 (E)*. Using the VLE data, the corresponding reactive driving force diagram is constructed as illustrated in *Figure 4.38 (E)*.

After that, the RD column is designed at the driving force diagram. The result of application of reactive McCabe-Thiele method is shown below:

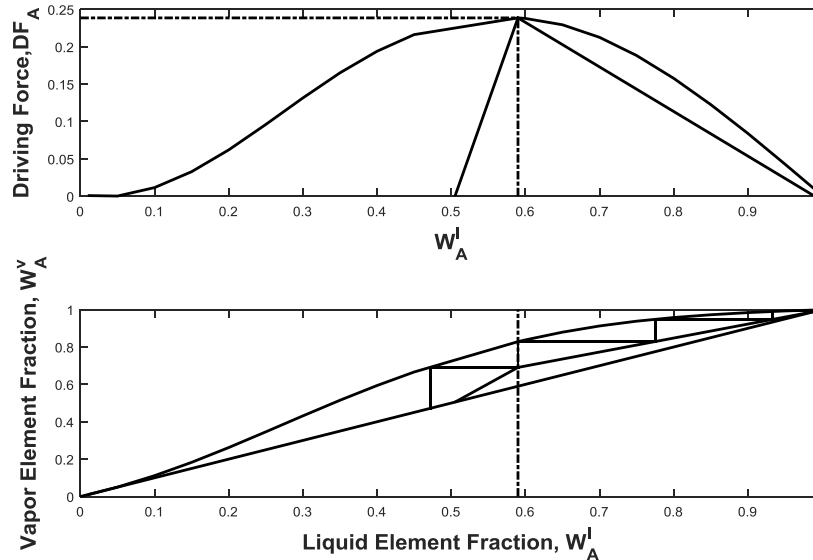


Figure 4.25 Reactive distillation column design for ETBE binary -element system at 15 atm.

#### 4.6.2.2 Step 2b: Optimal design-control issues

Differential driving force diagram (*Figure 4.39E*) shows a similar curve with unique minima as Case study 1. Hence, similar conclusion follows.

### 4.6.3 Step 3: Verification through simulation and analysis

#### 4.6.3.1 Step 3a: Control structure verification

Similarly as Case study 1,  $RGA$  and  $N_I$  are calculated using the linearized state space model (*Table 4.11*). Since the values are close to unity and positive respectively, it can be deduced that the control loop interaction is minimal.

### 4.6.3.2 Step 3b: Dynamic open loop and closed loop analysis

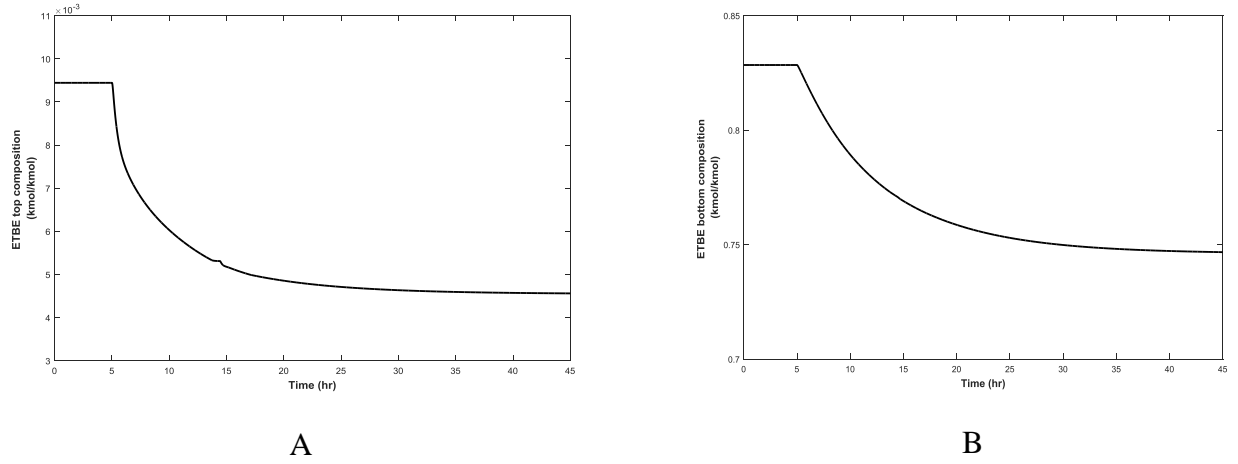


Figure 4.26 Open-loop response of the optimal design control solution to step change in feed flow rate, Case study 5: A) top; B) bottom.

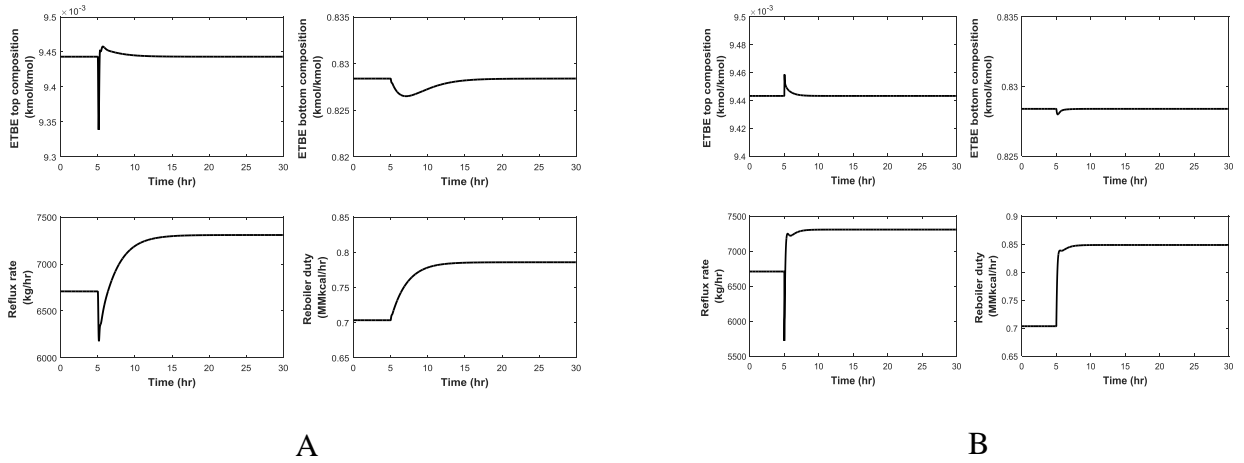
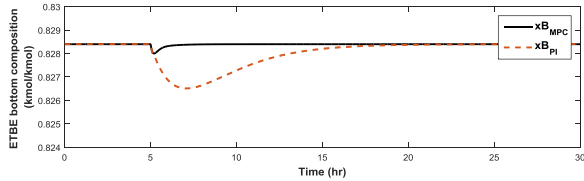
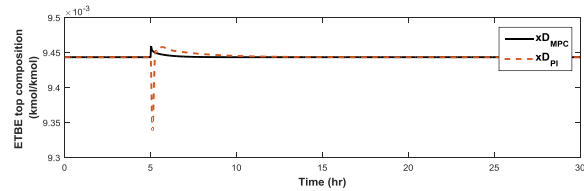
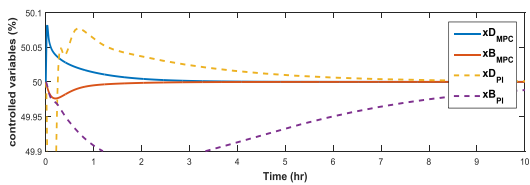
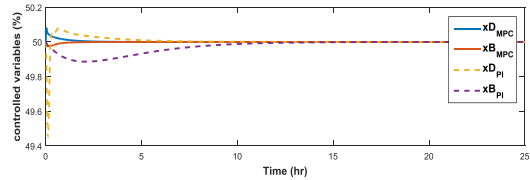


Figure 4.27 Close-loop response of the optimal design control solution for step change in feed flow rate, Case study 5: A) PI controller; B) MPC controller



A



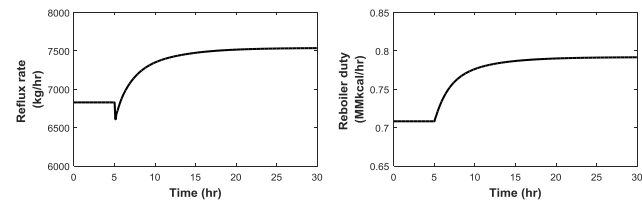
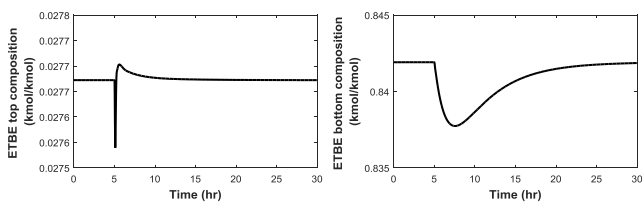
B

Figure 4.28 Comparison between controlled outputs under MPC and PI controllers for the design-control solution, Case study 5: A) composition B) percent deviation

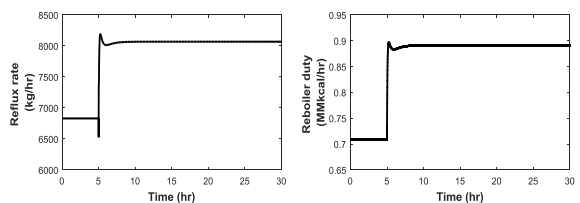
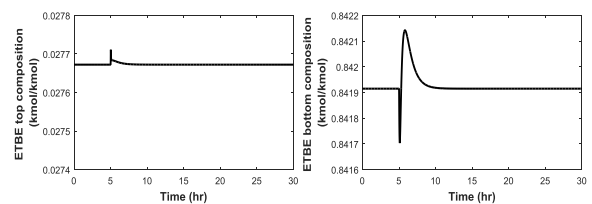
#### 4.6.3.3 Step 3c: Final selection

The parameters in Equation 4.1 are calculated and listed in Table 4.13.

#### 4.6.4 Step 4: Comparison with RD design not at the maximum driving force



A



B

Figure 4.29 Close-loop response of the alternative design for step change in feed flow rate, Case study 5: A) PI controller; B) MPC controller.

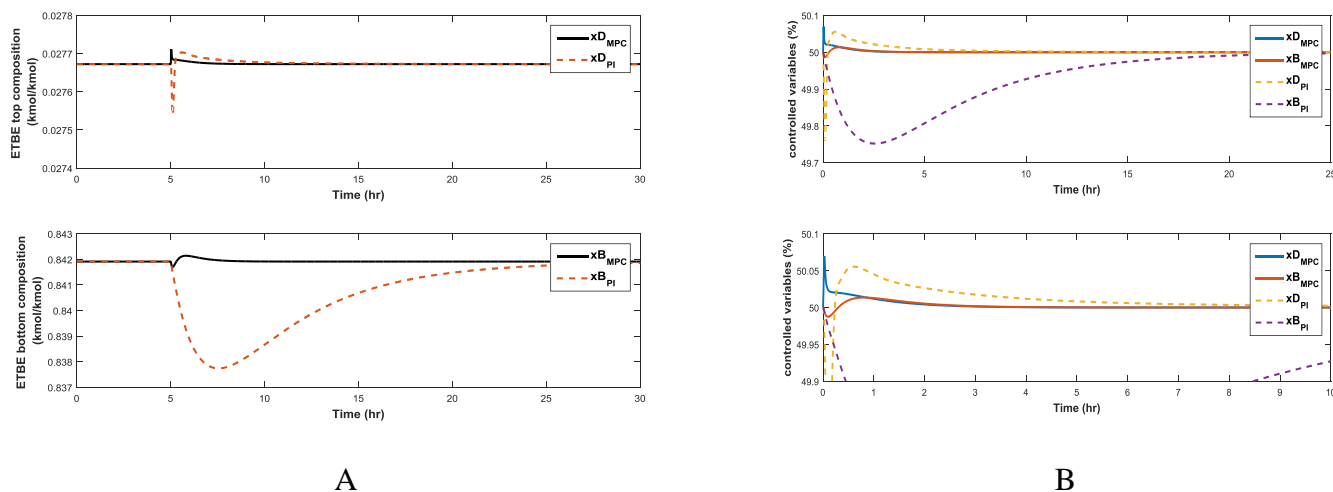


Figure 4.30 Comparison between controlled outputs under MPC and PI controllers for the alternative design, Case study 5: A) composition B) percent deviation.

To compare the performance with design-control solution, the parameters are calculated and listed in *Table 4.17*.

## 4.7 Case study 6: TAME production

### 4.7.1 Step 1: Data collection and problem formulation

Luyben, 2013 considered three simultaneous reversible reactions for the production of TAME, together with recycle streams and prereactor. However, in this study a simplified RD process is demonstrated that achieves comparable TAME purity at the bottom by incorporating a binary element reactive system. For that purpose, only the reaction between 2-methyl-1-butene (2M1B) and methanol to produce TAME is considered. This liquid phase reversible reaction can be expressed as follows:



The reaction kinetics for TAME synthesis are proposed by several researchers (Baur et al., 2003) (Al-Arfaj & Luyben, 2004). This study uses the simple power law model, with the kinetics parameters for the forward and reverse reactions proposed by Al-Arfaj & Luyben, 2004. The

feed conditions for the production of TAME are taken from Luyben, 2013, and rescaled for 100 kmol/hr feed flow rate. At the operating pressure, methanol forms an azeotrope. Therefore, the distillate from the reactive column contains 26-28% methanol. The design targets and product specifications are summarized in *Table 4.6*. Note however, that the primary design target is to achieve high purity TAME (> 97%) at the bottom of the reactive column.

Table 4.6 Design targets and product specifications for TAME system.

Component	Molar composition		
	Feed	Distillate	Bottom
2M1B (C <sub>5</sub> H <sub>10</sub> )	0.6	-	-
Methanol (CH <sub>4</sub> O)	0.4	< 0.28	-
TAME (C <sub>6</sub> H <sub>14</sub> O)	0.0	-	> 0.97
Feed flowrate: 100 kmol/h; Feed temperature and Pressure: 356K and 4 bar.			

The choice of elements and corresponding element matrix are given in

*Table 4.8*.

## 4.7.2 Step 2: Integrated Design-Control

### 4.7.2.1 Step 2a: Design Issues

Wilson model is selected to calculate liquid phase activity coefficients and SRK equation is used to calculate the vapor phase fugacity coefficients. The resulting  $T - W_A^l - W_A^v$  phase diagrams is shown in *Figure 4.37* (F). Using the VLE data, the corresponding reactive driving force diagram is constructed as illustrated in *Figure 4.38* (F).

Following the same steps as mentioned in Case study 1, the RD column is designed using the driving force diagram. The result of application of reactive McCabe-Thiele method is shown below.



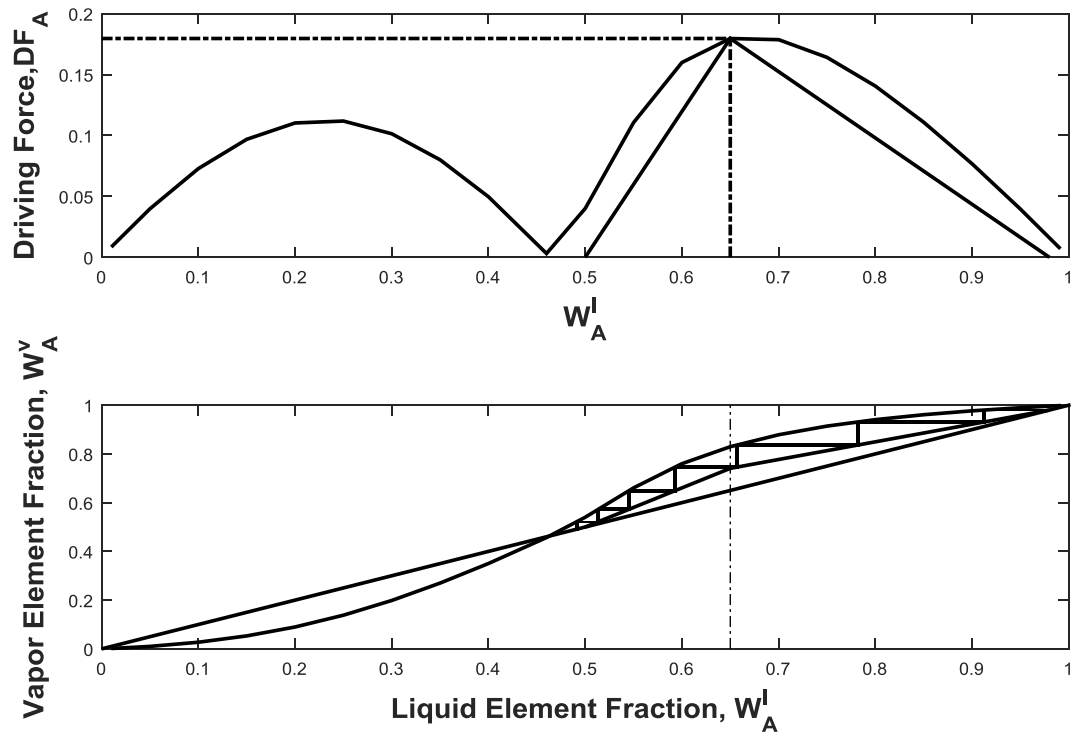


Figure 4.31 Reactive distillation column design for TAME at 4 bar.

#### 4.7.2.2 Step 2b: Optimal design-control issues

The differential driving force diagram (*Figure 4.39F*) suggests that the design at the maximum driving force should be optimally controllable, since the sensitivity to feed disturbance is minimum at the maximum driving force.

### 4.7.3 Step 3: Verification through simulation and analysis

#### 4.7.3.1 Step 3a: Control structure verification

The  $RGA$  and  $N_I$  values supports the conclusion obtained using the driving force diagram, i.e., the system is very easily controllable as the loop interaction is minimal.

### 4.7.3.2 Step 3b: Dynamic Open loop and closed-loop analysis

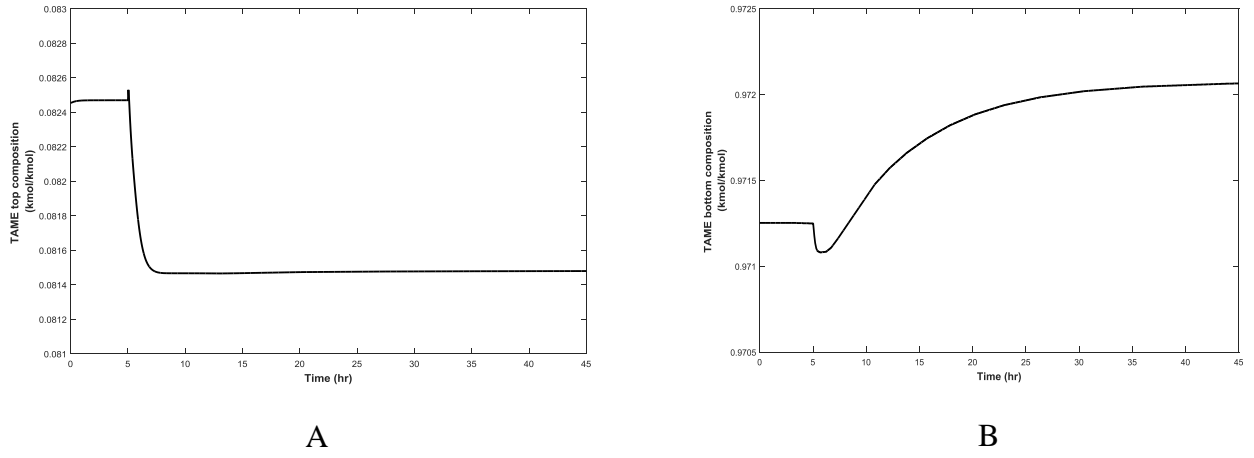


Figure 4.32 Open-loop response of the optimal design control solution to step change in feed flow rate, Case study 6: A) top; B) bottom.

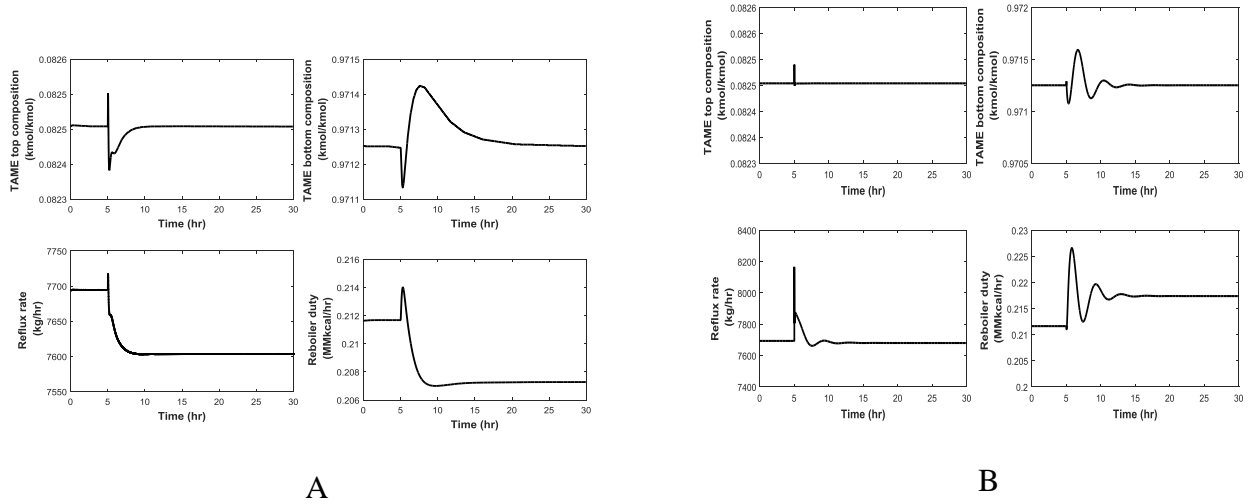
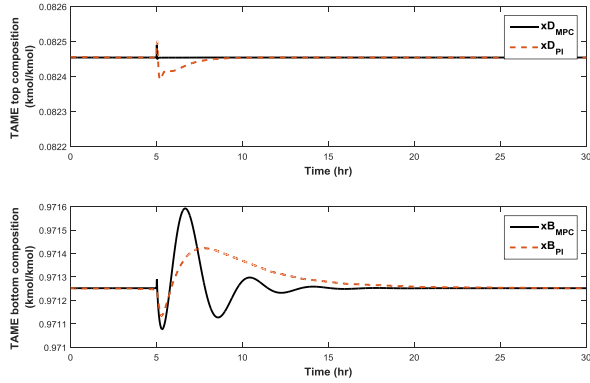
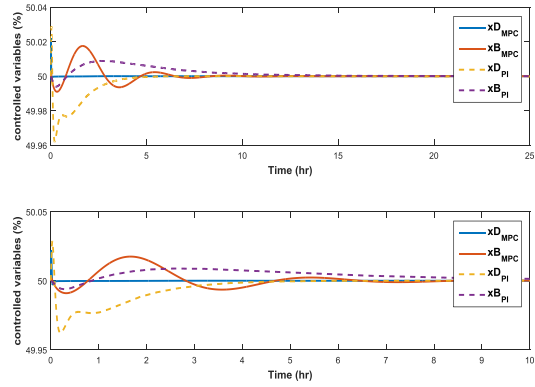


Figure 4.33 Close-loop response of the optimal design control solution for step change in feed flow rate, Case study 6: A) PI controller; B) MPC controller



A



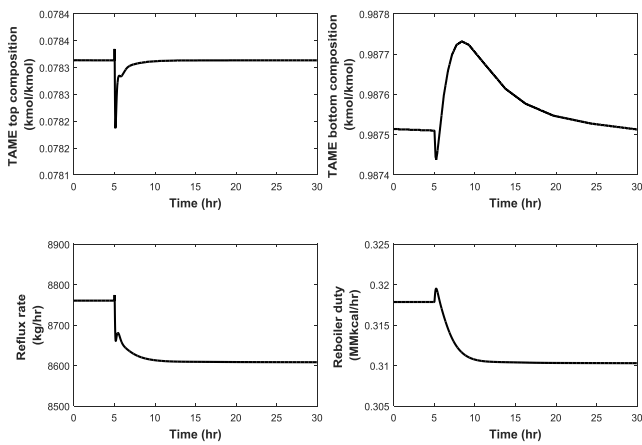
B

Figure 4.34 Comparison between controlled outputs under MPC and PI controllers for the design-control solution, Case study 6: A) composition B) percent deviation

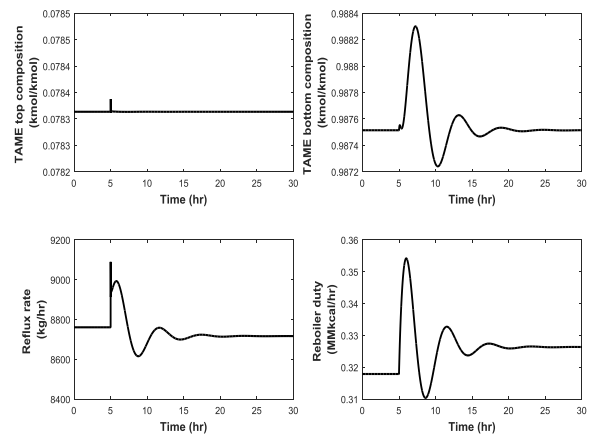
### 4.7.3.3 Step 3c: Final selection

The objective function values are calculated and summarized in Table 4.13.

### 4.7.4 Step 4: Comparison with RD design not at the maximum driving force



A



B

Figure 4.35 Close-loop response of the alternative design for step change in feed flow rate, Case study 6: A) PI controller; B) MPC controller

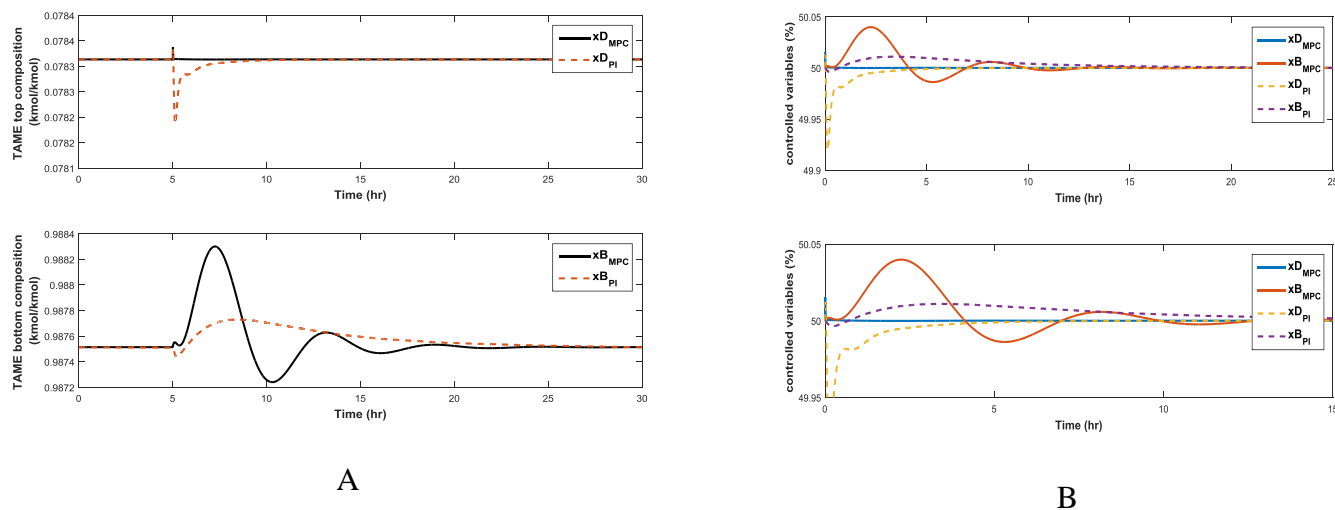


Figure 4.36 Comparison between controlled outputs under MPC and PI controllers for the alternative design, Case study 6: A) composition B) percent deviation

Finally, the performance comparison between design-control solution and alternative design is summarized in *Table 4.17*.

#### 4.8 Summarized results and discussions

Table 4.7 Key information for problem formulation (step 1).

Case study	Reactions	Catalyst	Number of elements	Main design target	Number of Feed
1	isobutene + methanol $\leftrightarrow$ MTBE	Sulfuric acid	2	MTBE > 80% at bottom	single
2	isobutene + methanol $\leftrightarrow$ MTBE	Acidic catalyst	3	MTBE > 90% at bottom	single

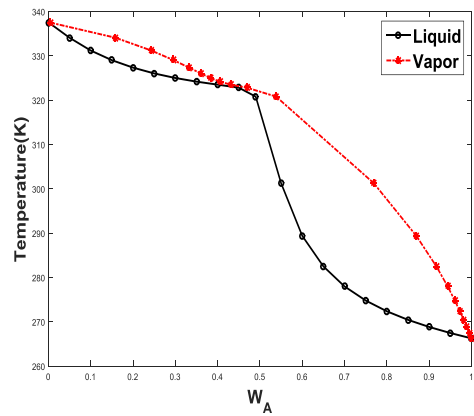
3	$\text{MeOH} + \text{HOAc} \rightleftharpoons \text{MeOAc} + \text{Water}$	Sulfuric acid	3	MeOAc > 99% at distillate	double
4	$2 \text{ Toluene} \rightleftharpoons \text{Benzene} + o\text{-xylene}$	zeolite	2	Benzene > 97% at distillate	single
5	$\text{isobutene} + \text{ethanol} \rightleftharpoons \text{ETBE}$	Ion exchange resin	2	ETBE > 80% at bottom	single
6	$2\text{M1B} + \text{methanol} \rightleftharpoons \text{TAME}$	Acid ion exchange resin	2	TAME > 97% at bottom	single

Table 4.8 The element matrix and element reaction for the binary element reactive systems.

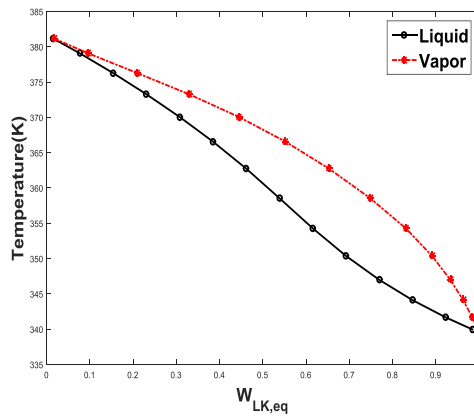
Case study	Element definition and reaction	Components	Formula Matrix	
			A	B
1	$A = \text{C}_4\text{H}_8$ ; $B = \text{CH}_4\text{O}$ $A + B \rightleftharpoons AB$	Isobutene ( $\text{C}_4\text{H}_8$ )	1	0
		Methanol ( $\text{CH}_4\text{O}$ )	0	1
		MTBE ( $\text{C}_5\text{H}_{12}\text{O}$ )	1	1
4	$A = \text{C}_6\text{H}_6$ $B = \text{CH}_2$ $2AB \rightleftharpoons A + AB_2$	Benzene ( $\text{C}_6\text{H}_6$ )	1	0
		Toluene ( $\text{C}_6\text{H}_6(\text{CH}_2)$ )	1	1
		<i>o</i> -xylene ( $\text{C}_6\text{H}_6(\text{CH}_2)_2$ )	1	2
5	$A = \text{C}_4\text{H}_8$ ; $B = \text{C}_2\text{H}_6\text{O}$ $A + B \rightleftharpoons AB$	Isobutene ( $\text{C}_4\text{H}_8$ )	1	0
		Ethanol ( $\text{C}_2\text{H}_6\text{O}$ )	0	1
		ETBE( $\text{C}_6\text{H}_{14}\text{O}$ )	1	1
6	$A = \text{C}_5\text{H}_{10}$ $B = \text{CH}_4\text{O}$ $A + B \rightleftharpoons AB$	2M1B ( $\text{C}_5\text{H}_{10}$ )	1	0
		methanol ( $\text{CH}_4\text{O}$ )	0	1
		TAME ( $\text{C}_6\text{H}_{14}\text{O}$ )	0	1

Table 4.9 The element matrix and element reaction for the multi-element reactive systems.

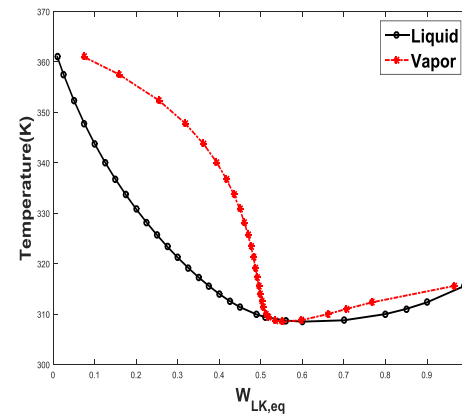
Case study	Element definition and reaction	Components	Formula Matrix		
			A	B	C
2	$A = C_4H_8$ $B = CH_4O$ $C = C_4H_8$ (isomer) $A + B + C \longleftrightarrow AB + C$	Isobutene ( $C_4H_8$ )	1	0	0
		Methanol ( $CH_4O$ )	0	1	0
		MTBE ( $C_5H_{12}O$ )	1	1	0
		1-butene( $C_4H_8$ )	0	0	1
3	$A = CH_4O$ $B = C_2H_2O$ $C = H_2O$ $A + BC \longleftrightarrow AB + C$	Methanol ( $CH_4O$ )	1	0	0
		Acetic Acid ( $C_2H_4O_2$ )	0	1	1
		Methyl Acetate ( $C_3H_6O_2$ )	1	1	0
		Water ( $H_2O$ )	0	0	1



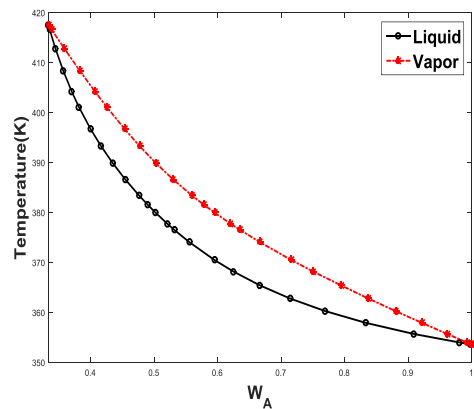
A



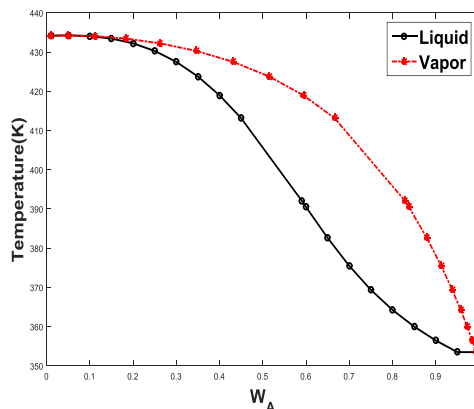
B



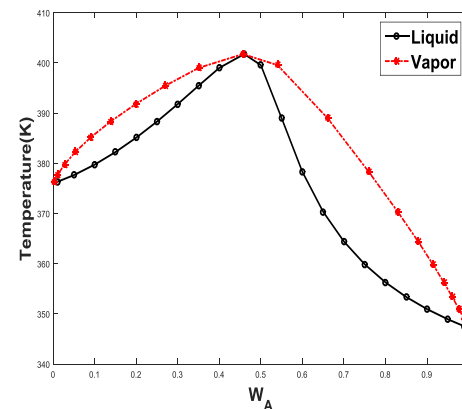
C



D



E



F

Figure 4.37 Calculated VLE phase diagram for the 6 reactive systems; A) MTBE without inert (1 atm); B) MTBE with inert (11 atm); C) Methyl-acetate (1 atm); D) Toluene disproportionation (1 atm); E) ETBE (15 atm); F) TAME (4 bar).

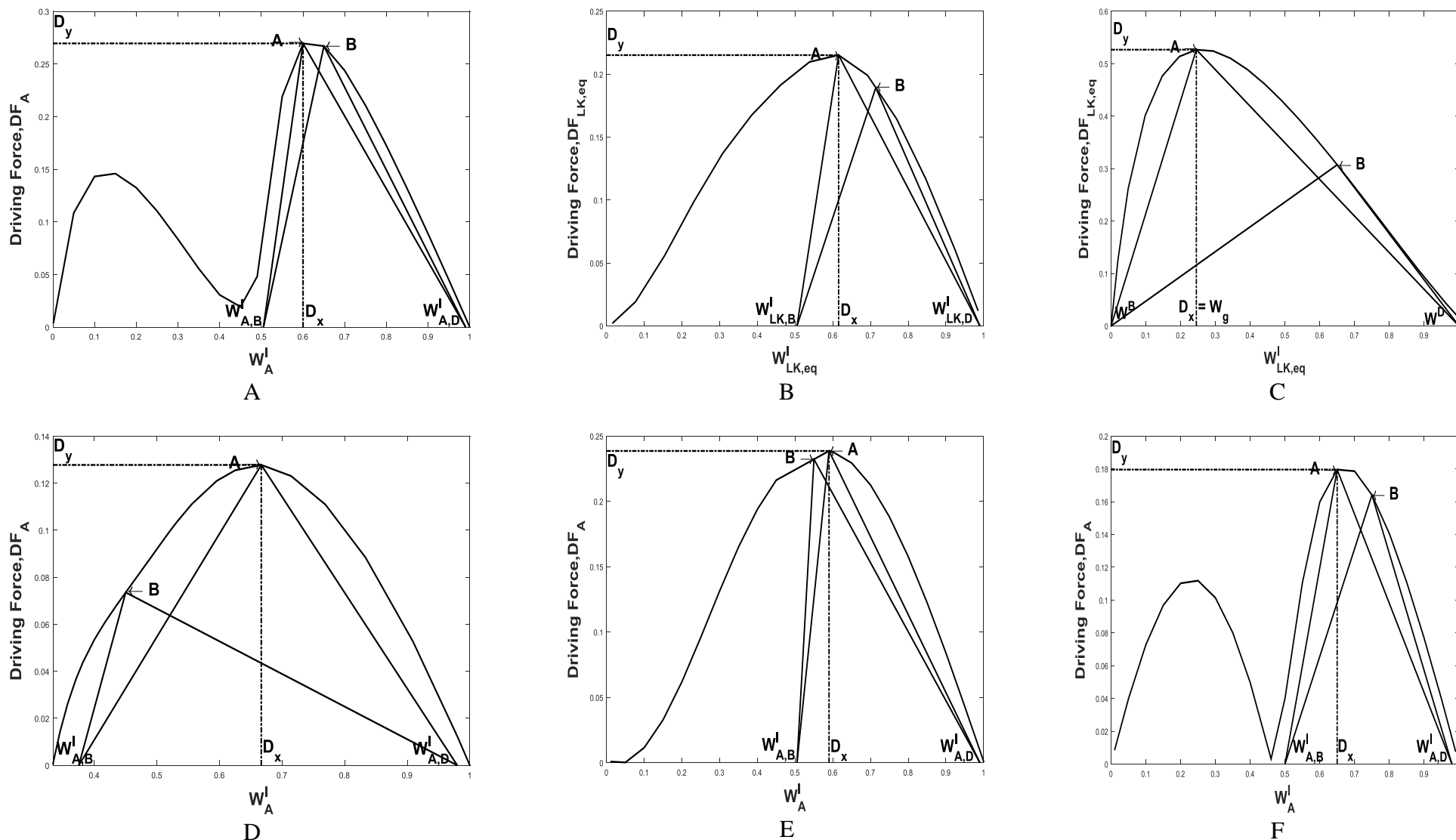
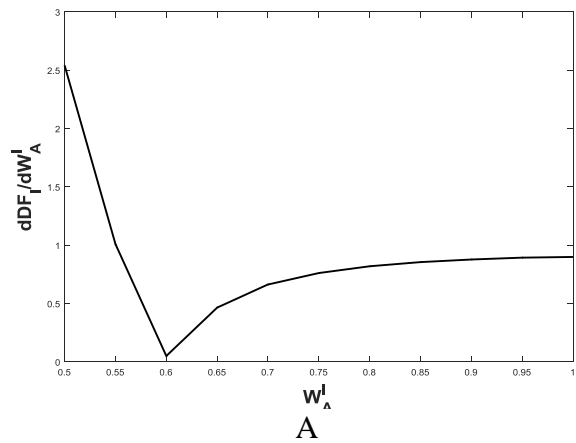


Figure 4.38 Calculated reactive driving force diagram for the 6 reactive systems; A) MTBE without inert (1 atm); B) MTBE with inert (11 atm); C) Methyl-acetate (1 atm); D) Toluene disproportionation (1 atm); E) ETBE (15 atm); F) TAME (4 bar).

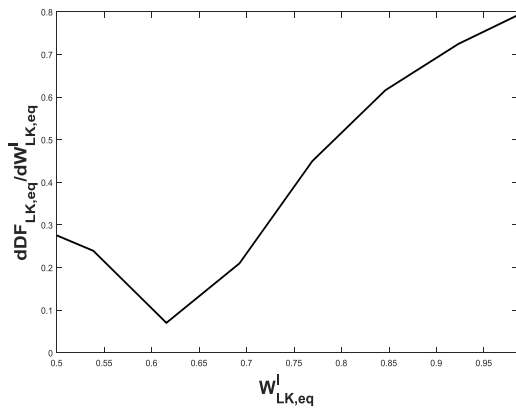


Table 4.10 Summary of design parameters for design-control solutions and alternative designs.

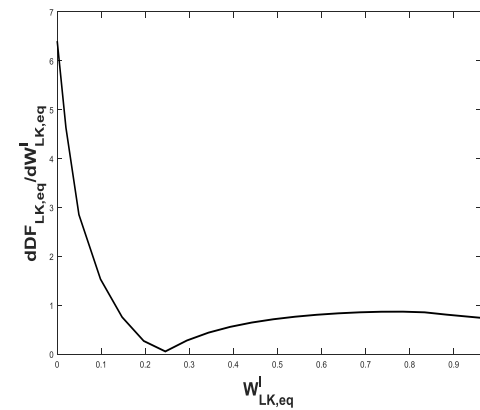
Case studies	Design	Number of stages	Feed stage		Reflux ratio	Reboiler duty (kW)	Condenser duty (kW)	Total Carbon Footprint (CO <sub>2</sub> eq per kg feed)
1	Design-Control solution	6	2		3.88	421.22	1296.11	0.195297
	Alter. 1	6	3		5	616.69	1490.57	0.230943
2	Design-Control solution	7	4		2.813	427.53	530.8	0.094138
	Alter. 1	7	2		7	1055.74	1162.44	0.211983
3	Design-Control solution	45	7	12	1.86	3110.34	5244.92	0.197642
	Alter. 1	45	9	12	6.28	6075.34	8059.79	0.317962
4	Design-Control solution	13	6		7.51	930.98	2961.04	0.23594
	Alter. 1	13	8		9	1448.46	3478.34	0.28614
5	Design-Control solution	6	3		3	818.108	729.646	0.126743
	Alter. 1	6	4		3	823.797	740.773	0.128382
6	Design-Control solution	9	4		2.6326	246.134	1248.96	0.160808
	Alter. 1	9	3		3	369.664	1370.41	0.180676



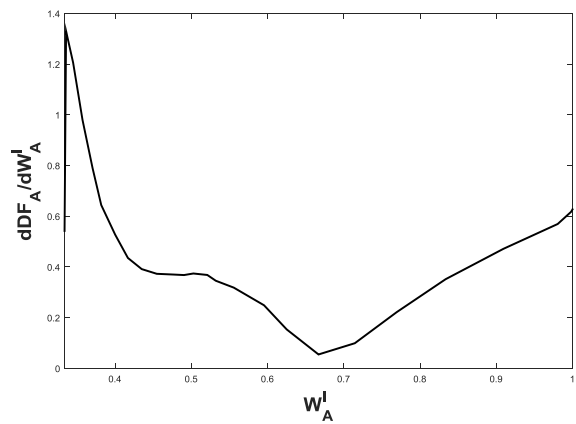
A



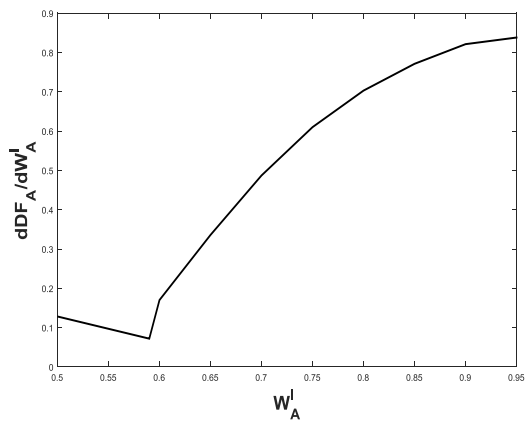
B



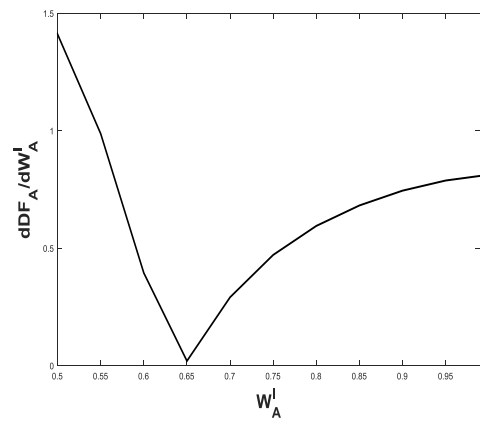
C



D



E



F

Figure 4.39 Calculated reactive differential driving force diagram for the 6 reactive systems; A) MTBE without inert (1 atm); B) MTBE with inert (11 atm); C) Methyl-acetate (1 atm); D) Toluene disproportionation (1 atm); E) ETBE (15 atm); F) TAME (4 bar).

Table 4.11 *RGA*, Niederlinski index ( $N_I$ ) and system stability for the design at the maximum driving force.

Case studies	Relative Gain Array ( <i>RGA</i> )	Niederlinski index ( $N_I$ )	Stability
1	$\begin{bmatrix} 1.26 & -0.26 \\ -0.26 & 1.26 \end{bmatrix}$	0.7919	Stable
2	$\begin{bmatrix} 1.26 & -0.26 \\ -0.26 & 1.26 \end{bmatrix}$	0.7914	Stable
3	$\begin{bmatrix} 1.09 & -0.09 \\ -0.09 & 1.09 \end{bmatrix}$	0.9110	Stable
4	$\begin{bmatrix} 0.85 & 0.15 \\ 0.15 & 0.85 \end{bmatrix}$	1.2101	Stable
5	$\begin{bmatrix} 0.98 & 0.02 \\ 0.02 & 0.98 \end{bmatrix}$	1.0263	Stable
6	$\begin{bmatrix} 1.10 & -0.10 \\ -0.10 & 1.10 \end{bmatrix}$	0.7662	Stable

Table 4.12 Disturbance scenarios

Case studies	Disturbance scenarios	
1	+10% step change in isobutene flow rate.	
2	+16.5% step change in methanol flow rate.	
3	Disturbance 1	Disturbance 2
	+10% step change in methanol	+10% step change in acetic acid
4	+5% step change in Toluene flow rate.	
5	+10% step change in isobutene flow rate.	
6	+10% step change in 2M1B flow rate.	

Table 4.13 Performance objective function values of PI and MPC controller for Case study 1,2,4,5 & 6 at the design-control solution

Objective function parameter	Case study 1	Case study 2	Case study 4	Case study 5	Case study 6
$J_1$ [KW]	1717.33	958.34	3892.02	1547.75	1495.09
$J_{2,D}$ [hr] (PI)	6.06E-07	0.0010	4.19E-05	4.7E-05	8.96E-05
$J_{2,D}$ [hr] (MPC)	6.2E-10	1.65E-07	5.84E-04	7.75E-06	1.24E-06
$J_{2,B}$ [hr] (PI)	7.7E-04	9.84E-04	0.0058	0.0107	0.0010
$J_{2,B}$ [hr] (MPC)	4E-05	7.48E-04	2.2E-05	2.9E-04	7.42E-04

$J_{3,D}$ [-] (PI)	378.19	803.3	1.84E+03	1.66E+03	138.99
$J_{3,D}$ [-] (MPC)	264.3	2.4E+03	2.05E+03	1.64E+03	696.48
$J_{3,B}$ [-] (PI)	0.008	4585	0.047	0.0825	0.0097
$J_{3,B}$ [-] (MPC)	0.0062	6.01E+04	0.0791	0.1377	0.0420
$J_4$ [-]	$\begin{bmatrix} 1.26 & -0.26 \\ -0.26 & 1.26 \end{bmatrix}$	$\begin{bmatrix} 1.26 & -0.26 \\ -0.26 & 1.26 \end{bmatrix}$	$\begin{bmatrix} 0.85 & 0.15 \\ 0.15 & 0.85 \end{bmatrix}$	$\begin{bmatrix} 0.98 & 0.02 \\ 0.02 & 0.98 \end{bmatrix}$	$\begin{bmatrix} 1.10 & -0.10 \\ -0.10 & 1.10 \end{bmatrix}$
$J_5$ [-]	0.7919	0.7915	1.21	1.026	0.7662
$J_6$ [CO <sub>2</sub> eq per kg feed]	0.195297	0.094138	0.23594	0.126743	0.160808

Table 4.14 RGA, Niederlinski index ( $N_I$ ) and system stability for the alternative designs

Case studies	Relative Gain Array (RGA)	Niederlinski index ( $N_I$ )	Stability
1	$\begin{bmatrix} -1.58 & 2.58 \\ 2.58 & -1.58 \end{bmatrix}$	-0.629	Unstable
2	$\begin{bmatrix} 1.41 & -0.41 \\ -0.41 & 1.41 \end{bmatrix}$	0.706	Stable
3	$\begin{bmatrix} 0.14 & 0.86 \\ 0.86 & 0.14 \end{bmatrix}$	7.288	Stable
4	$\begin{bmatrix} -0.32 & 1.32 \\ 1.32 & -0.32 \end{bmatrix}$	-3.0788	Unstable
5	$\begin{bmatrix} 0.82 & 0.18 \\ 0.18 & 0.82 \end{bmatrix}$	1.2076	Stable
6	$\begin{bmatrix} 0.46 & 0.54 \\ 0.54 & 0.46 \end{bmatrix}$	2.168	Stable

Table 4.15 Performance objective parameter values of the PI and MPC controllers for Case study 3 at the design-control solution.

Case study 3	$J_1$ [KW]	$J_{2,D}$ [hr] (PI)	$J_{2,D}$ [hr] (MPC)	$J_{2,B}$ [hr] (PI)	$J_{2,B}$ [hr] (MPC)	$J_{3,D}$ [-] (PI)	$J_{3,D}$ [-] (MPC)	$J_{3,B}$ [-] (PI)	$J_{3,B}$ [-] (MPC)	$J_4$ [-]	$J_5$ [-]	$J_6$ [CO <sub>2</sub> eq per kg feed]
Dist. 1	8355.26	7.8E-05	0.0062	0.004	6.1E-04	1.57E+03	2.1E+04	0.718	11.48	$\begin{bmatrix} 1.09 & -0.09 \\ -0.09 & 1.09 \end{bmatrix}$	0.911	0.197642
Dist. 2		1.67E-04	0.0126	0.025	0.0042	3.2E+03	2.2E+04	2.007	15.64			

Table 4.16 Summary of the comparison of performance objective function terms for design-control solution and alternative designs for PI and MPC control structure for case study 1, 2 & 4.

Objective Function Parameter	Case study 1		Case study 2		Case study 4	
	Design-control solution	Alternative 1	Design-control solution	Alternative 1	Design-control solution	Alternative 1
$J_1$ [kW]	1717.33	2107.26	958.34	2218.18	3892.02	4926.8
$J_{2,D}$ [hr] (PI)	6.06E-07	2.88E-06	0.001	6.12E-04	4.19E-05	1.24E-04
$J_{2,D}$ [hr] (MPC)	6.2E-10	1.63E-08	1.65E-07	8.61E-06	5.84E-04	9.36E-04
$J_{2,B}$ [hr] (PI)	7.7E-04	0.0029	9.84E-04	0.0385	0.0058	0.1033
$J_{2,B}$ [hr] (MPC)	4E-05	2.57E-04	7.48E-04	7.4E-04	2.21E-05	2.58E-05
$J_{3,D}$ [-] (PI)	378.19	445.1	803.3	2867	1.84E+03	1.51E+03
$J_{3,D}$ [-] (MPC)	264.4	1.13E+03	2.4E+03	6.49E+03	2.05E+03	5.32E+03
$J_{3,B}$ [-] (PI)	0.008	0.0264	4585	48195	0.047	0.0753
$J_{3,B}$ [-]	0.0062	0.0422	6.02E+04	3.105E+05	0.0791	0.2361
$J_4$ [-]	$\begin{bmatrix} 1.26 & -0.26 \\ -0.26 & 1.26 \end{bmatrix}$	$\begin{bmatrix} -1.58 & 2.58 \\ 2.58 & -1.58 \end{bmatrix}$	$\begin{bmatrix} 1.26 & -0.26 \\ -0.26 & 1.26 \end{bmatrix}$	$\begin{bmatrix} 1.41 & -0.41 \\ -0.41 & 1.41 \end{bmatrix}$	$\begin{bmatrix} 0.85 & 0.15 \\ 0.15 & 0.85 \end{bmatrix}$	$\begin{bmatrix} -0.32 & 1.32 \\ 1.32 & -0.32 \end{bmatrix}$
$J_5$ [-]	0.7919	-0.687	0.7914	0.706	1.21	-3.07

Table 4.17 Summary of the comparison of performance objective function terms for design-control solution and alternative designs for PI and MPC control structure for case study 5 & 6.

Objective Function Parameter	Case study 5		Case study 6	
	Design-control solution	Alternative 1	Design-control solution	Alternative 1
$J_1$ [kW]	1547.754	1564.57	1495.094	1740.074
$J_{2,D}$ [hr] (PI)	4.7E-05	9.78E-05	8.96E-05	8.1E-05
$J_{2,D}$ [hr] (MPC)	7.75E-06	1.68E-05	1.24E-06	1.26E-06
$J_{2,B}$ [hr] (PI)	0.0107	0.0332	0.0010	0.0018
$J_{2,B}$ [hr] (MPC)	2.91E-04	3.96E-04	7.42E-04	0.0025
$J_{3,D}$ [-] (PI)	1.66E+03	1.15E+03	138.99	220.38
$J_{3,D}$ [-] (MPC)	1.64E+03	1.89E+03	696.4857	880.3836
$J_{3,B}$ [-] (PI)	0.0825	0.0834	0.0097	0.0109
$J_{3,B}$ [-]	0.1377	0.1828	0.0420	0.1170
$J_4$ [-]	$\begin{bmatrix} 0.98 & 0.02 \\ 0.02 & 0.98 \end{bmatrix}$	$\begin{bmatrix} 0.82 & 0.18 \\ 0.18 & 0.82 \end{bmatrix}$	$\begin{bmatrix} 1.1 & -0.1 \\ -0.1 & 1.1 \end{bmatrix}$	$\begin{bmatrix} 0.46 & 0.54 \\ 0.54 & 0.46 \end{bmatrix}$
$J_5$ [-]	1.026	1.2076	0.766197	2.168

Table 4.18 Summary of the comparison of the performance objective function terms for the design-control solution and the alternative designs for the PI and MPC control structure for case study 3.

Objective Function Parameter	Disturbance Scenario 1		Disturbance Scenario 2	
	Design-control solution	Alternative 1	Design-control solution	Alternative 1
$J_1$ [kW]	8355.26	14135.13	8355.26	14135.13
$J_{2,D}$ [hr] ( $x_{MeOAc}^D$ by R) (PI)	7.8E-05	10.1979	1.67E-04	0.0116
$J_{2,D}$ [hr] ( $x_{MeOAc}^D$ by R) (MPC)	0.0062	0.0454	0.0126	0.0055
$J_{2,B}$ [hr] ( $x_{water}^B$ by $Q_R$ ) (PI)	0.004	0.1145	0.025	0.0123

$J_{2,B}$ [hr] ( $x_{water}^B$ by $Q_R$ ) (MPC)	6.09E-04	0.1284	0.0042	0.0105
$J_{3,D}$ [-] (PI)	1.57E+03	7.86E+04	3.2E+03	5.04E+03
$J_{3,D}$ [-] (MPC)	2.1E+04	9.43E+04	2.26E+04	4.28E+04
$J_{3,B}$ [-] (PI)	0.718	33.2587	2.007	2.4028
$J_{3,B}$ [-] (MPC)	11.4826	36.92	15.64	25.4562
$J_4$ [-]	$\begin{bmatrix} 1.09 & -0.09 \\ -0.09 & 1.09 \end{bmatrix}$	$\begin{bmatrix} 0.14 & -0.86 \\ -0.86 & 0.14 \end{bmatrix}$	$\begin{bmatrix} 1.09 & -0.09 \\ -0.09 & 1.09 \end{bmatrix}$	$\begin{bmatrix} 0.14 & -0.86 \\ -0.86 & 0.14 \end{bmatrix}$
$J_5$ [-]	0.911	7.288	0.911	7.288
$J_6$ [CO <sub>2</sub> eq per kg feed]	0.197642	0.317962	0.197642	0.317962

As can be seen from Figure 4.2 - Figure 4.36, the closed-loop response under both the PI and MPC controller for the optimal design control solution which is operating at the maximum driving force, is able to reject the disturbance and restore the controlled variables to their original set-points with relatively small efforts in the manipulated variables in both the top and bottom loops. This was also expected from the RGA matrix since the values close to unity implying minimal interactions between the control loops, thereby, facilitating the disturbance rejection. For the alternative designs, the controller is not able to sufficiently restore all the controlled variables to their set points. Furthermore, a relatively longer settling time is observed in the controlled variables. The quantified results listed in Table 4.16 - Table 4.18 further verifies that moving away from the maximum driving force will result in a more difficult control of RD column, as indicated by greater values of integral absolute error (IAE) and variation of input (TV).

**CHAPTER 5**  
**OVERVIEW OF THE REACTIVE**  
**DISTILLATION TOOLBOX**



## 5 OVERVIEW OF THE REACTIVE DISTILLATION TOOLBOX

This chapter aims to give a walkthrough of the integrated design-control toolbox. As part of the walkthrough, a case study is selected, and the subsequent steady state simulation, dynamic state space model generation, MPC MATLAB script generation and simulation is shown.

### 5.1 The Reactive Distillation Toolbox

The Reactive Distillation toolbox works as a bridge between the user and the simulation and control software (ASPEN PLUS, MATLAB) by performing the following tasks:

1. Auto generating flowsheet
2. Auto generating MATLAB scripts
3. Providing a single user interface that facilitates problem setup, steady state simulation, dynamic closed loop MPC simulation and analysis of the responses.

As part of the overview of the toolbox, Case study 2 is selected. Note that the choice is arbitrary. The overview will consist of 3 sections as follows

1. Setting up steady state simulation
2. Generating state space matrices and MPC scripts
3. Running the simulation and observing the dynamic responses

### 5.2 Setting up steady state simulation

**Step 1:** Add the compounds (methanol, isobutene, 1-butene, and MTBE) by searching from the database by their CAS ID or Aspen ID or Chemical name. Click 'Next' to go to the next tab (Figure 5.1).

**Step 2:** Click 'Add Inlet' once, since this is a single feed process. After that click on the inlet arrow to enter the feed conditions and molar flow rates of the compounds as shown below.

**Step 3:** After entering the values, click 'Save'. After that click 'Next' to go to the next tab (Figure 5.2).

**Step 4:** In the 'Define Reactions' tab, enter the reaction stoichiometry, and the reaction order for both forward and backward reactions. After that, click 'Next' (Figure 5.3).

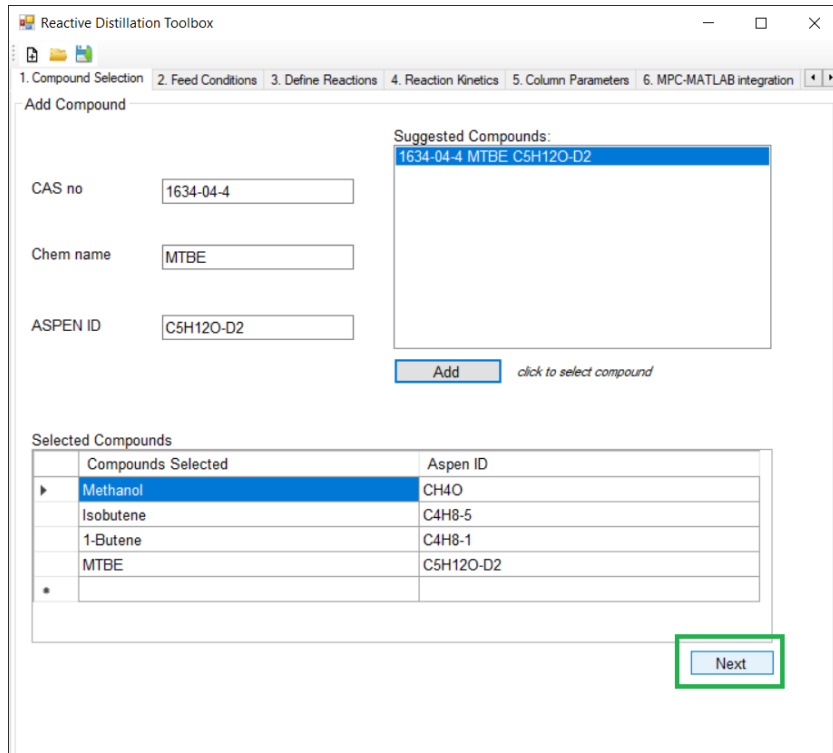


Figure 5.1 Compound selection

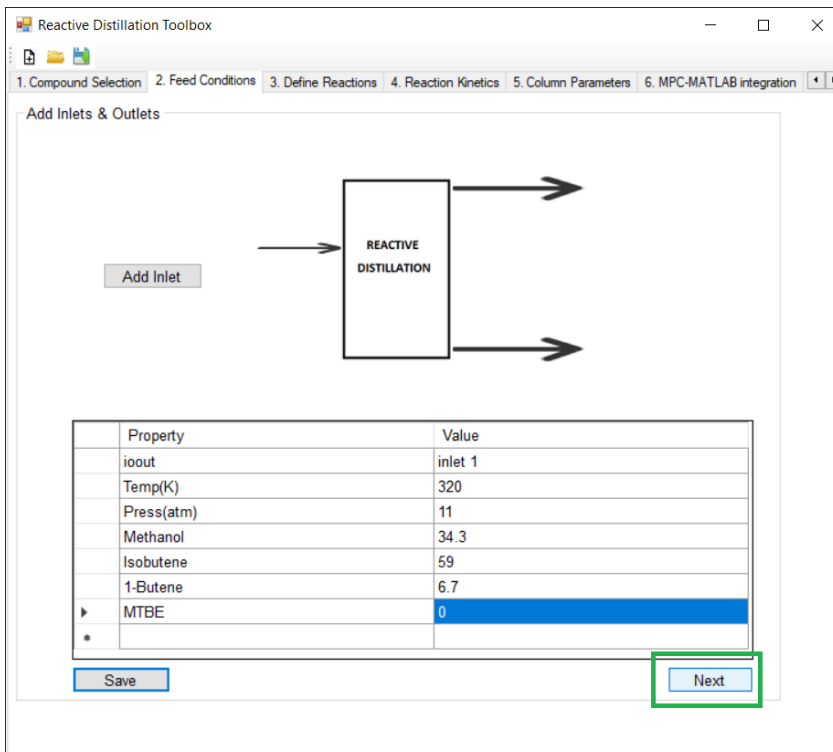


Figure 5.2 Feed specification

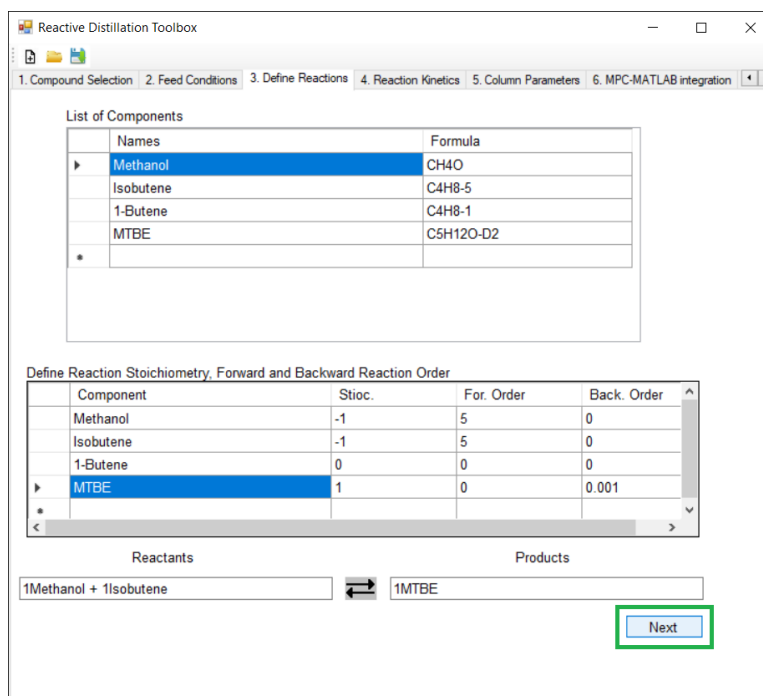


Figure 5.3 Reaction Definition

**Step 5:** In the 'Reaction Kinetics' tab, enter the pre-exponential factor, activation energy, and temperature exponent for the forward and backward reaction. Please note that the pre-exponential factor has to be entered in the SI unit, i.e,  $\text{kmol/s/m}^3$ . Activation energy values must be entered in  $\text{cal/mol}$  unit. If the reactive distillation is modeled using an irreversible reaction, enter 0 for both pre-exponential and activation energy values. Select light key and heavy key for the process in consideration. After that, click 'Next' to go the 'Column Parameters' tab (Figure 5.4).

**Step 6:** In this tab, in addition to the values required to specify the reactive distillation column, enter the converge algorithm to be used by ASPEN to solve the system of model equations (Figure 5.5).

**Step 7:** After clicking the 'Generate ASPEN input file' button, the aspen input file is generated in the debug folder as shown below (Figure 5.6).

**Step 8:** Load this aspen input file to ASPEN PLUS. The process flowsheet is auto generated. Note the 'Required Input Complete' is shown at the bottom left corner which confirms that the all required input values for steady-state simulation are successfully translated as shown in Figure 5.7.

Reactive Distillation Toolbox

1. Compound Selection | 2. Feed Conditions | 3. Define Reactions | 4. Reaction Kinetics | 5. Column Parameters | 6. MPC-MATLAB integration

Reaction Parameters

Rate constants:  $k = AT^m e^{-E/T}$

	Forward	Backward
Pre-Exponential Factor (A):	2.49E+07	1.85E+18
Activation Energy (E):	12600	31100
Temperature factor (m):	2	0

Element Selection

Light Key: Isobutene

Heavy Key: Methanol

Next

Figure 5.4 Reaction Kinetics

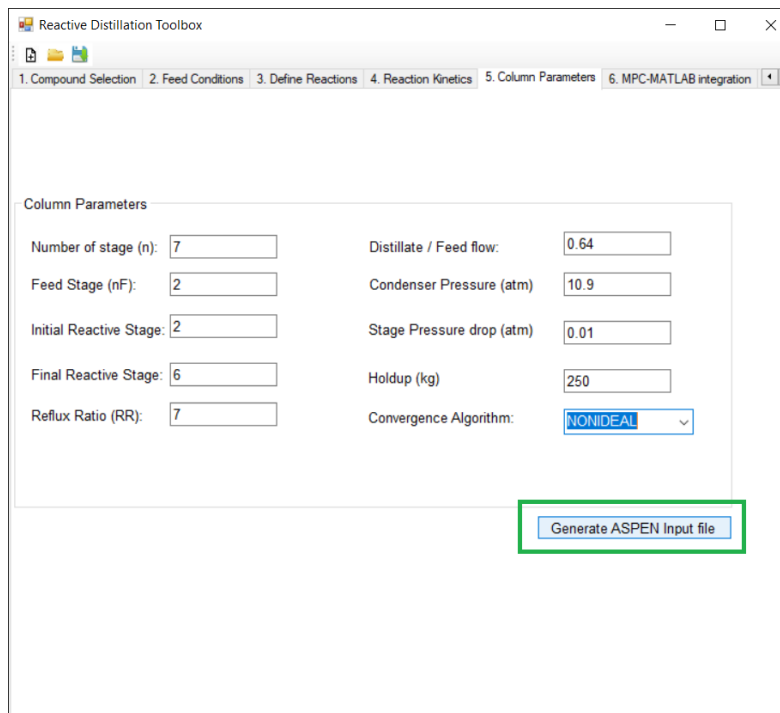


Figure 5.5 RD Column Design parameters

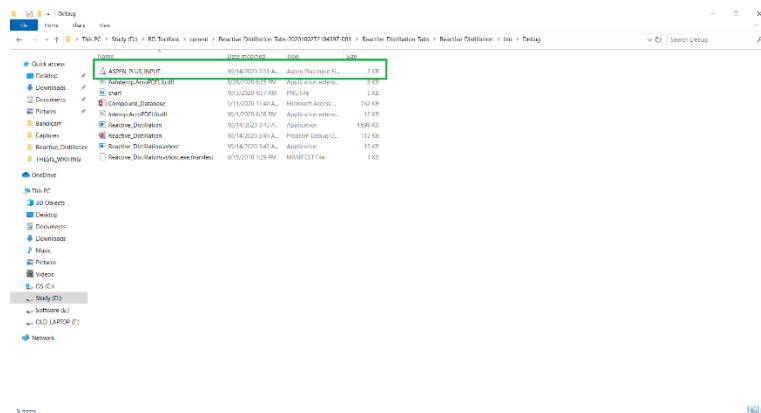


Figure 5.6 Aspen Input file generation

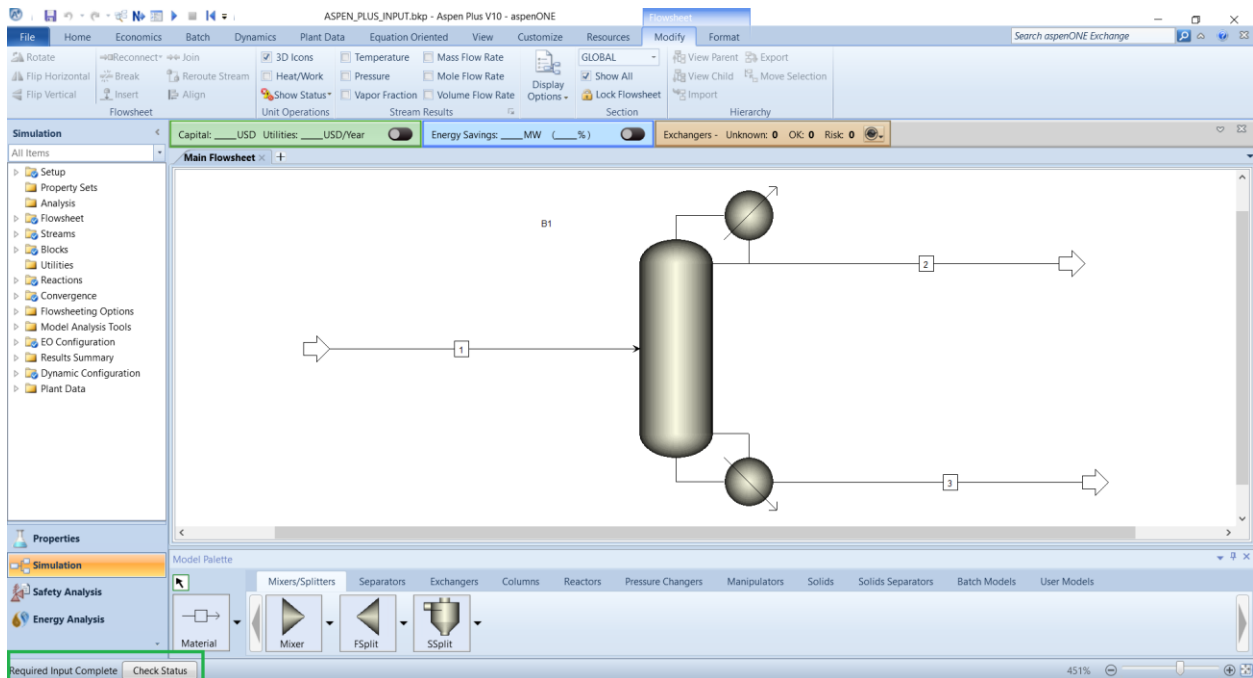


Figure 5.7 Input file translation to ASPEN PLUS

**Step 9:** Run the ASPEN PLUS to perform steady-state simulation as shown in Figure 5.8 . Observe that the steady-state simulation converges as 'Results Available' is displayed at the bottom left corner without any error.

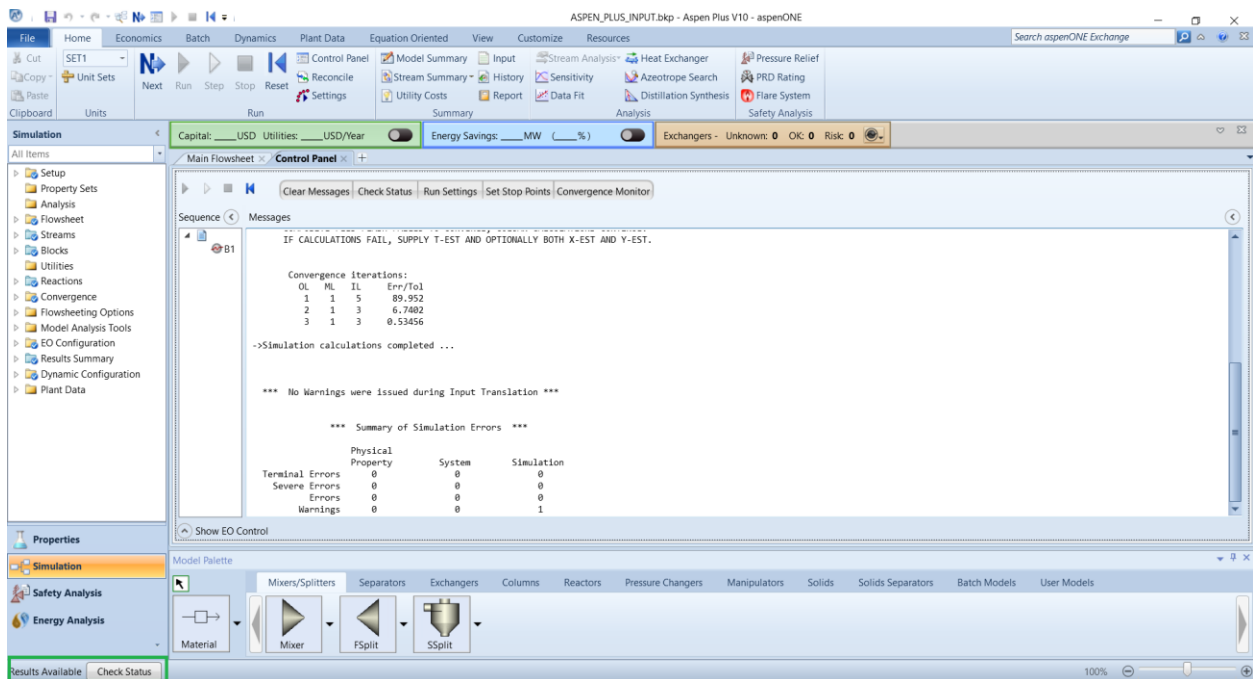


Figure 5.8 Converged steady state simulation

### 5.3 Generating state space matrices and MPC scripts

**Step 1:** After the successful steady state simulation switch to dynamic mode and provide the required dynamic data (reflux drum, sump level, hydraulics). Since for all the case studies, it is assumed that the pressure drop is negligible, export a flow driven dynamic model to ASPEN PLUS DYNAMICS as shown in Figure 5.9.

**Step 2:** Go back to the ‘MPC-MATLAB integration’ tab in the Reactive Distillation Toolbox. Specify the controlled variables, block names and disturbance streams. After that, click on the ‘Generate CDI script’ button as shown in Figure 5.10. The control-design interface (CDI) script is generated in the ‘debug’ folder as shown in Figure 5.11.

**Step 3:** In the generated ASPEN PLUS dynamic file, remove the controllers, initialize at time 0. After that, create a new script and load the contents in the generated CDI script as shown in Figure 5.12. Then, invoke the script, and the state space matrices are generated in the ‘debug’ folder as shown in Figure 5.13. Note that the DAT files contain the system state. Thus the user is relieved of manually writing the code for state space model generation.

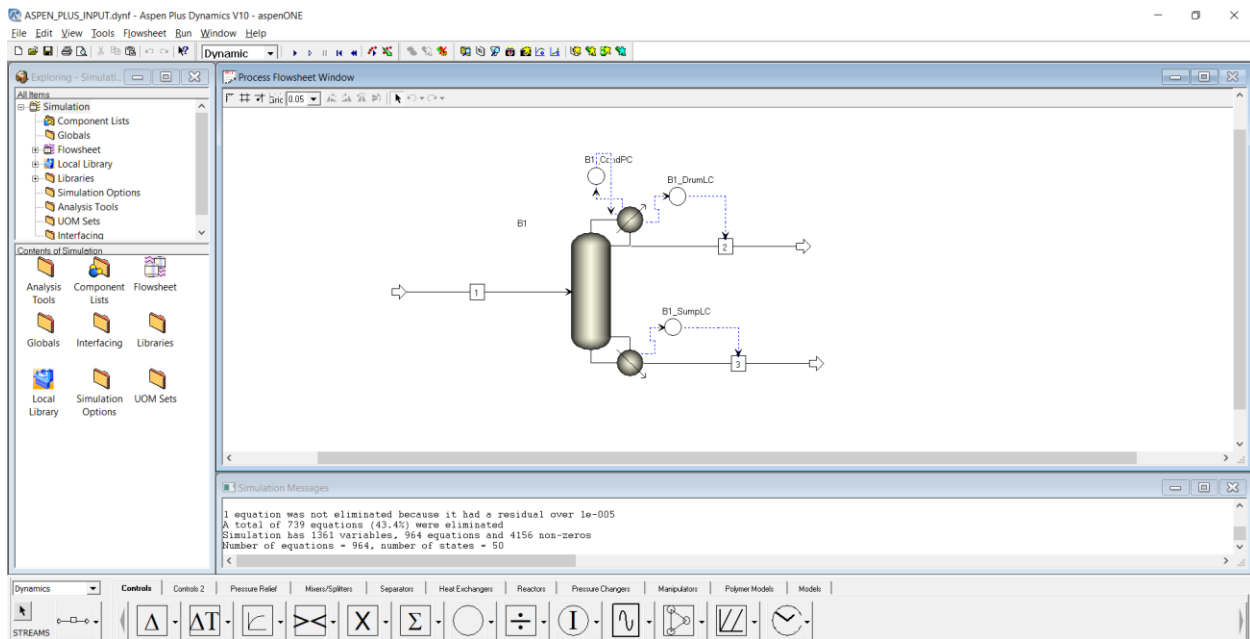


Figure 5.9 Flow driven ASPEN PLUS Dynamics file





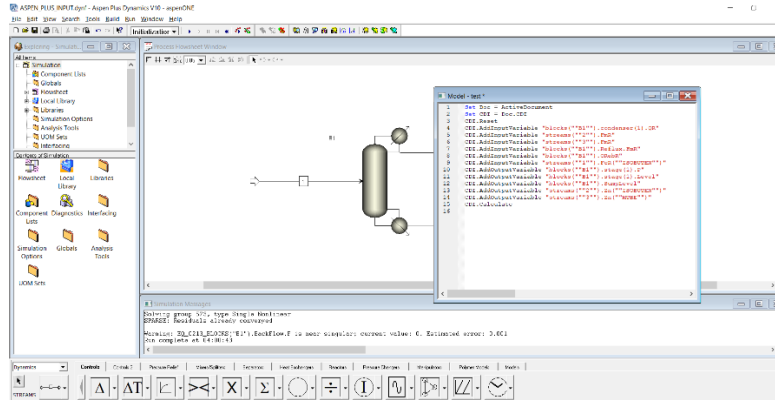


Figure 5.12 CDI script invoke

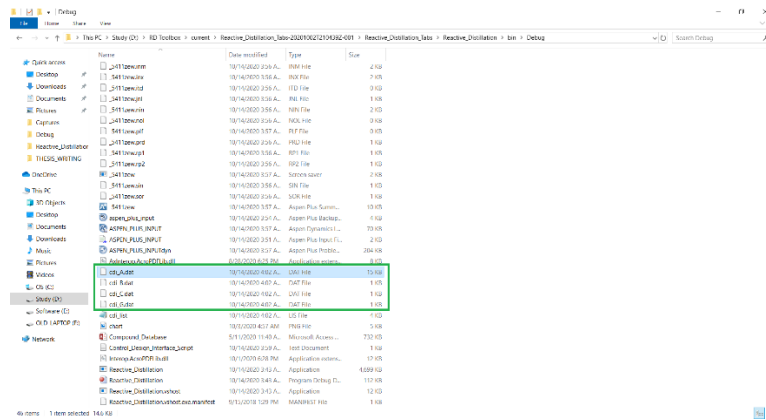


Figure 5.13 State space matrices generation

**Step 4:** provide the required values for MPC simulation. These include all the nominal values for controlled and manipulated variables, weights on the controlled and manipulated variables, weights on the rate of change of manipulated variables, simulation time and tuning parameters (prediction horizon, control horizon). After that click on the ‘MATLAB MPC m file’ as shown in Figure 5.14. Note that the m file is generated in the ‘debug’ folder as shown in Figure 5.15.

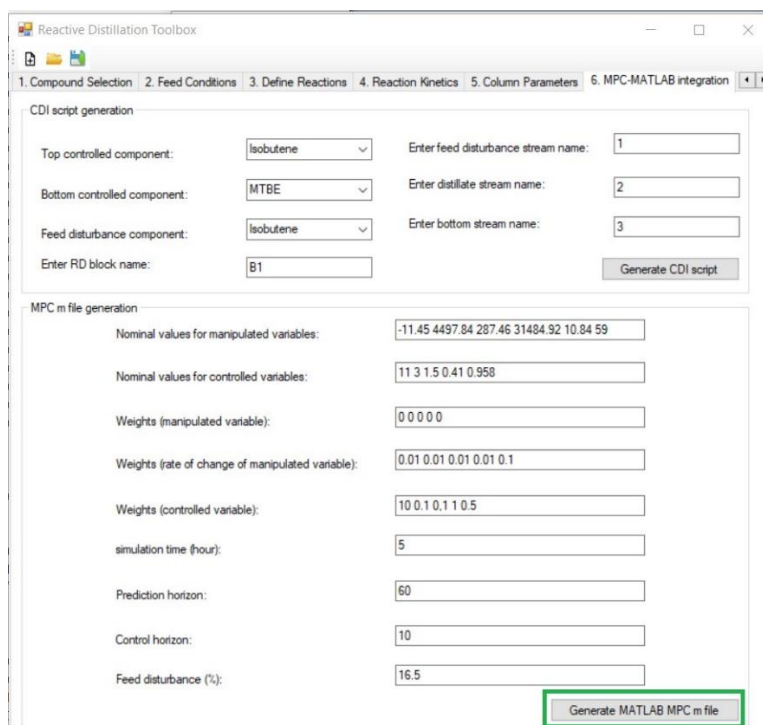


Figure 5.14 MATLAB MPC m file generation

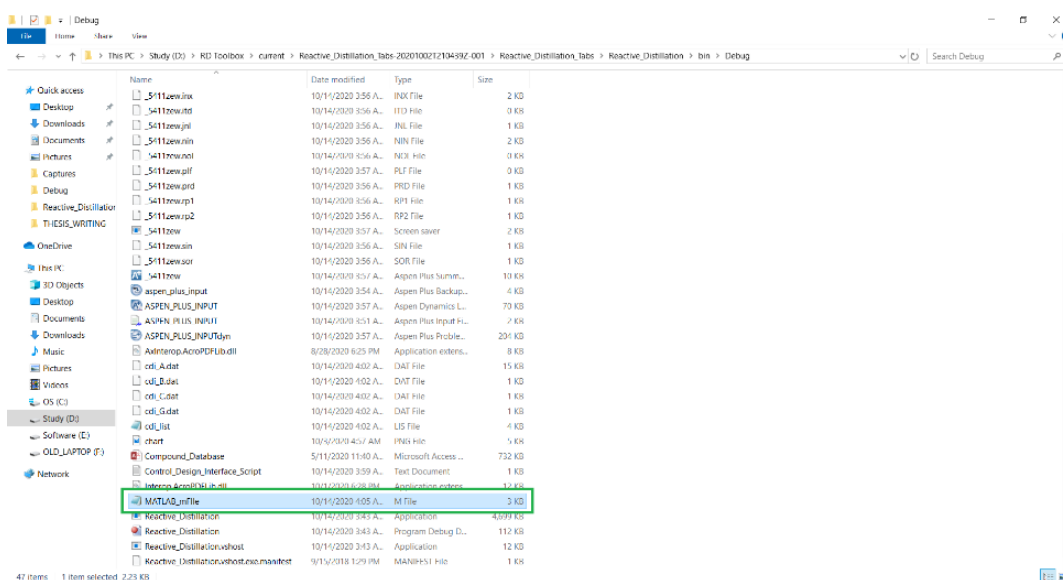


Figure 5.15 Generated m file for MPC simulation

## 5.4 Running the simulation and observing the dynamic responses

**Step 1:** Load the m file in MATLAB (Figure 5.16). After that run the program. When the simulation is complete, an excel file containing the closed loop data is generated as shown in Figure 5.17. Note that the code is auto generated. Thus the user is relieved of writing any code for MPC simulation.

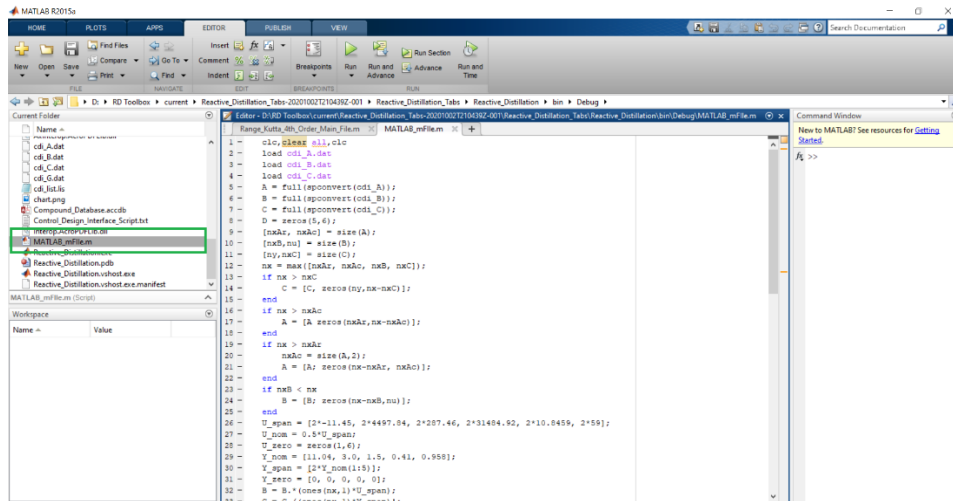


Figure 5.16 Opening MPC m file in MATLAB

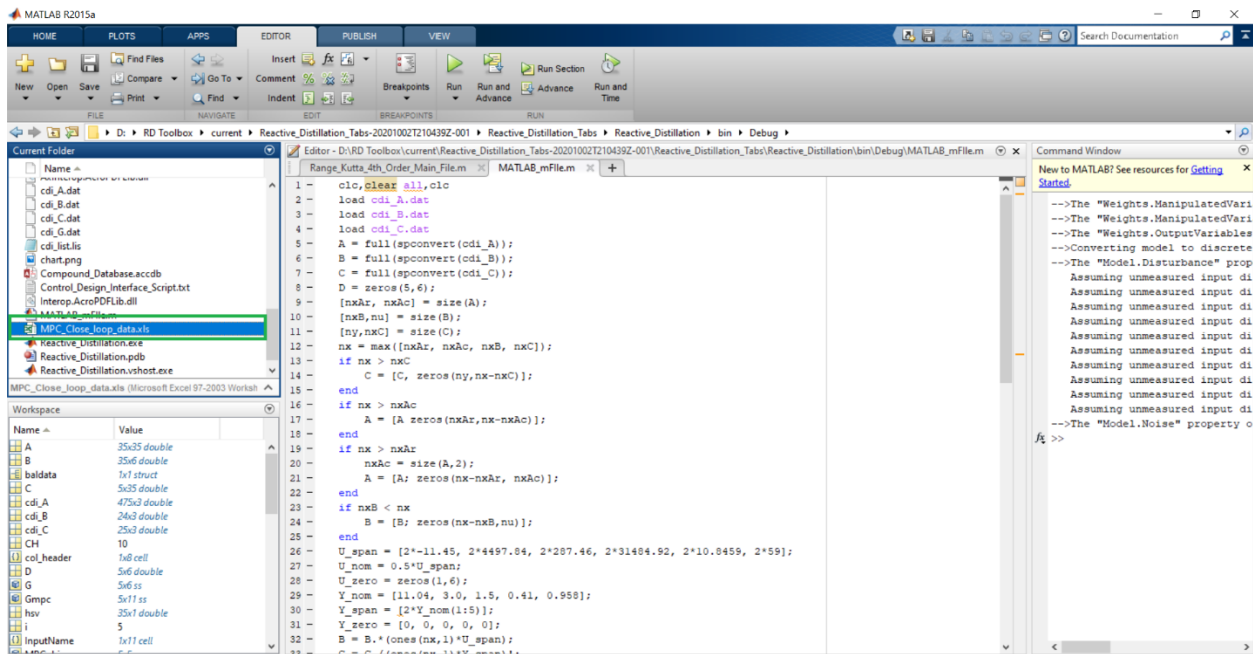


Figure 5.17 MPC simulation data

**Step 2:** To observe the response, go to the ‘Dynamic Response’ tab in the Reactive Distillation Toolbox. Click on the ‘Close Loop MPC’ sub tab. After that click on ‘Choose File’ button to locate the generated excel file. Specify the sheet name where the data is stored and click on ‘Load Data’. Then click on ‘Show Response’ button to observe the closed loop response as shown in Figure 5.18. Note that the MPC close loop simulation is based on percentage deviation where the nominal set point is at 50%.

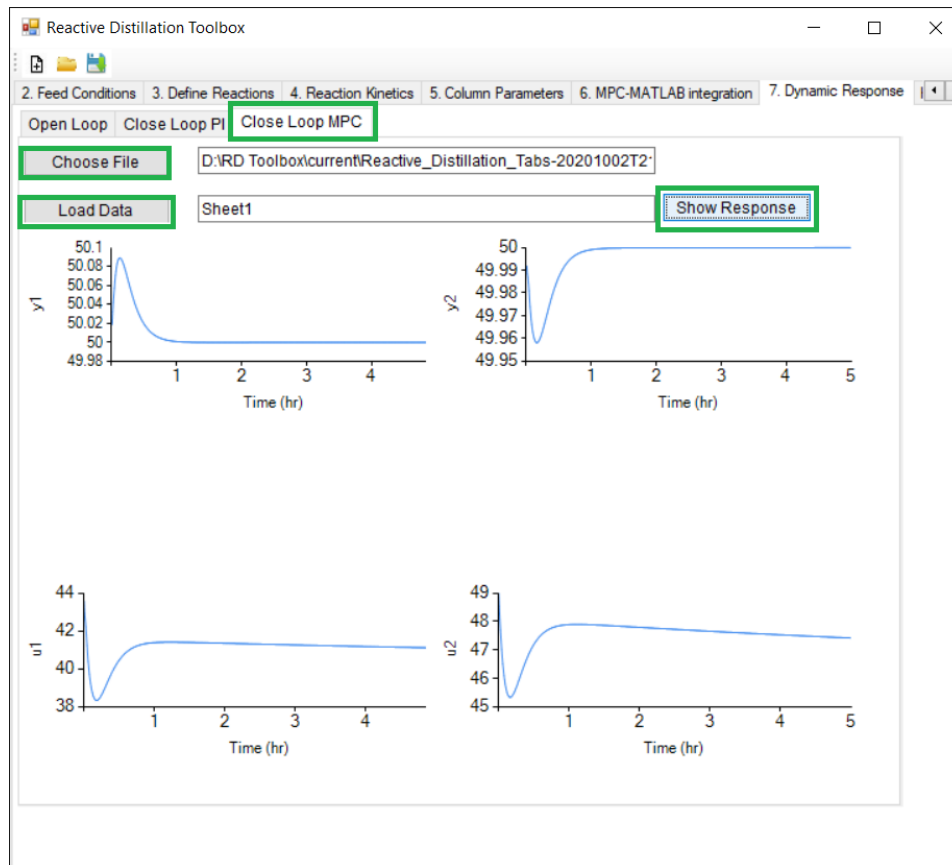


Figure 5.18 Dynamic MPC closed loop simulation

To observe the open loop and close loop PI response, follow the steps described in Step 2. For this case study the following responses are observed (Figure 5.19).

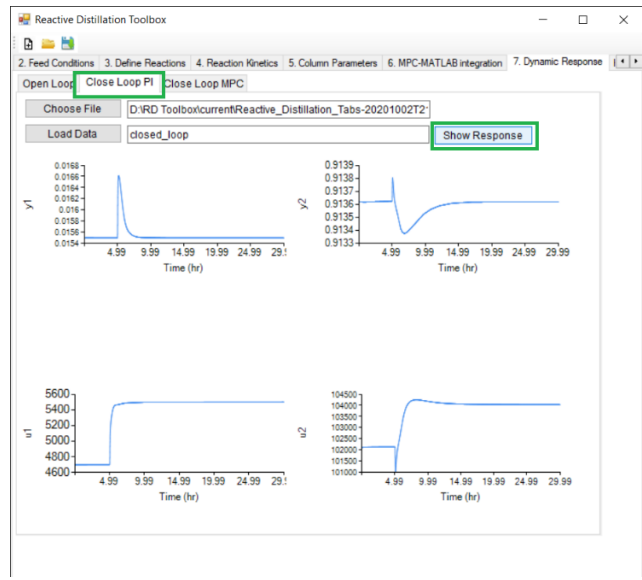
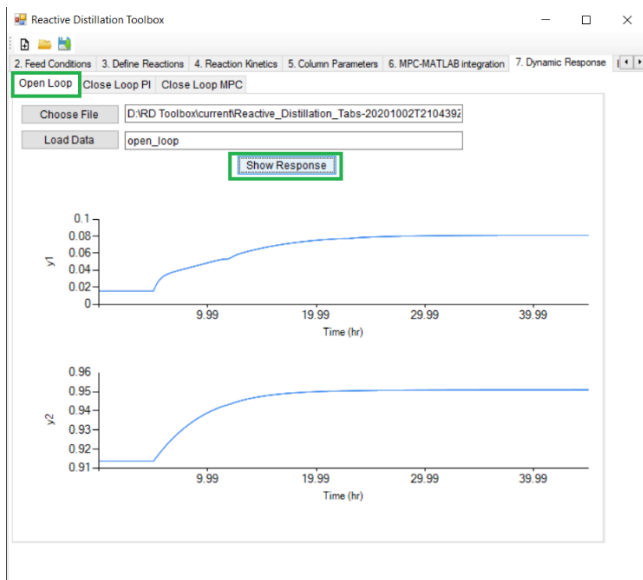


Figure 5.19 Open loop and Close loop PI response

**CHAPTER 6**  
**CONCLUSION AND FUTURE WORKS**

## 6 CONCLUSION AND FUTURE WORKS

This chapter describes the contribution of this thesis work and the direction for future works.

### 6.1 Conclusions

In this thesis work, the enhanced design and superior controllability of reactive distillation processes obtained through an integrated design-control framework using the driving force concept has been demonstrated. The integrated design-control framework has been converted to a computer aided toolbox for fast and efficient RD problem formulation, design and control analysis. The framework has been applied to study six RD systems: MTBE without inert (single feed binary element), MTBE with inert (single feed multi-element), Methyl Acetate production (double feed multi-element), Toluene disproportionation (single feed binary element), ETBE without inert (single feed binary element) and TAME production without inert (single feed binary element). A performance objective function that takes into account the steady state sustainability metrics (total energy consumption, total carbon footprint) and dynamic control performance (total variations in manipulated variables, the integral absolute error in controlled variables) has been employed. The main contributions of this thesis work are summarized below:

1. The integrated design-control framework covers design-control options so that RD systems in terms of configuration as well as reactive systems can be easily introduced. The framework allows for different configurations of the RD column and integrates the controller designs through a common set of variables that define both the design and control of the RD column operation. For example, product purity (a specification for process design, also serves as a set-point value for the controller) is paired with reflux ratio (which is optimized in process design, and serves as a reference value for the manipulated variable) at the maximum achievable driving force.
2. The advantages of driving force based integrated design-control of RD systems are demonstrated for both liquid phase and vapor phase reactive systems.

3. Application and evaluation of advanced controllers such as MPC is carried out. The results show that the RD systems designed at the maximum driving force can be more easily controlled with less error through the PI controllers as well as the MPC controller.
4. For each RD system, the control performance at the maximum driving force is better than any other designs which are based on non-maximal driving force.
5. For a double feed multi-element system (methyl-acetate), it has also been demonstrated that the PI and MPC control structures can successfully reject the disturbances introduced through either of the two feeds.
6. The extended framework has been converted to a computer-aided toolbox that guides the user through the steps of the work-flow of the integrated design-control method, provides access to in-house and/or external tools needed at each step, and, transfers the data from one step to another. For a reactive system, the toolbox based on the framework guides the user through the steps of the design and control algorithms and sets up the closed-loop simulation for verification.

Therefore, it can be concluded that the design at the maximum driving force facilitates the control structure design and results in better controller performance, regardless of the choice of the controller (MPC or PI), compared to designs not at the maximum driving force.

## **6.2 Directions for future works**

The future research direction in this subject area can be listed as follows:

- 1) Further equipping the implemented integrated design-control toolbox with additional features to enable efficient, reliable and systematic studies of a wide range of RD systems.
- 2) Simulation and investigation of driving force based integrated design and control of RD systems with multiple feed and side streams.
- 3) Controllability analysis of RD systems designed using the IDEAS (infinite dimensional state space) approach can be explored.



## References

- Agreda, V. H., & Partin, L. R. (1984). *Reactive distillation process for the production of methyl acetate* (Patent No. Patent 4435595 A).
- Al-Arfaj, M. A., & Luyben, W. L. (2002). Comparative control study of ideal and methyl acetate reactive distillation. *Chemical Engineering Science*, *57*(24), 5039–5050. [https://doi.org/10.1016/S0009-2509\(02\)00415-3](https://doi.org/10.1016/S0009-2509(02)00415-3)
- Al-Arfaj, M. A., & Luyben, W. L. (2004). Plantwide control for TAME production using reactive distillation. *AIChE Journal*, *50*(7), 1462–1473. <https://doi.org/10.1002/aic.10138>
- Al-Jarallah, A. M., Lee, A. K. K., & Siddiqui, M. A. B. (1988). Kinetics of methyl tertiary butyl ether synthesis catalyzed by sulphuric acid. *The Chemical Engineering Journal*, *39*(3), 169–174. [https://doi.org/10.1016/0300-9467\(88\)80024-8](https://doi.org/10.1016/0300-9467(88)80024-8)
- Almeida-Rivera, C. P., Swinkels, P. L. J., & Grievink, J. (2004). Designing reactive distillation processes: Present and future. *Computers and Chemical Engineering*, *28*(10), 1997–2020. <https://doi.org/10.1016/j.compchemeng.2004.03.014>
- Alvarado-Morales, M., Hamid, M. K. A., Sin, G., Gernaey, K. V., Woodley, J. M., & Gani, R. (2010). A model-based methodology for simultaneous design and control of a bioethanol production process. *Computers and Chemical Engineering*, *34*(12), 2043–2061. <https://doi.org/10.1016/j.compchemeng.2010.07.003>
- An, W., Lin, Z., Chen, J., & Zhu, J. (2014). Simulation and analysis of a reactive distillation column for removal of water from ethanol-water mixtures. *Industrial and Engineering Chemistry Research*, *53*(14), 6056–6064. <https://doi.org/10.1021/ie403906z>
- Androulakis, I. P. (2000). Kinetic mechanism reduction based on an integer programming approach. *AIChE Journal*, *46*(2), 361–371. <https://doi.org/10.1002/aic.690460214>
- Avami, A., Marquardt, W., Saboohi, Y., & Kraemer, K. (2012). Shortcut design of reactive distillation columns. *Chemical Engineering Science*, *71*, 166–177. <https://doi.org/10.1016/j.ces.2011.12.021>
- Avraam, M. P., Shah, N., & Pantelides, C. C. (1999). A decomposition algorithm for the optimisation of hybrid dynamic processes. *Computers and Chemical Engineering*, *23*(SUPPL. 1), S451–S454. [https://doi.org/10.1016/S0098-1354\(99\)80111-2](https://doi.org/10.1016/S0098-1354(99)80111-2)
- Babi, D. K., Lutze, P., Woodley, J. M., & Gani, R. (2014). A process synthesis-intensification framework for the development of sustainable membrane-based operations. *Chemical Engineering and Processing: Process Intensification*, *86*, 173–195. <https://doi.org/10.1016/j.cep.2014.07.001>
- Bahakim, S. S., & Ricardez-Sandoval, L. A. (2014). Simultaneous design and MPC-based control for dynamic systems under uncertainty: A stochastic approach. *Computers and Chemical Engineering*, *63*, 66–81. <https://doi.org/10.1016/j.compchemeng.2014.01.002>
- Balasubramhanya, L. S., & Doyle, F. J. (2000). Nonlinear model-based control of a batch

- reactive distillation column. *Journal of Process Control*, 10(2), 209–218.  
[https://doi.org/10.1016/S0959-1524\(99\)00024-4](https://doi.org/10.1016/S0959-1524(99)00024-4)
- Baur, R., Taylor, R., & Krishna, R. (2003). Bifurcation analysis for TAME synthesis in a reactive distillation column: Comparison of pseudo-homogeneous and heterogeneous reaction kinetics models. *Chemical Engineering and Processing*, 42(3), 211–221.  
[https://doi.org/10.1016/S0255-2701\(02\)00090-9](https://doi.org/10.1016/S0255-2701(02)00090-9)
- Bek-Pedersen, E., & Gani, R. (2004). Design and synthesis of distillation systems using a driving-force-based approach. *Chemical Engineering and Processing: Process Intensification*, 43(3), 251–262. [https://doi.org/10.1016/S0255-2701\(03\)00120-X](https://doi.org/10.1016/S0255-2701(03)00120-X)
- Bek-Pedersen, E., Gani, R., & Levaux, O. (2000). Determination of optimal energy efficient separation schemes based on driving forces. *Computers and Chemical Engineering*, 24(2–7), 253–259. [https://doi.org/10.1016/S0098-1354\(00\)00474-9](https://doi.org/10.1016/S0098-1354(00)00474-9)
- Biegler, L. T. (2007). An overview of simultaneous strategies for dynamic optimization. *Chemical Engineering and Processing: Process Intensification*, 46(11), 1043–1053.  
<https://doi.org/10.1016/j.cep.2006.06.021>
- Bristol, E. H. (1966). On a new measure of interaction for multivariable process control. *IEEE Transactions on Automatic Control*, 11(1), 133–134.  
<https://doi.org/10.1109/TAC.1966.1098266>
- Chien, I. L., Chen, K., & Kuo, C. L. (2008). Overall control strategy of a coupled reactor/columns process for the production of ethyl acrylate. *Journal of Process Control*, 18(3–4), 215–231. <https://doi.org/10.1016/j.jprocont.2007.02.006>
- Chiu, M. Sen, & Arkun, Y. (1991). A new result on Relative Gain Array, Niederlinski Index and decentralized stability condition:  $2 \times 2$  plant cases. *Automatica*, 27(2), 419–421.  
[https://doi.org/10.1016/0005-1098\(91\)90093-H](https://doi.org/10.1016/0005-1098(91)90093-H)
- Corriou, J. (2004). *Process Control Theory and Applications*. Springer-Verlog London.
- Dimian, A. C., Bildea, C. S., & Kiss, A. A. (2014). Integrated Process and Product Design. In *Computer Aided Chemical Engineering* (Vol. 35, pp. 1–33). Elsevier B.V.  
<https://doi.org/10.1016/B978-0-444-62700-1.00001-2>
- Doherty, MF; Malone, M. (2001). *Conceptual design of distillation systems*. McGraw-Hill, New York.
- Dragomir, R. M., & Jobson, M. (2005). Conceptual design of single-feed kinetically controlled reactive distillation columns. *Chemical Engineering Science*, 60(18), 5049–5068.  
<https://doi.org/10.1016/j.ces.2005.03.045>
- Engell, S., & Fernholz, G. (2003). Control of a reactive separation process. *Chemical Engineering and Processing*, 42(3), 201–210. [https://doi.org/10.1016/S0255-2701\(02\)00089-2](https://doi.org/10.1016/S0255-2701(02)00089-2)
- Flores-Tlacuahuac, A., & Biegler, L. T. (2007). Simultaneous mixed-integer dynamic optimization for integrated design and control. *Computers and Chemical Engineering*, 31(5–6), 588–600. <https://doi.org/10.1016/j.compchemeng.2006.08.010>

- Francisco, M., Vega, P., & Álvarez, H. (2011). Robust Integrated Design of processes with terminal penalty model predictive controllers. *Chemical Engineering Research and Design*, 89(7), 1011–1024. <https://doi.org/10.1016/j.cherd.2010.11.023>
- Françoise, O., & Thyron, F. C. (1991). Kinetics and mechanism of ethyl tert-butyl ether liquid-phase synthesis. *Chemical Engineering and Processing*, 30(3), 141–149. [https://doi.org/10.1016/0255-2701\(91\)85003-7](https://doi.org/10.1016/0255-2701(91)85003-7)
- Gani, R., Baldyga, J., Biscans, B., Brunazzi, E., Charpentier, J. C., Drioli, E., Feise, H., Furlong, A., Van Geem, K. M., de Hemptinne, J. C., ten Kate, A. J. B., Kontogeorgis, G. M., Manenti, F., Marin, G. B., Mansouri, S. S., Piccione, P. M., Povoia, A., Rodrigo, M. A., Sarup, B., ... Woodley, J. M. (2020). A multi-layered view of chemical and biochemical engineering. *Chemical Engineering Research and Design*, 155, 133–145. <https://doi.org/10.1016/j.cherd.2020.01.008>
- Georgiadis, M. C., Schenk, M., Pistikopoulos, E. N., & Gani, R. (2002). The interactions of design, control and operability in reactive distillation systems. *Computers and Chemical Engineering*, 26(4–5), 735–746. [https://doi.org/10.1016/S0098-1354\(01\)00774-8](https://doi.org/10.1016/S0098-1354(01)00774-8)
- Harmsen, G. J. (2007). Reactive distillation: The front-runner of industrial process intensification. A full review of commercial applications, research, scale-up, design and operation. *Chemical Engineering and Processing: Process Intensification*, 46(9 SPEC. ISS.), 774–780. <https://doi.org/10.1016/j.cep.2007.06.005>
- Harmsen, J. (2010). Process intensification in the petrochemicals industry: Drivers and hurdles for commercial implementation. *Chemical Engineering and Processing: Process Intensification*, 49(1), 70–73. <https://doi.org/10.1016/j.cep.2009.11.009>
- Heath, J. A., Kookos, I. K., & Perkins, J. D. (2000). Process control structure selection based on economics. *AIChE Journal*, 46(10), 1998–2016. <https://doi.org/10.1002/aic.690461012>
- Jantharasuk, A., Gani, R., Górak, A., & Assabumrungrat, S. (2011). Methodology for design and analysis of reactive distillation involving multielement systems. *Chemical Engineering Research and Design*, 89(8), 1295–1307. <https://doi.org/10.1016/j.cherd.2011.04.016>
- Kawathekar, R., & Riggs, J. B. (2007). Nonlinear model predictive control of a reactive distillation column. *Control Engineering Practice*, 15(2), 231–239. <https://doi.org/10.1016/j.conengprac.2006.07.004>
- Kiss, A. A. (2019). Novel Catalytic Reactive Distillation Processes for a Sustainable Chemical Industry. *Topics in Catalysis*, 62(17–20), 1132–1148. <https://doi.org/10.1007/s11244-018-1052-9>
- Kiss, A. A., & Bildea, C. S. (2012). A review of biodiesel production by integrated reactive separation technologies. In *Journal of Chemical Technology and Biotechnology* (Vol. 87, Issue 7, pp. 861–879). John Wiley & Sons, Ltd. <https://doi.org/10.1002/jctb.3785>
- Kookos, I. K., & Perkins, J. D. (2001). An algorithm for simultaneous process design and control. *Industrial and Engineering Chemistry Research*, 40(19), 4079–4088. <https://doi.org/10.1021/ie000622t>
- Lee, H. Y., Jan, C. H., Chien, I. L., & Huang, H. P. (2010). Feed-splitting operating strategy of a

- reactive distillation column for energy-saving production of butyl propionate. *Journal of the Taiwan Institute of Chemical Engineers*, 41(4), 403–413.  
<https://doi.org/10.1016/j.jtice.2010.03.003>
- Lee, J. H. (2011). Model predictive control: Review of the three decades of development. In *International Journal of Control, Automation and Systems* (Vol. 9, Issue 3, pp. 415–424). Springer. <https://doi.org/10.1007/s12555-011-0300-6>
- Lobão, M. W. N., Alberton, A. L., Melo, S. A. B. V., Embiruçu, M., Monteiro, J. L. F., & Pinto, J. C. (2012). Kinetics of toluene disproportionation: Modeling and experiments. In *Industrial and Engineering Chemistry Research* (Vol. 51, Issue 1, pp. 171–183). American Chemical Society. <https://doi.org/10.1021/ie2015526>
- Lopez-Arenas, T., Mansouri, S. S., Sales-Cruz, M., Gani, R., & Pérez-Cisneros, E. S. (2019). A Gibbs energy-driving force method for the optimal design of non-reactive and reactive distillation columns. *Computers and Chemical Engineering*, 128, 53–68.  
<https://doi.org/10.1016/j.compchemeng.2019.05.024>
- Lucia, A., Amale, A., & Taylor, R. (2008). Distillation pinch points and more. *Computers and Chemical Engineering*, 32(6), 1342–1364.  
<https://doi.org/10.1016/j.compchemeng.2007.06.019>
- Luyben, W. (2013). *Distillation Design and Control Using Aspen<sup>TM</sup> Simulation*. John Wiley & Sons, Ltd.
- Malcolm, A., Polan, J., Zhang, L., Ogunnaike, B. A., & Linninger, A. A. (2007). Integrating systems design and control using dynamic flexibility analysis. *AIChE Journal*, 53(8), 2048–2061. <https://doi.org/10.1002/aic.11218>
- Mansouri, S. (2016). *Integrated Process Design, Control and Analysis of Intensified Chemical Processes*. Technical University of Denmark.
- Mansouri, S. S., Huusom, J. K., Gani, R., & Sales-Cruz, M. (2016). Systematic integrated process design and control of binary element reactive distillation processes. *AIChE Journal*, 62(9), 3137–3154. <https://doi.org/10.1002/aic.15322>
- Mansouri, S. S., Sales-Cruz, M., Huusom, J. K., & Gani, R. (2016a). Integrated Process Design and Control of Multi-element Reactive Distillation Processes. *IFAC-PapersOnLine*, 49(7), 735–740. <https://doi.org/10.1016/j.ifacol.2016.07.272>
- Mansouri, S. S., Sales-Cruz, M., Huusom, J. K., & Gani, R. (2016b). Systematic integrated process design and control of reactive distillation processes involving multi-elements. *Chemical Engineering Research and Design*, 115, 348–364.  
<https://doi.org/10.1016/j.cherd.2016.07.010>
- McCabe, W. L., & Thiele, E. W. (1925). Graphical Design of Fractionating Columns. *Industrial and Engineering Chemistry*, 17(6), 605–611. <https://doi.org/10.1021/ie50186a023>
- Medina-Herrera, N., Tututi-Avila, S., Jiménez-Gutiérrez, A., & Segovia-Hernández, J. G. (2017). Optimal design of a multi-product reactive distillation system for silanes production. *Computers and Chemical Engineering*, 105, 132–141.  
<https://doi.org/10.1016/j.compchemeng.2017.01.014>

- Michelsen, M. L. (1994). Calculation of multiphase equilibrium. *Computers and Chemical Engineering*, 18(7), 545–550. [https://doi.org/10.1016/0098-1354\(93\)E0017-4](https://doi.org/10.1016/0098-1354(93)E0017-4)
- Mohideen, M. J., Perkins, J. D., & Pistikopoulos, E. N. (1996). Optimal synthesis and design of dynamic systems under uncertainty. *Computers and Chemical Engineering*, 20(SUPPL.2), S895–S900. [https://doi.org/10.1016/0098-1354\(96\)00157-3](https://doi.org/10.1016/0098-1354(96)00157-3)
- Moon, J., Kim, S., & Linninger, A. A. (2011). Embedded control for optimizing flexible dynamic process performance. *Industrial and Engineering Chemistry Research*, 50(9), 4993–5004. <https://doi.org/10.1021/ie1014052>
- Nielsen, T. L., Abildskov, J., Harper, P. M., Papaconomou, I., & Gani, R. (2001). The CAPEC database. *Journal of Chemical and Engineering Data*, 46(5), 1041–1044. <https://doi.org/10.1021/je000244z>
- Pérez Cisneros, E. S., Gani, R., & Michelsen, M. L. (1997). Reactive separation systems - I. Computation of physical and chemical equilibrium. *Chemical Engineering Science*, 52(4), 527–543. [https://doi.org/10.1016/S0009-2509\(96\)00424-1](https://doi.org/10.1016/S0009-2509(96)00424-1)
- Rafiei, M., & Ricardez-Sandoval, L. A. (2020). New frontiers, challenges, and opportunities in integration of design and control for enterprise-wide sustainability. *Computers and Chemical Engineering*, 132. <https://doi.org/10.1016/j.compchemeng.2019.106610>
- Ricardez-Sandoval, L. A., Budman, H. M., & Douglas, P. L. (2009). Integration of design and control for chemical processes: A review of the literature and some recent results. In *Annual Reviews in Control* (Vol. 33, Issue 2, pp. 158–171). Pergamon. <https://doi.org/10.1016/j.arcontrol.2009.06.001>
- Rivera, D. E., Morarl, M., & Skogestad, S. (1986). Internal Model Control: Pid Controller Design. *Industrial and Engineering Chemistry Process Design and Development*, 25(1), 252–265. <https://doi.org/10.1021/i200032a041>
- Sánchez Daza, O., Pérez-Cisneros, E. S., Bek-Pedersen, E., & Gani, R. (2003). Graphical and Stage-to-Stage Methods for Reactive Distillation Column Design. *AIChE Journal*, 49(11), 2822–2841. <https://doi.org/10.1002/aic.690491115>
- Sander, S., Flisch, C., Geissler, E., Schoenmakers, H., Ryll, O., & Hasse, H. (2007). Methyl Acetate Hydrolysis in a Reactive Divided Wall Column. *Chemical Engineering Research and Design*, 85(1 A), 149–154. <https://doi.org/10.1205/cherd06106>
- Schoenmakers, H. G., & Bessling, B. (2003). Reactive and catalytic distillation from an industrial perspective. *Chemical Engineering and Processing*, 42(3), 145–155. [https://doi.org/10.1016/S0255-2701\(02\)00085-5](https://doi.org/10.1016/S0255-2701(02)00085-5)
- Seborg, Dale; Edgar, Thomas; Mellichamp, Duncan; Doyle III, F. (2010). *Process Dynamics and Control* (3rd ed.). John Wiley & Sons.
- Segovia-Hernández, J. G., Hernández, S., & Bonilla Petriciolet, A. (2015). Reactive distillation: A review of optimal design using deterministic and stochastic techniques. In *Chemical Engineering and Processing: Process Intensification* (Vol. 97, pp. 134–143). Elsevier. <https://doi.org/10.1016/j.cep.2015.09.004>

- Sendin, O. H., Moles, C. G., Alonso, A. A., & Banga, J. R. (2004). Chapter D4 Multi-objective integrated design and control using stochastic global optimization methods. In *Computer Aided Chemical Engineering* (Vol. 17, Issue C, pp. 555–581). Elsevier. [https://doi.org/10.1016/S1570-7946\(04\)80074-9](https://doi.org/10.1016/S1570-7946(04)80074-9)
- Shah, M., Kiss, A. A., Zondervan, E., & De Haan, A. B. (2012). A systematic framework for the feasibility and technical evaluation of reactive distillation processes. *Chemical Engineering and Processing: Process Intensification*, *60*, 55–64. <https://doi.org/10.1016/j.cep.2012.05.007>
- Sharma, N., & Singh, K. (2012). Model predictive control and neural network predictive control of TAME reactive distillation column. *Chemical Engineering and Processing: Process Intensification*, *59*, 9–21. <https://doi.org/10.1016/j.cep.2012.05.003>
- Skogestad, S. (2003). Simple analytic rules for model reduction and PID controller tuning. *Journal of Process Control*, *13*(4), 291–309. [https://doi.org/10.1016/S0959-1524\(02\)00062-8](https://doi.org/10.1016/S0959-1524(02)00062-8)
- Sneesby, M. G., Tadé, M. O., Datta, R., & Smith, T. N. (1997). ETBE Synthesis via Reactive Distillation. 1. Steady-State Simulation and Design Aspects. *Industrial and Engineering Chemistry Research*, *36*(5), 1855–1869. <https://doi.org/10.1021/ie960283x>
- Tian, Y., Demirel, S. E., Hasan, M. M. F., & Pistikopoulos, E. N. (2018). An overview of process systems engineering approaches for process intensification: State of the art. In *Chemical Engineering and Processing - Process Intensification* (Vol. 133, pp. 160–210). Elsevier B.V. <https://doi.org/10.1016/j.cep.2018.07.014>
- Tula, Anjan K., Wang, J., Chen, X., Mansouri, S. S., & Gani, R. (2020). ProCADC: A computer-aided versatile tool for process control. *Computers and Chemical Engineering*, *136*, 106771. <https://doi.org/10.1016/j.compchemeng.2020.106771>
- Tula, Anjan Kumar, Babi, D. K., Bottlaender, J., Eden, M. R., & Gani, R. (2017). A computer-aided software-tool for sustainable process synthesis-intensification. *Computers and Chemical Engineering*, *105*, 74–95. <https://doi.org/10.1016/j.compchemeng.2017.01.001>
- Tula, Anjan Kumar, Eden, M. R., & Gani, R. (2015). Process synthesis, design and analysis using a process-group contribution method. *Computers and Chemical Engineering*, *81*, 245–259. <https://doi.org/10.1016/j.compchemeng.2015.04.019>
- Umar, M., Patel, D., & Saha, B. (2009). Kinetic studies of liquid phase ethyl tert-butyl ether (ETBE) synthesis using macroporous and gelular ion exchange resin catalysts. *Chemical Engineering Science*, *64*(21), 4424–4432. <https://doi.org/10.1016/j.ces.2009.07.015>
- Venkateswarlu, C., & Reddy, A. D. (2008). Nonlinear model predictive control of reactive distillation based on stochastic optimization. *Industrial and Engineering Chemistry Research*, *47*(18), 6949–6960. <https://doi.org/10.1021/ie070972g>
- Wang, S. J., Cheng, S. H., Chiu, P. H., & Huang, K. (2014). Design and control of a thermally coupled reactive distillation process synthesizing diethyl carbonate. *Industrial and Engineering Chemistry Research*, *53*(14), 5982–5995. <https://doi.org/10.1021/ie402923p>
- Yuan, Z., Chen, B., Sin, G., & Gani, R. (2012). State-of-the-art and progress in the optimization-

based simultaneous design and control for chemical processes. In *AICHE Journal* (Vol. 58, Issue 6, pp. 1640–1659). John Wiley & Sons, Ltd. <https://doi.org/10.1002/aic.13786>

# **APPENDICES**



# Appendix - A

MATLAB code for Reactive McCabe Thiele, Driving Force and Differential Driving force diagram generation for Case study 2

```
clc
clear all
close all
lk=1;hk=2;%A=1;B=2;C=3
upp=0.714;%liquid composition after max driving force point
lwp=0.55;%liquid composition before max driving force point
x=10;y=6;a=0;aa=0;c=0;cc=0;d=0;dd=0;e=0;ee=0;b=0;bb=0;f=0;ff=0;t=2;lm=1;
dc=0.80;%Component distillate composition
rc=0.90;%Component reboiler composition
fc=0.59;%Component feed composition
nr=1;%number of reactions
nc=4;%number of components
ne=nc-nr;%number of elements
m=1.2;%multiplication factor of Reflux Ratio and min Ref ratio

fm=[1 0 0 1;0 1 0 1;0 0 1 0];%formula matrix

wrc=0.505;wdc=0.99;wfc=0.63;
exf=xlsread('MTBEFWI');
temp=exf(:,5);
for i=1:1:length(exf)
for j=1:1:nc
a=(exf(i,x).*fm(1,j));
c=(exf(i,x).*fm(2,j));
b=(exf(i,x).*fm(1,j))+(exf(i,x).*fm(2,j))+(exf(i,x).*fm(3,j));
e=(exf(i,y).*fm(1,j));
d=(exf(i,y).*fm(2,j));
f=(exf(i,y).*fm(1,j))+(exf(i,y).*fm(2,j))+(exf(i,y).*fm(3,j));
x=x+1;
y=y+1;
aa=a+aa;
cc=c+cc;
bb=b+bb;
ee=e+ee;
dd=d+dd;
ff=f+ff;
end
aaa(i)=aa;
ccc(i)=cc;
bbb(i)=bb;
eee(i)=ee;
ddd(i)=dd;
fff(i)=ff;
a=0;b=0;c=0;d=0;e=0;f=0;g=0;h=0;x=10;y=6;aa=0;bb=0;ee=0;ff=0;cc=0;dd=0;
end
wla=aaa./bbb;
```

```

wlb=ccc./bbb;
wva=eee./fff;
wvb=ddd./fff;

for w=1:1:length(wla)
    wl(w)=wla(w)/(wla(w)+wlb(w));
    wv(w)=wva(w)/(wva(w)+wvb(w));
end

df=abs(wl-wv);
dfd=[0 df];wld=[0 wl];

for d=1:1:length(df)
    ddf(d)=abs(dfd(d)-dfd(d+1));
    dwl(d)=abs(wld(d)-wld(d+1));
    ddfwl(d)=ddf(d)/dwl(d);
end

maxv=max(df);

maxp=find(df==maxv);

mem=1/((maxv/(wdc-wl(maxp))));%Slope for Enriching Section for min RR

RRm=abs((mem/(mem-1)));%Min Reflux Ratio

RR=m*RRm;%Reflux Ratio

me=RR/(1+RR);%Slope for Enriching Section

ce=wdc/(1+RR);%Straight line constant for top op line

xin=wl(maxp);yin=me*xin+ce;%operating lines intersecting point

ms=(yin-wrc)/(xin-wrc);%Slope for Stripping Section

RB=1/(ms-1);% Reboiler Ratio

cs=yin-(ms*xin);%Straight line constant for bottom op line

mf=(yin-wfc)/(xin-wfc);%Slope of feed operating line

q=mf/(mf-1);%quality of feed

xdfgdz=[wl(maxp) wl(maxp)];ydfgdz=[0 maxv];%In driving force diagram
xdfgdy=[0 wl(maxp)];ydfgdy=[maxv maxv];

plot(wl,temp,'ko-',wv,temp,'r*-.')% temperature Diagram
set(gcf,'color','white')
xlabel('W_{LK,eq}'); ylabel('Temperature(K)');legend('Liquid','Vapor')

figure % Differential Driving Force Diagram

```

```

plot(wl,ddfwl,'k')
set(gcf,'color','white')
xlabel('W^{1}_{LK,eq}'); ylabel('dDF_{LK,eq}/dW^{1}_{LK,eq}');
xlim([0.5 1]);

figure

subplot(2,1,1)%Driving Force Diagram

x3=[wrc wl(maxp)];y3=[0 maxv];x4=[wdc wl(maxp)];y4=[0 maxv];
%y5=(wdc-wl(maxp))/(me);x5=[wdc wl(maxp)];y5=[0 y5];x6=[wrc
wl(maxp)];y6=[y5];

plot(wl,df,'k',x3,y3,'k',x4,y4,'k',xdfgd,x,ydfgd,'k-.',xdfgd,y,ydfgd,'k-.')
set(gcf,'color','white')
xlabel('W^{1}_{LK,eq}');ylabel('Driving Force,DF_{LK,eq}')

subplot(2,1,2)%McCabe Thiele Diagram
xx=[0 1];yy=[0 1];
xe=[wdc xin];ye=[wdc yin];% top operating line
xs=[wrc xin];ys=[wrc yin];%bottom operating line
ydfgd,x,ydfgd,'k-.')
xlim([0 1]);ylim([0 1])
xlabel('Liquid Element Fraction, W^{1}_{LK,eq}');ylabel('Vapor Element
Fraction, W^{v}_{LK,eq}')
set(gcf,'color','white')

yp=wdc;

for k=1:100
    if yp>max(wv)
        Ev=[(ceil(yp*10))/10 wv];
        El=[(ceil(yp*10))/10 wl];
    else
        Ev=[wv];El=[wl];
    end

    p=find(Ev>=yp);
    xp=El(p(1)-1)+((El(p(1)-1)-(El(p(1))))*(yp-(Ev(p(1)-1))))/(Ev(p(1)-
1)-(Ev(p(1))));
    if yp>=yin
        xp1=(yp-ce)/me;
        fr1(lm)=xp1;
    else
        xp1=(yp-cs)/ms;
        fr1(lm)=xp1;
    end
x6=[xp xp1];
y6=[yp yp];
if xp>=xin
    yp1=me*xp+ce;
    optf=k;
    fr=xp;

```

```

else
    yp1=ms*xp+cs;

    if yp1<=xp;
        yp1=xp;
    end
end
end
x7=[xp xp];
y7=[yp yp1];
hold on
plot(x6,y6, 'k',x7,y7, 'k');
yp=yp1;
if xp<=wrc
    break
end
lm=lm+1;
end

for ii=1:length(fr1)
    if fr1(ii)>0
        fr2=fr1(ii);
        break
    end
end

optf=optf+abs((fr-xin)/(fr-fr2))+1;
TN=(k-1)+((xp1-wrc)/(xp1-xp))+2;

dbf=(wfc-wrc)/(wdc-wrc);

NN=round(TN);

Nf=0;FN(1)=1;RRR(1)=NaN;RBB(1)=NaN;Dx=[];

for i=1.1:0.1:NN-2
    Nf=Nf+1;
    Dx(Nf+1)=1-i/(TN);
    pp=find(wl>=Dx(Nf+1));
    Dy(Nf+1)=df(pp(1)-1)+((df(pp(1)-1)-(df(pp(1))))*(Dx(Nf+1)-(wl(pp(1)-1))))/(wl(pp(1)-1)-(wl(pp(1)))));
    MEm(Nf+1)=1/abs(Dy(Nf+1)/(Dx(Nf+1)-wdc));%Slope for Enriching Section for min RR

    RRM(Nf+1)=abs(MEm(Nf+1)/(1-MEm(Nf+1)));%Min Reflux Ratio

    RRR(Nf+1)=m*RRM(Nf+1);%Reflux ratio

FN(Nf+1)=1+i+1

end
FN(Nf+2)=NN;RRR(Nf+2)=NaN;

```

```

inputvariable={'LK in Dist';'LK in Bot';'Feed comp';'Number of Rxn';'No of
Comp'};
inputdata=[wdc;wrc;wfc;nr;nc];
outputvariable={'Ref Ratio';'Reb Ratio';'No of Stage';'Opt Feed
Location';'Dist to Feed Ratio'};
outputdata=[RR;RB;TN;optf;dbf];

table(inputvariable,inputdata,outputvariable,outputdata)

Optimum_feed_stage=FN';
Reflux_Ratio=RRR';
table(Optimum_feed_stage,Reflux_Ratio)

figure%Driving Force Diagram

qq=find(wl>=upp);

dfupp=df(qq(1)-1)+((df(qq(1)-1))-(df(qq(1))))*(upp-(wl(qq(1)-1)))/((wl(qq(1)-
1))-(wl(qq(1)))));

rr=find(wl>=lwp);

dflwp=df(rr(1)-1)+((df(rr(1)-1))-(df(rr(1))))*(lwp-(wl(rr(1)-1)))/((wl(rr(1)-
1))-(wl(rr(1)))));

x3=[wrc wl(maxp)];y3=[0 maxv];x4=[wdc wl(maxp)];y4=[0 maxv];
x7=[wrc upp];y7=[0 dfupp];x8=[wdc upp];y8=[0 dfupp];
x9=[wrc lwp];y9=[0 dflwp];x10=[wdc lwp];y10=[0 dflwp];
x11=[0 wl(maxp)];y11=[maxv maxv];x12=[wl(maxp) wl(maxp)];y12=[0 maxv];

plot(wl,df,'k',x3,y3,'k',x4,y4,'k',x7,y7,'k',x8,y8,'k',x9,y9,'k',x10,y10,'k',
x11,y11,'k-.',x12,y12,'k-.')
set(gcf,'color','white')
xlabel('W^{1}_{LK,eq}');ylabel('Driving Force,DF_{LK,eq}')
txt = 'A \rightarrow';
text(0.54,0.225,txt);
txt = '\leftarrow B';
text(0.65,0.22,txt);
txt = 'C \rightarrow';
text(0.49,0.22,txt);
txt = 'D_{y}';
text(0.005,0.22,txt);
txt = 'D_{x}';
text(0.605,0.01,txt);
txt = 'W^{1}_{LK,D}';
text(0.9,0.0125,txt);
txt = 'W^{1}_{LK,B}';
text(0.43,0.0125,txt);

```

# Appendix -B

ASPEN PLUS INPUT file for flowsheet auto generation and steady state simulation

DYNAMICS

DYNAMICS RESULTS=ON

IN-UNITS MET PRESSURE=bar TEMPERATURE=C DELTA-T=C PDROP=bar &  
INVERSE-PRES='1/bar' SHORT-LENGTH=mm

DEF-STREAMS CONVEN ALL

MODEL-OPTION

DATABANKS 'APV100 PURE36' / 'APV100 AQUEOUS' / 'APV100 SOLIDS' &  
/ 'APV100 INORGANIC' / 'APESV100 AP-EOS' / &  
'NISTV100 NIST-TRC' / NOASPENPCD

PROP-SOURCES 'APV100 PURE36' / 'APV100 AQUEOUS' / &  
'APV100 SOLIDS' / 'APV100 INORGANIC' / 'APESV100 AP-EOS'  
&  
/ 'NISTV100 NIST-TRC'

COMPONENTS

Methanol CH4O /  
Isobutene C4H8-5 /  
1-Butene C4H8-1 /  
MTBE C5H12O-D2

SOLVE

RUN-MODE MODE=SIM

FLOWSHEET

BLOCK B1 IN=1 OUT=2 3

PROPERTIES UNIFAC

STREAM 1

SUBSTREAM MIXED TEMP=320 <K> PRES=11 <atm>  
MOLE-FLOW Methanol 34.3 / Isobutene 59 / 1-Butene 6.7 / MTBE  
0

BLOCK B1 RADFRAC

PARAM NSTAGE=7 ALGORITHM=NONIDEAL INIT-OPTION=STANDARD &  
MAXOL=200 DAMPING=NONE  
COL-CONFIG CONDENSER=TOTAL

FEEDS 1 2 ON-STAGE  
PRODUCTS 2 1 L / 3 7 L  
P-SPEC 1 10.9 <atm>  
COL-SPECS D:F=0.64 DP-STAGE=0.01 <atm> MOLE-RR=7  
REAC-STAGES 2 6 R-1  
HOLD-UP 2 6 MASS-LHLDP=250.

EO-CONV-OPTI

STREAM-REPOR MOLEFLOW

REACTIONS R-1 REAC-DIST  
REAC-DATA 1 KINETIC  
REAC-DATA 2 KINETIC  
RATE-CON 1 PRE-EXP=2.49E+07 ACT-ENERGY=12600 &  
TEMP-EXPONEN=2  
RATE-CON 2 PRE-EXP=1.85E+18 ACT-ENERGY=31100  
STOIC 1 Methanol -1 / Isobutene -1 / 1-Butene 0 / MTBE 1  
STOIC 2 MTBE -1 / 1-Butene 0 / Isobutene 1 / Methanol 1  
POWLAW-EXP 1 Methanol 5 / Isobutene 5 / 1-Butene 0 / MTBE 0  
POWLAW-EXP 2 MTBE 0.001 / 1-Butene 0 / Isobutene 0 /  
Methanol 0

# Appendix - C

## Control Design Interface (CDI) script for Case study 2

```
Set Doc = ActiveDocument
Set CDI = Doc.CDI
CDI.Reset
CDI.AddInputVariable "blocks("B1").condenser(1).QR"
CDI.AddInputVariable "streams("2").FmR"
CDI.AddInputVariable "streams("3").FmR"
CDI.AddInputVariable "blocks("B1").Reflux.FmR"
CDI.AddInputVariable "blocks("B1").QRebR"
CDI.AddInputVariable "streams("1").FcR("ISOBUTEN")"
CDI.AddOutputVariable "blocks("B1").stage(1).P"
CDI.AddOutputVariable "blocks("B1").stage(1).Level"
CDI.AddOutputVariable "blocks("B1").SumpLevel"
CDI.AddOutputVariable "streams("2").Zn("ISOBUTEN")"
CDI.AddOutputVariable "streams("3").Zn("MTBE")"
CDI.Calculate
```



# Appendix - D

## MATLAB script for MPC simulation for Case study 2

```
clc,clear all,clc
load cdi_A.dat
load cdi_B.dat
load cdi_C.dat
A = full(spconvert(cdi_A));
B = full(spconvert(cdi_B));
C = full(spconvert(cdi_C));
D = zeros(5,6);
[nxAr, nxAc] = size(A);
[nxB,nu] = size(B);
[ny,nxC] = size(C);
nx = max([nxAr, nxAc, nxB, nxC]);
if nx > nxC
    C = [C, zeros(ny,nx-nxC)];
end
if nx > nxAc
    A = [A zeros(nxAr,nx-nxAc)];
end
if nx > nxAr
    nxAc = size(A,2);
    A = [A; zeros(nx-nxAr, nxAc)];
end
if nxB < nx
    B = [B; zeros(nx-nxB,nu)];
end
U_span = [2*-11.45, 2*4497.84, 2*287.46, 2*31484.92, 2*10.8459, 2*59];
U_nom = 0.5*U_span;
U_zero = zeros(1,6);
Y_nom = [11.04, 3.0, 1.5, 0.41, 0.958];
Y_span = [2*Y_nom(1:5)];
Y_zero = [0, 0, 0, 0, 0];
B = B.*(ones(nx,1)*U_span);
C = C./(ones(nx,1)*Y_span)';
G = ss(A, B, C, D);
G.TimeUnit = 'hours';
G.u = {'Qc', 'Qr', 'R', 'D', 'B', 'F'};
G.y = {'P', 'RLev', 'Slev', 'xD', 'xB'};
[hsv, baldata] = hsvd(G);
order = find(hsv>0.01,1,'last');
Options = balredOptions('StateElimMethod', 'Truncate');
G = balred(G, order, baldata, Options);
U_nom_pct = (U_nom - U_zero)*100./U_span;
Y_nom_pct = (Y_nom - Y_zero)*100./Y_span;
Gmpc = ss(G.a, G.b(:, [1:6,1:5]), G.c, zeros(5,11), 'TimeUnit', 'hours');
InputName = cell(1,11);
for i = 1:5
    InputName{i} = G.InputName{i};
    InputName{i+6} = [G.InputName{i}, '-UD'];
end
```

```

InputName{6} = G.InputName{6};
Gmpc.InputName = InputName;
Gmpc.InputGroup = struct('MV', 1:5, 'MD', 6, 'UD', 7:11);
Gmpc.OutputName = G.OutputName;
Ts = 30/3600;
PH = 60;
CH = 10;
MPCobj = mpc(Gmpc, Ts, PH, CH);
MPCobj.Weights.ManipulatedVariables = [0, 0, 0, 0, 0];
MPCobj.Weights.ManipulatedVariablesRate = [0.01, 0.01, 0.01, 0.01, 0.1];
MPCobj.Weights.OutputVariables = [10, 0.1, 0.1, 1, 0.5];
MPCobj.Model.Nominal.U = [U_nom_pct'; zeros(5,1)];
MPCobj.Model.Nominal.Y = Y_nom_pct';
T = 5*120;
r = Y_nom_pct;
v = U_nom_pct(6)+16.5;
SimOptions = mpcsimopt(MPCobj);
SimOptions.InputNoise = [0 0 0 0 0];
[y_L, t_L, u_L] = sim(MPCobj, T, r, v, SimOptions);
XD = y_L(:,4);
XB = y_L(:,5);
reflux = u_L(:,4);
QR = u_L(:,5);
Time = t_L;
xlswrite('MPC_Close_loop_data.xls', [Time, XD, Time, XB, Time, reflux, Time, QR]);
col_header={'Time', 'XD', 'Time', 'XB', 'Time', 'RR', 'Time', 'RD'};
xlswrite('MPC_Close_loop_data.xls', col_header);

```